OPTIMIZATION OF 3-D NEURAL CULTURE AND EXTRACELLULAR ELECTROPHYSIOLOGY FOR STUDYING INJURY-INDUCED MORPHOLOGICAL AND FUNCTIONAL CHANGES

A Dissertation
Presented to
The Academic Faculty

by

Varadraj Nagesh Vernekar

In Partial Fulfillment
of the Requirements for the Degree
Doctor of Philosophy in the
Department of Biomedical Engineering

Georgia Institute of Technology
May 2010

OPTIMIZATION OF 3-D NEURAL CULTURE AND EXTRACELLULAR ELECTROPHYSIOLOGY FOR STUDYING INJURY-INDUCED MORPHOLOGICAL AND FUNCTIONAL CHANGES

Approved by:

Dr. Michelle C. LaPlaca, Advisor
School of Biomedical Engineering
Georgia Institute of Technology

Dr. Nael C. McCarty
Department of Pediatrics
Emory University, School of Medicine

Dr. Mark G. Allen
School of Electrical and Computer Engineering
Georgia Institute of Technology

Dr. Steven M. Potter
School of Biomedical Engineering
Georgia Institute of Technology

Dr. Stephen P. DeWeerth
School of Biomedical Engineering
Georgia Institute of Technology

Date Approved: April 2, 2010.

To my parents

ACKNOWLEDGEMENTS

I could not have done this work alone without the help of so many people along the way. I cannot thank my advisor Dr. Michelle LaPlaca enough for her interest, patience, and support throughout all my projects. She helped sustain my motivation for successfully finishing this big task, and inspired me with her open mindedness, encouraging spirit, sense of fairness, and responsible conduct. Michelle's wise judgment effectively shaped my progression through my doctoral studies. I will never forget some of her words: "It's all a game," "We want to look forward," "Make it part of your being," "By now you need to have developed a thick skin, they don't mean to be mean to you," "Be objective," and the list goes on...

I would like to thank my thesis committee members: Drs. Mark Allen, Stephen DeWeerth, Nael McCarty, and Steven Potter for their guidance, critical oversight, and interest which helped to shape my thesis work. Collectively, along with Michelle, they made sure that I finished strong in this experience. They directed me to objectively and critically analyze my own work and taught me that sound conclusions stand on statistically robust results. As I worked on my thesis, I also learned a lot about team work from my collaborators in the Bioengineering Research Partnership (BRP) project. Particularly in BRP, I would like to acknowledge Dr. Yoonsu Choi, and Dr. Gregory Brewer. In influencing my development, my Master's thesis advisor Dr. Robert Latour from Clemson University has a big share too - he was the one who introduced me to the research path that brought me to Georgia Tech.

I would like to thank the Georgia Tech community for providing state-of-the-art facilities for research and an excellent environment for learning. The funding for my research came from the National Institute of Health – BRP grant NIBIB/NINDS (BRP EB000786), the Biomedical Engineering Department, and microPerfusions Inc. without which my work would not be possible. I would like to thank Dr. Andrés García, Dr. Brent Carter, Dr. Amanda Walls Bridges, Cameron Sullards and David Bostwick for sharing their equipment and technical expertise with me, and Sandra Wilson, Chris Ruffin, and Amber Burris for their administrative support.

I would like to acknowledge the TI:GER program (Technological Innovations : Generating Economic Resources) for giving me a chance to explore aspects of technology innovation, entrepreneurship, and business, while working on my doctoral research. So would I also like to acknowledge Jane Chisholm, Ruth Schowalter, and Dr. Karen Head for working with me in improving my linguistic and conceptual communication skills written and spoken.

I would like to recognize all the present and past LaPlaca group members, especially Drs. Kacy Cullen, and Hillary Irons for strengthening me in weak areas. I would like to thank Brock Wester, JT Shoemaker, and Drs. Chris Lessing and Maxine McClain for their amiable companionship in lab. I would also like to acknowledge the work of many undergraduate students who made this work possible: Megan Springman, Winston Pewin, Tulika Raj, Nishil Patel, Nishit Jain, Rafeed Chaudhury, Angela Liu, Ruchir Karmali, Ellen Field, Camila Santiago, Melody Keith, Rebekah Hamrick, and Willa Ni. I would not have finished my thesis without your commitment and dedication. During my graduate work, I benefited from my interactions with Peter Passaro, and Drs.

Douglas Backum and Radhika Madhavan, members of the Potter group, and the collaborative environment of the Neurolab.

I am very grateful for the support of my friends and colleagues John Slanina, Lukasz Gadowski, Dr. Vishwas Aiyanger, Anna Pavlova, Veer Mahajan, Dr. Krishna Sarangapani, Arpit Singhal, and Dr. Mahesh Dodla as I made my passage through the academic rigor at Georgia Tech. I must thank Rebekah Hamrick and Melody Keith for sharing their expertise of English communication with me. So must I thank Lydia DePue, Joshua Steele, Daniel Kestranek, and Brian Young for ensuring my love for health and fitness, which helped me balance the academic stress of the doctoral program. Special thanks go to Ken and Jen for their support through these trying years. The accomplishment seems amazing, looking back at my clueless states, having had no idea how to wade through this journey. I truly thank Georgia Tech for offering me such a great pottery wheel to mold my intellectual clay.

I dedicate this work to my parents, Geeta and Nagesh, without whom, I would not have come all this way. I must thank my friend Jai and brother Pratik for their love and support. I am grateful to all my family, friends, mentors, colleagues, and foes. Moreover, I am grateful to God and this universe for allowing me a part.

Varadraj Nagesh Vernekar

April 2010

TABLE OF CONTENTS

LIST OF TABLES

LIST OF FIGURES

SUMMARY

Interfacing micron-sized electrodes with neural tissue could potentially transform the treatment of pathological conditions such as depression, pain, paralysis, and neural trauma. To realize these possibilities, one must first understand neural network dynamics and processing capabilities through long-term neuronal signal recording. Although putative *in vitro* neural network studies employ planar 2-D culture, they may not accurately represent *in vivo* cellular and network level functions. In contrast, a 3-D *in vitro* culture model more closely mimics the microenvironments of *in vivo* neural networks without the extra confounding variables of *in vivo* neural tissue.

This work characterized an *in vitro* 3-D neural co-culture model electrophysiologically via multi electrode arrays (MEAs), and morphologically via immunocytochemistry. Since MEA surface insulation SU-8 2000 can be used in neural micro- and multi- electrode arrays, this investigation first developed techniques to make SU-8 2000 cytocompatible. The *in vitro* 3-D neural co-culture model was then used to study viability and electrophysiological responses to physical injury as well as drugs known to affect network signaling. 1) SU-8 2000 cytotoxicity to neuronal cultures was linked to both poor adhesive properties and toxic components, such as solvents and photo acid generator elements. Surface treatments of oxygen plasma or parylene coating following optimal combinations of heat and isopropanol sonication showed improvement in SU-8 2000 cytocompatibility. 2) The 3-D neural networks within the 3-D co-cultures maintained considerable process outgrowth and complex 3-D structure. The cultures were viable up to three weeks *in vitro* with functional synaptic connections and

spontaneous electrophysiological activity that was responsive to chemical modulation. This electrophysiological activity was modulated by synaptic inhibition. 3) Injury experiments demonstrated that both shear and compression loading significantly increased acute membrane permeability of cells in a strain rate dependent manner. Cell death correlated with higher membrane permeability, and shear resulted in more death than compression in these 3-D cultures.

While techniques were developed for making a major micro-fabrication material cytocompatible, engineering the 3-D neural co-culture resulted in a more physiologically-representative neural tissue platform, allowing an increased understanding of structure-function relationships. Overall, this research established and characterized a neural culture system for the mechanistic study of cell growth, cell-cell and cell-matrix interactions, as well as the responses to chemical or mechanical perturbations. This is the first investigation of the network-level electrophysiological activity of 3-D dissociated cultures. This system can be used to model various pathological states *in vitro*, testing various reparative drugs; cell-, and tissue-engineering based strategies; as well as for pre-animal and pre-clinical testing of neural implants.

CHAPTER 1

INTRODUCTION

Research Motivation

Neural-electronic interfaces allow an increased understanding of neuronal communication and a direct means to manipulate network behavior. Electronic interfaces between micron-sized electrodes and neural tissue could potentially transform the treatment of pathological conditions including depression, pain, paralysis, and effects of neural trauma. Electrical signals sent directly to a limb-actuating muscle or to a prosthetic limb could bypass an injured spinal cord or nerves, allowing paralyzed patients to regain functional use of limbs. A neural tissue-implanted electrochemical sensor could cause electrical stimulus or chemical release of reservoir-stored serotonin reuptake inhibitor in response to depression-induced chemical imbalances. An implant responsive to neural trauma could send molecular sealing bandages to ruptured cells, thus minimizing cell death and brain damage.

The first step in realizing these possibilities is to understand neural network dynamics, neural processing capabilities, and neural response to pathological stimuli and therapeutic treatments through electrophysiological recording from neurons. Neural network recordings have been used to understand neural plasticity, trauma, disease, age-related degeneration [1]; deafness, memory deficits, epilepsy [2-3]**;** and neuroprostheses [4]. In researching these pertinent fields with respect to neural network properties, both *in vivo* and *in vitro* models are used. *In vivo* animal models are complex and often confound data interpretation, while single-cell studies (both *in vivo* and *in vitro*) preclude

robust network-level analysis. In contrast, *in vitro* cell culture models provide for a relatively controlled study environment and allow for simpler experimental manipulation at the network level.

Although *in vitro* neural network studies employ planar 2-D culture, they may not accurately represent *in vivo* cellular and network level functions, because *in vivo* conditions are 3-D in nature. Therefore, a 3-D *in vitro* culture model may more closely mimics the microenvironment of *in vivo* neural networks. The presence of 3-D growth and interactions may be crucial because the matrix surrounding cells, as is typical of the 3-D *in vivo* environment, has been shown to affect cellular function for a variety of cell types [5-6] including neural cells [7-9]. There is evidence that 3-D culture conditions may better approximate the morphology, cytoarchitecture, gene expression, proliferation of neural tissue [6, 10-12], organization and types of cell-cell and cell-matrix interactions, [13] than 2-D culture conditions.

We established a 3-D co-culture model of a neural network to closer approximate *in vivo* tissue, by harvesting embryonic cortical neurons and astrocytes of newborn rats and mixing them homogeneously within a 3-D hydrogel-based bioactive scaffold, Matrigel™. The cell culture model interfaced with an array of microelectrodes where external electronics recorded the electrophysiological activity.

We studied the structural and functional development of the neural networks within this 3-D neural co-culture model using microscopic imaging and 3-D multi electrode array (MEA) based electrophysiological recording. MEA technology has been used to study neural electrophysiological activity in 2-D dissociated spinal cord [14], cortical [15], hippocampal, acute retina [16-17], and cardiac myocyte cultures [18].

However, few studies exist on the electrophysiological activity of 3-D dissociated neural culture[19]. The study published by Irons et al. in 2008, is probably the only study presenting electrophysiological activity recording from 3-D neural cultures; However, that study was done using the patch clamp technique and merely showed that the neurons in the 3-D cultures were electrophysiologically active; it did not characterize the 3-D network level activity and it's development with respect to time. Unlike the patch clamp technique, 3-D MEA technology allows simultaneous multi-location recording in 3-D environments. Here we tracked the spontaneous electrophysiological (functional) and structural changes involved in 3-D neural network development in culture with respect to days *in vitro* (DIV). We hypothesized that *in vitro* spontaneous electrophysiological activity of the cultured 3-D neural networks would directly correlate with neuronal and synaptic densities. Therefore, to investigate the dynamic electrophysiological capability based on the structural organization of a neural network, we compared field potential based measurements of spike and burst rates over three weeks *in vitro* to markers of synaptic distribution and neuronal maturation. In addition, we compared the native spontaneous activity of the cultures to the activity during known pharmacologically altered states to confirm the biological response, learn more about the nature of these 3-D neural networks developed *in vitro*, and to assess the possibility of using these networks for pharmacological and toxcicological testing.

However, this approach assumes MEAs are cytocompatible for the test cultures to be healthy and viable. Therefore, we developed processing protocols to increase the cytocompatibility of SU-8 2000, a microelectrode fabrication material that insulates the MEA substrates, and; therefore, would be the main material to come in contact with the

3-D neural cultures. Processing increased cytocompatibility and allowed for the structural and functional (electrophysiological) characterization and pharmacological modulation of the cultures, without poor cytocompatibility interference from the MEA surface insulation. Moreover, this work provided a methodology for increasing the potential for SU-8 2000 to be a primary microfabrication material for biological microelectromechanical systems (bioMEMS) and other biomedical applications. In our pharmacological modulation studies we observed that excitatory drugs could increase the culture activity. This pharmacological modulation provided insight into the neural network development within these 3-D cultures. Furthermore, this model can be used to test various therapies such as single dose, time-release, mono- and combination drug therapies; drug-releasing devices; cell-based therapies such as stem cell delivery; study pathological conditions resulting from traumatic neural injury; characterize and validate tissue engineering strategies; and characterize and validate neural implants for continuous monitoring, diagnostic, and therapeutic applications to the nervous system.

Because of the anisotropy and three-dimensionality of the neural network structure in these cultures, the resulting strain fields at the cellular level, upon dynamic deformation, are inherently heterogeneous [20]. Therefore, this 3-D culture model can more realistically represent the 3-D dynamic loading conditions including heterogeneous strain fields induced during traumatic neural injury *in vivo* than 2-D cell culture models. Furthermore, they better mimic *in vivo* cytoarchitecture and the distribution of cell-cell and cell-matrix interactions than 2-D cultures, potentially affecting the mechano-transduction of the injury at a molecular level. Cells respond differently to traumatic loading depending on the deformation mode (tensile, shear, or compression), cell

population (different cell type morphologies manifest in different cellular mechanical properties), cell orientation with respect to the bulk strain field (affecting principle axes of local cellular strains), and the number of cellular processes (affecting the complexity of the strain field). Therefore, these multi-cell type comprised 3-D cell cultures offer a controlled and reproducible platform to better represents the mechanical injury and its associated pathological pathways than 2-D cultures, along with the continued benefits of real-time imaging and precise micro-environmental control. Therefore, we used our 3-D co-culture model to study traumatic neural injury, specifically we evaluated alterations in plasmalemma permeability as a function of bulk deformation mode (shear versus compression), loading parameters (strain and strain rate), and time post-insult (milliseconds to hours) in our 3-D co-culture model. These studies contributed to an increased understanding of cellular tolerance to injury and can be useful in computer modeling to more accurately predict structural and functional damage of neural tissue in response to large magnitude , high rate deformation.

Thus, our multi-faceted research offers multiple applications. Amongst them are the testing of different drugs and new therapeutic responses to pathologies such as traumatic injury, and the characterization and validation of neural implants for continuous monitoring, diagnostic, and therapeutic applications to the nervous system.

Purpose Statement

We developed and characterized 3-D co-culture models as a more relevant alternative to *in vitro* 2-D dissociated neural networks. After addressing the cytocompatibility issues with SU-8 2000, a material used in MEA fabrication, we used MEAs and immunocytochemistry to characterize the structural and functional (electrophysiological) development of these 3-D networks. We also applied this 3-D culture model for studying pharmacological and injury response of neural networks using 3-D MEA and confocal microscopic techniques. This thesis is a product of a multi-faceted project, broken up in to three specific aims: SU-8 2000 compatibility to neural networks, development of spontaneous neural network activity in a 3-D neuronal-astrocytic co-culture model, and neural network response to traumatic neural injury.

Specific Aims and Research Hypotheses

Execution of this research work fulfilled the following three aims, each with specific hypotheses: improve SU-8 2000 an MEA fabrication material compatibility to neural networks, structural and electrophysiological (MEA) analysis of 3-D neural network development in culture, and neural network response to traumatic neural injury. The interrelationship of the three specific aims is illustrated in Figure 1.1.

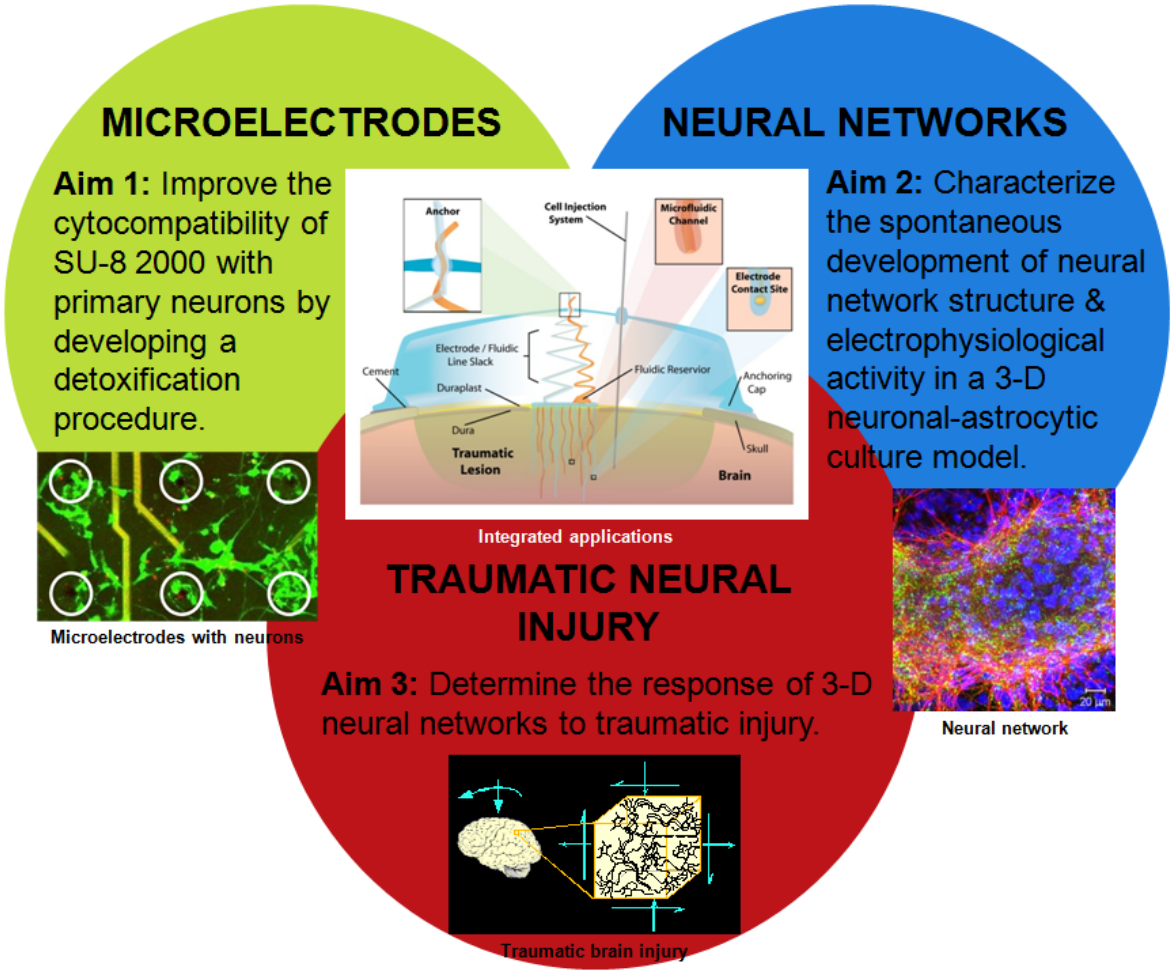

Figure 1.1. Interrelationship of the three specific aims of this thesis work. This research work bring together the fields of microelectrode technology, neural networks analysis, cell culture, and traumatic neural injury. Applications lie at the intersections of these fields in the area of neuroengineering; bioMEMS; neural prosthetics; neurobiology; cell culture; tissue engineering; traumatic neural injury; and *in vitro* drug, disease, and diagnostic testing technologies.

<u>Aim 1.</u> Develop a procedure to improve the cytocompatibility of SU-8 2000. The thermal and chemical stability of SU-8 2000 makes it ideal for the fabrication of high-aspect ratio 3-D microelectrode systems for neurological applications. In addition, its dielectric properties make it an excellent insulation material for micro electrode arrays (MEAs). However, thick untreated SU-8 2000 substrates ($\geq$ 100 μm) do not support living neural cells, potentially because of toxic leaching, and poor cell-adhesive characteristics. SU-8 2000 being hydrophobic, resists aqueous wetting and macromolecular adsorption, adversely affecting neural adhesion and growth [21-22]. Characterizing and improving the cytocompatibility of this material opens possibilities for SU-8 2000 to be used more frequently as a fabrication material for neural devices. This study is the first reported characterization of SU-8 2000 cytocompatibility for *in vitro* neurobiological applications, and presents several preparatory treatments for improved compatibility with neurons. This work expands the applicability of SU-8 2000 in the fabrication of 3-D microelectrode systems, such as in neural prosthetics, and offers cytocompatibility techniques for other cytotoxic microfabrication materials as well, especially those that are SU-8 based.

Study 1. Improve the cytocompatibility of SU-8 2000 substrates by reducing potentially toxic leaching and by promoting adhesion of neural cultures to SU-8 2000 surfaces. *First, it was hypothesized that the toxic leaching of chemicals from SU-8 2000 and its poor cell-adhesive character diminished its cytocompatibility. Second, it was hypothesized that SU-8 2000 substrates can be made cytocompatible by one or a combination of the following treatments: CO_2 supercritical extraction, ultra violet (UV) light exposure, and heating to potentially reduce toxic leaching. Finally, it was*

hypothesized that surface treatments such as glow discharge treatment, poly-D-lysine coating and laminin coating will improve neural culture adhesion to SU-8 2000 surfaces by increasing surface roughness, hydrophilicity, and protein adhesiveness.

<u>Aim 2.</u> Characterize the spontaneous development of neural network structure and electrophysiological activity in a 3-D neuronal-astrocytic co-culture model. Neural-electronic interfaces within cell culture models allow the controlled study of specific components of neuronal behavior, such as understanding the spatial and temporal development of neural network activity. Since 3-D cultures may better mimic the *in vivo* environment than 2-D cultures, we engineered 3-D culture models of neural tissue to study neural network-level properties. Since cell type, viability, connection patterns, and synaptic density in a neural network contribute to electrophysiological activity, we characterized these 3-D cultures using both immunocytochemistry and 3-D multielectrode array (MEA) recordings. We characterized network structure and electrophysiological activity in a 3-D dissociated neural culture model, so that we can understand the development of these neural networks, potentially comparing it to *in vivo* tissue behavior, and using it for the several applications discussed in the first section of this chapter. Structural characteristics such as synaptic distribution and neuronal maturation were compared to electrophysiological activity to better understand structure-function relationships in network development. To confirm a biological response, the electrophysiological activity of these 3-D co-cultures was assessed in response to agents known to interfere with synaptic transmission and neuronal action potential firing.

Study 2. Correlate synaptic distribution and neuronal maturity with electrophysiological activity. *It is hypothesized that the spontaneous*

electrophysiological activity of 3-D neural networks in culture will be a function of the synaptic distribution and neuronal maturation. To investigate this hypothesis, we recorded the spontaneous electrophysiological activity of dissociated cortical cultures, measuring the spike and burst rates over three weeks *in vitro*, while correlating them with synaptic density and neuronal maturation marker staining. Spontaneous spike and burst parameters represent stable modes of electrophysiological activity in neural networks that occur irrespective of stimulation.

Aim 3. Determine the response of 3-D neural networks to traumatic injury. Traumatic mechanical loading to central nervous system cells can lead to devastating consequences. Neural cells in the brain have a unique fluidic and osseous protection system, and; therefore, are not normally subjected to large deformations. Supra-threshold physical loading, resulting in acute cell death or sub-lethal cellular and network damage, can lead to traumatic brain injury (TBI), which is a leading cause of death and disability in the United States [23-24]. TBI is unique from any other neurological affliction in that it is induced by a physical event. The long-term outcomes of TBI are dependent on the severity of the primary physical event due to the mechanical insult and are compounded by multi-faceted secondary events due to the deleterious effects of dying cells and the activation of other pathways and systems (see [25-27] for reviews). Collectively, these events may result in significant functional deficits and progressive neural degeneration [28-29]. Currently, there are no effective therapeutic interventions that directly attenuate injury-induced neural pathology. Therefore, attention to the tissue and cellular biomechanics of injury is critically important in refining neural tolerance criteria to injury

and developing mechanistically-driven targeted therapies for this affliction. The immediate physical consequences of loading on the cellular level may range from complete structural failure, such as major somatic disruption and axotomy, to more subtle damage, such as cytoskeletal breakdown, decoupling of sub-cellular structures/organelles, and micro- or nano-tears in the plasmalemma. However, it is challenging to establish these potentially subtle physical effects as a direct consequence of loading, because secondary pathophysiology can induce similar structural damage. In particular, physical disruption of the plasmalemma, termed "mechanoporation", acutely increasing neuronal plasma membrane permeability through nano- and micro-scale tears, may be one of the initial responses and is particularly devastating as it may trigger disruption of normal cell function in a positive feedback manner. The increase in permeability may disturb the ionic homeostasis of cells by allowing atypical flux of ions across the membrane, directly affecting electrical activity [27]. In a positive feedback fashion, these undesirable ionic currents concomitant with an excessive excitatory neurotransmitter release, result in prolonged increases of intracellular Ca^{2+}, initiating many secondary detrimental pathways that may induce short- and long-term changes in neurons including cell death [27, 30-36]. This study focused on the primary, sub-acute, and acute components of injury by limiting analysis to the millisecond-to-seconds-to-minutes periods immediately following injury, and the first 48 hours. We evaluated alterations in plasmalemma permeability as a function of bulk deformation mode (shear versus compression), loading parameters (strain and strain rate), and time post-insult (milliseconds to hour) by inducing complex, three-dimensional shear or compressive strain fields in our 3-D neuronal-astrocytic co-culture model. Studying the acute effects

of injury on neurons and neural networks can help to understand the related pathology and rationally develop clinical therapies for immediate action after traumatic brain injuries.

Study 3. Evaluate acute cell permeability and sub-acute cell viability as functions of strain rate resulting from compression and shear deformations. *It is postulated that there is an important link between the physical parameters of traumatic loading, such as loading strain, strain rate, and modality; and the physiological consequences of neural injury.* Therefore, trauma-specific mechanisms of physical damage should be identified. *Furthermore, it is hypothesized that the level/intensity of injury in 3-D neural co-cultures for both compressive and shear deformations will directly correlate to the strain rates for these two modes of deformation. Moreover, based on the viscoelastic properties of brain tissue, it is postulated that neural cells are more sensitive to shear deformation than compression.* As discussed before, since plasmalemma disruptions leading to increased cellular permeability is one of the primary physiological disturbances of injury we quantified cell membrane disruptions *during and following injury* by analyzing per cell uptake of normally cell-impermeant dyes calcein and ethidium homodimer-1 as a measure of the level/intensity of the injury response. *Furthermore, it is hypothesized that permeabilized cells during injury will directly correlate to subsequently dead cells.* Therefore, cell viability was tested 48 hours after injury.

Conclusion

Collectively, these studies investigated the cytocompatibility of the MEA fabrication material SU-8 2000, correlated the electrophysiological development with the structural development of 3-D neural networks via MEAs and microscopic analysis, and modeled traumatic neural injury with a 3-D neural network *in vitro*. Cytocompatibility protocols for SU-8 2000 potentiate the possibilities for biologically interfacing MEAs and other bioMEMS devices with high aspect ratios made using SU-8 2000. The biologically developed 3-D culture models could serve as test-beds for studying neural network development, drug response, and pathological conditions such as those resulting from traumatic neural injury. These studies propose the development of hybrid-neural-interfaces that could diagnose, improve, or resolve functional deficits in the nervous system that result from damage, disease, and dysfunction.

To inform the readers with the background for this research work and provide context for the motivation relating to existing, relevant studies, Chapter 2 presents a broader review of the literature. The Journal of Biomedical Materials Research published the results of the experiments conducted under Aim 1, which Chapter 3 presents. The work conducted under Aim 2, presented in Chapter 4, reports the development of spontaneous neural network activity in a 3-D neuronal-astrocytic co-culture model. The work conducted under Aim 3 is included in Chapter 5, the study of 3-D neural injury *in vitro*. Chapter 6 holds a broader summary of this body of work, its major conclusions, and its significance. Discussions of the potential applications of these results and their relevance to current and future research are also found in this chapter.

References

1. Heetderks, W. and F. Hambrecht, *Applied neural control in the 1990s.* Proceedings of the IEEE, 1988. **76**(9): p. 1115-1121.
2. Dalbasti, T., et al., *Multielectrode array for simultaneous recording of glucose, oxygen and electrocorticography from cerebral cortex in experimental focal epilepsy.* Biosensors and Bioelectronics, 1998. **13**(7-8): p. 881-888.
3. Marzella, P. and G. Clark, *Growth factors, auditory neurones and cochlear implants: a review.* Acta oto-laryngologica, 1999. **119**(4): p. 407-412.
4. Lauer, R., et al., *Applications of cortical signals to neuroprosthetic control: acritical review.* IEEE Transactions on Rehabilitation Engineering, 2000. **8**(2): p. 205-208.
5. Cukierman, E., et al., *Taking Cell-Matrix Adhesions to the Third Dimension.* Science, 2001. **294**(5547): p. 1708.
6. Schindler, M., et al., *Living in three dimensions: 3D nanostructured environments for cell culture and regenerative medicine.* Cell biochemistry and biophysics, 2006. **45**(2): p. 215-227.
7. Kiryushko, D., V. Berezin, and E. Bock, *Regulators of neurite outgrowth: role of cell adhesion molecules.* Annals of the New York Academy of Sciences, 2004. **1014**(1 Gastroenteropancreatic Neuroendocrine Tumor Disease Molecular and Cell Biological Aspects): p. 140-154.
8. Loers, G. and M. Schachner, *Recognition molecules and neural repair.* Journal of neurochemistry, 2007. **101**(4): p. 865.
9. Venstrom, K. and L. Reichardt, *Extracellular matrix. 2: Role of extracellular matrix molecules and their receptors in the nervous system.* The FASEB Journal, 1993. **7**(11): p. 996-1003.
10. Hoffman, R., *To do tissue culture in two or three dimensions? That is the question.* Stem Cells, 1993. **11**(2).
11. Fawcett, J.W., R.A. Barker, and S.B. Dunnett, *Dopaminergic neuronal survival and the effects of bFGF in explant, three dimensional and monolayer cultures of embryonic rat ventral mesencephalon.* Exp Brain Res, 1995. **106**(2): p. 275-82.
12. Smalley, K.S.M., M. Lioni, and M. Herlyn, *Life Isn't Flat: Taking Cancer Biology to the Next Dimension.* In Vitro Cellular & Developmental Biology - Animal, 2006. **42**(8 & 9): p. 242-247.
13. Schmeichel, K.L. and M.J. Bissell, *Modeling tissue-specific signaling and organ function in three dimensions.* J Cell Sci, 2003. **116**(Pt 12): p. 2377-88.
14. Streit, J., et al., *The generation of rhythmic activity in dissociated cultures of rat spinal cord.* European Journal of Neuroscience, 2001. **14**(2): p. 191-202.
15. Maeda, E., H. Robinson, and A. Kawana, *The mechanisms of generation and propagation of synchronized bursting in developing networks of cortical neurons.* Journal of Neuroscience, 1995. **15**(10): p. 6834-6845.
16. Hämmerle, H., et al., *Extracellular recording in neuronal networks with substrate integrated microelectrode arrays.* Biosensors & Bioelectronics, 1994. **9**(9-10): p. 691.

17. Meister, M., J. Pine, and D. Baylor, *Multi-neuronal signals from the retina: acquisition and analysis.* Journal Of Neuroscience Methods, 1994. **51**(1): p. 95-106.
18. Israel, D., et al., *An array of microelectrodes to stimulate and record from cardiac cells in culture.* American Journal of Physiology- Heart and Circulatory Physiology, 1984. **247**(4): p. 669-674.
19. Irons, H., et al., *Three-dimensional neural constructs: a novel platform for neurophysiological investigation.* Journal of Neural Engineering, 2008. **5**(3): p. 333-341.
20. Cullen, D. and M. LaPlaca, *Neuronal response to high rate shear deformation depends on heterogeneity of the local strain field.* Journal of neurotrauma, 2006. **23**(9): p. 1304-1319.
21. Chang, J.C. and B.C. Wheeler, *Patterning technologies for structuring neuronal networks on MEAs*, in *Advances in Network Electrophysiology Using Multi-Electrode Arrays*, T. M. and B. M., Editors. 2006, Springer Science + Business Media: New York. p. 153-189.
22. Hickman, J. and D.A. Stenger, *Culturing Neural Networks*, in *Enabling Technologies for Cultured Neural Networks*, S. D.A. and M. T.M., Editors. 1994, Academic Press: San Deigo. p. 510-76.
23. Langlois, J., W. Rutland-Brown, and K. Thomas, *Traumatic brain injury in the United States: emergency department visits, hospitalizations, and deaths*. 2004, Centers for Disease Control and Prevention, National Center for Injury Prevention and Control: Atlanta, GA. p. 1–68.
24. Langlois, J.A., W. Rutland-Brown, and M.M. Wald, *The epidemiology and impact of traumatic brain injury: a brief overview*. J Head Trauma Rehabil, 2006. **21**(5): p. 375-8.
25. McIntosh, T.K., et al., *Secondary brain injury: neurochemical and cellular mediators.* Traumatic brain injury, 1999.
26. Saatman, K., et al., *Classification of traumatic brain injury for targeted therapies.* Journal of neurotrauma, 2008. **25**(7): p. 719-738.
27. Raghupathi, R., *Cell death mechanisms following traumatic brain injury.* Brain Pathol, 2004. **14**(2): p. 215-22.
28. Smith, D., et al., *Progressive atrophy and neuron death for one year following brain trauma in the rat.* Journal of neurotrauma, 1997. **14**(10): p. 715-727.
29. Stein, S., et al., *Delayed and progressive brain injury in closed-head trauma: radiological demonstration.* Neurosurgery, 1993. **32**(1): p. 25.
30. Ellis, E., et al., *A new model for rapid stretch-induced injury of cells in culture: characterization of the model using astrocytes.* Journal of neurotrauma, 1995. **12**(3): p. 325-339.
31. Geddes, D. and R. Cargill, *An in vitro model of neural trauma: device characterization and calcium response to mechanical stretch.* Journal of biomechanical engineering, 2001. **123**: p. 247.
32. Geddes, D., R. Cargill, and M. LaPlaca, *Mechanical stretch to neurons results in a strain rate and magnitude-dependent increase in plasma membrane permeability.* Journal of neurotrauma, 2003. **20**(10): p. 1039-1049.

33. Katayama, Y., et al., *Massive increases in extracellular potassium and the indiscriminate release of glutamate following concussive brain injury.* Journal of neurosurgery, 1990. **73**(6): p. 889-900.
34. LaPlaca, M., V. Lee, and L. Thibault, *An in vitro model of traumatic neuronal injury: loading rate-dependent changes in acute cytosolic calcium and lactate dehydrogenase release.* Journal of neurotrauma, 1997. **14**(6): p. 355-368.
35. LaPlaca, M. and L. Thibault, *Dynamic mechanical deformation of neurons triggers an acute calcium response and cell injury involving the N-methyl-D-aspartate glutamate receptor*. Journal of neuroscience research, 1998. **52**(2).
36. Yoshino, A., et al., *Dynamic changes in local cerebral glucose utilization following cerebral conclusion in rats: evidence of a hyper-and subsequent hypometabolic state.* Brain Research, 1991. **561**(1): p. 106.

CHAPTER 2

BACKGROUND

In Vivo vs. *In Vitro* Study of Neural Networks

The continuous nature of electrochemical inputs and outputs across units in the nervous system complicates the understanding of neural network electrophysiological activity *in vivo*, because of the sheer amount of information recorded and the difficulty in isolating its components. In addition, *in vivo* analysis is confounded by, the structural complexity of the organization of neurons and synapses within the nervous system, tissue damage from recording electrode insertion, and only one time-point for post-mortem tissue analysis per animal studied. Furthermore, animal motion during such studies, interferes with the *in vivo* recording of activity. On the other hand, immobilizing or anaesthetizing animals can alter this activity potentially influencing the experimental variables in question [1].

As an alternative to *in vivo* study of neural networks in animal models, one can study neural network behavior in brain slices or dissociated neural cells cultured *in vitro*. Brain slices retain the brain's organization, providing a partial window for understanding the behavior of neural networks, in a piece-meal fashion. However, the health and mechanical integrity of tissue slices deteriorate over longer periods of time as cells die from nutrient deficiency resulting from insufficient diffusion of nutrients, and concomitant tissue degradation, making them preferable for acute studies. The other alternative, dissociated neural cultures, not only lack native tissue architecture but also lack the continuous spatiotemporal sensory inputs present *in vivo*. Therefore, great

caution needs to be exercised while applying the results obtained from *in vitro* studies with non-human models to understanding the *in vivo* state [2], especially with human systems with comparatively different cortical neuronal properties [3-4].

Although, *in vitro* dissociated culture networks, self-organized from randomized cell suspensions, hardly develop any "signature," *in vivo* micro-circuitry designed through coordinated development and afferent and efferent connections [5], these networks do share distinct qualities with the tissue from which the original cell type was obtained [6], implying partial behavioral similarity between dissociated networks in culture and the tissue of origin. Furthermore, isolated dissociated neural cultures provide good long-term viability, accessibility, and visibility. These characteristics make the dissociated neural network models viable alternative environments for detailed electrophysiological, pharmacological and genetic manipulations at the molecular, cellular, and network levels of neural networks over long periods of time. One can study the mechanisms of how neurons connect with each other to form a network in such models. On the other hand, *in vivo* environments do not allow such level of control over experimental parameters such as customizable network sizes for experimentation and observation. Furthermore, in dissociated neural cultures the changes in electrophysiological activity can be directly tracked to changes in the neuronal states within the culture, and no unknown external factors. In contrast, in *in vivo* studies, it is difficult to distinguish between intrinsic changes in the neuronal states, and those induced by the communication between the different regions of the nervous system that may be influenced by disparate parameters such as conventional inputs and outputs between the peripheral and central nervous systems.

2-D vs. 3-D Dissociated Neural Networks

Traditionally, *in vitro* dissociated neural culture models have comprised of dissociated cells plated on a two-dimensional (2-D) substrate. 2-D dissociated neural networks *in vitro*, while lacking the brain's three-dimensional architecture, still maintain some similarities in their synaptic mechanisms, inherent cellular electrophysiological characteristics, morphological properties, and pharmacological electrophysiological response to those *in vivo* [7-11].

However, 2-D models restrict spatial interaction. Likewise, the 2-D cell-plating process pre-defines the cell arrangement, fixing a generally random set of synaptic contacts for each *in vitro* cell. In contrast, *in vivo*, the 3-D arrangement allows cells to group themselves synaptically in a manner which is neither fixed nor random. As such, traditional planar 2-D culture models possess atypical cell-cell/cell-matrix interactions and cellular morphology [12]. Moreover, cells in 2-D cultures differ from *in vivo* according to density, proliferation rates [13-14], migration [15], gene expression [16-17], differentiation [14, 18], cellular signaling [19], and pathological susceptibility [13, 20-21].

Three-dimensional (3-D) *in vitro* models, in which cells grow within a scaffold, may more accurately represent the *in vivo* environment than traditional 2-D culture models, while maintaining many of the benefits of *in vitro* culture models. For example, 3-D culture models better mimic the cytoarchitecture of *in situ* tissue than cells grown on non-physiological, hard surfaces, as in most 2-D culture models. 2-D surfaces limit cell growth area, whereas 3-D cultures, through an added dimension, are expected to

magnifies growth and migration, lending support to other cell behaviors, such as differentiation or maturation. The 3-D scaffold, designed for physiological structural stability, may protect cells from environmental disturbances, such as media changes, whereas cells in 2-D cultures are more exposed. Scaffolds can also be designed for optimal permeability for nutrient and waste diffusion.

Fundamentally, 3-D configurations are more conducive to the interactions of cells with the matrix, soluble factors, and each other, whereas planar cultures constrain these interactions [12, 22-23]; [24]. Moreover, in 2-D culture, the hard, planar surface flattens out the cells. In contrast, cells stay more spherical when embedded in a 3-D scaffold, potentially facilitating outgrowth in all directions for neurons and other process-extending cells.

It has been shown that dopaminergic neurons, harvested from embryonic brain, live longer in 3-D than in 2-D cultures [25]. Neurites grow longer, cells survive more, and differentiation occurs in different patterns, relative to 2-D monolayer cultures [26-30]. For embryonic mesencephalon tissue, for instance, more cell death occurred dissociated in monolayers, while 3-D collagen-gel cultures survived to a much greater extent [31]. The same observations were made for hippocampal neurons grown on 3-D aragonite matrices, resulting in higher density networks [32]. In mechanical injury, 3-D cultures sustained more cell death than 2-D cultures subjected to the same strain magnitude and strain rate [33]. Thus, 3-D culture sustains a more *in vivo*-like environment than 2-D.

3-D cultures can be formed through various preparations: spherically forming re-aggregate cultures; rotary bioreactor cultures with cell aggregates, otherwise known as

microcarriers; cell cultures in polymeric hydrogel scaffolds; and organotypic slice cultures. Organotypic cultures are slices of tissue which maintain the *in situ* architecture, and thus, preserve networks in the cut plane. The other cultures utilize dissociated cells, which reorganize according to cell type, media conditions, substrate adhesiveness, or cell-cell interaction. Rotation-induced reassociation can form reaggregate cultures [28, 34]. With regards to semi-3-D cultures, neurons have been plated on top of hydrated collagen matrices [35-37], recapitulating aspects of 3-D morphology; however, cell-cell and cell-matrix interactions are spatially limited. Cells that are grown within a 3-D scaffold or matrix produce perhaps the most controllable 3-D culture models, since cell type(s) can be chosen, and the extracellular composition controlled [31, 38-40].

3-D scaffolds allow tissue-like, multi-dimensional cell-cell/cell-matrix contacts. 3-D cultures allow construction of a defined system with respect to cell type, cell ratios, and orientation (whether random for a more uniform response, or patterned in some way, allowing for designed culture architecture). Transgenic animal cells also be introduced, allowing identification of a cell subpopulation or study of a specific mechanistic pathway. Extracellular proteins and biomarkers can be added to bind to or enter cells, respectively. Moreover, these cultures easily accept synthetic components, like electrodes or artificial micro-vessels, since one can "cast" these cultures around micro-machined devices.

3-D cultures may be developed to mimic *in vivo* cellular densities. The human cortex has approximately 10^5 neurons/mm^3, transmitting thousands of synapses locally and over long distances. Interneurons largely compose the central nervous system with 1000s of synapses to other neurons. Some of these neurons, as well as the projection

neurons, synapse with distant neurons. Given this composition, several methods for manipulating cell density to resemble the brain have been explored: layered 3-D neuronal networks using silica beads allowed elaborate networks to form, manipulating the density with bead size [41]; a convective microperfusion chamber permitted the survival of high density cultures [42]. These developments allow 3-D neural cultures systems to continue to mimic the *in vivo* state even more closely.

As mentioned previously, the benefits of studying dissociated neural cultures *in vitro* come at the loss of the native-tissue structural integrity, organizational architecture, and network connections; and with affected electrophysiological resting potentials, firing patterns, and other network functional aspects [5]. Despite such differences, *in vitro* still maintains comparative advantages over *in vivo*, and 3-D *in vitro* dissociated neural culture systems likely upgrade those advantages.

Criteria for Choice of 3-D Cell Culture Scaffold

Several criteria should be met while choosing a scaffold for 3-D dissociated cultures, including cell type and surface adhesion receptors; and scaffold stability and cytocompatibility [43]. Such consideration is vital, because scaffolds may affect gene expression and other functions [44]. Scaffolds for 3-D cultures must have a porous structure allowing for cell adherence, process-extension (neurons) and cell migration (microglia), while also allowing for adequate media diffusion/perfusion. The scaffold should preferably have a defined composition. Ideally, the scaffold should have adjustable mechanical properties, for example by adjusting the scaffold component concentration because properties of neural tissue vary. In order to realistically re-create

ECM, specific ECM proteins (e.g., hyaluronic acid, HSPGs, collagens, etc) should compose the scaffold in physiological quantities. Since the ECM of the brain contains little collagen / fibrillar components, collagen I scaffolds to mimic neural tissue is questionable. However, given the gelation and mechanical properties of collagen I, it serves as a useful structural component (natural or denatured) in combination with Matrigel™ [45] or other proteins or peptides. The scaffold selection should also consider cell adhesion surface receptors as ECM receptor interactions influence neuronal survival, process outgrowth, and signalling.

Considering synthetic over natural components for a 3-D culture scaffold opens the possibility of developing bioartificial or combination scaffolds. *N*-(2-hydroxypropyl) methacrylamide polymer HPMA + collagen I hydrogels, for example, also have potential as a 3-D neural scaffold [40]. Other synthetic scaffold materials include poly(ethylene oxide) (PEO), poly(glycolic acid) (PGA), poly(L-lactic acid) (PLLA), polycaprolactone, polyester urethane, methylcellulose, poly(acrylonitrile) (PAN), poly(acrylonitrile), poly(vinyl chloride) (PAN/PVC), and polysulfone (PS). The cytocompatibility of the material and the breakdown products should be carefully assessed (see [46-47] for more on cytocompatiblity assays). Biological scaffolds include Matrigel™, as well as chitosan [48], collagens, fibronectin, laminin, fibrin, hyaluronic acid derivatives, and decellularized tissue [43]. We chose Matrigel™, for our studies, because of its biological origin, rich ECM molecular composition, gelation characteristics at physiological temperatures, and high porosity.

The *porosity* is critical to cell performance within a 3-D culture. The scaffold should be permeable to low molecular weight molecules, gases and nutrients, and avoid

waste buildup or trapping. Sufficient pore volume should exist to permit cell-cell interactions, migration, and neurite extension. In addition, the surface area should maximize cell attachment and spreading. Scaffolds should balance ligand density with stiffness and pore-size, a relationship that may vary for different materials. For example, a decrease in pore size was observed in agarose gels when coupled to laminin peptides [49].

The scaffold's *stiffness* relates to its *pore size*. Distance between cross-links, a degree of stiffness, in the polymer chains will correlate with the pore size of the hydrogel. For example, in agarose gels, the average pore size decreased exponentially as the concentration (i.e. the stiffness) increased [50]. The elastic modulus of poly(2-hydroxyethyl methacrylate (pHEMA) hydrogels was not, however, affected by increased porosity until pores became interconnected [51]. This *tortuosity*, or path windiness among the pores will also play an important role in cell behavior, as neurites extend and synapses form. The *charge* of the gel will also affect the porosity and the cell function. For example, positive charge was shown to facilitate neurite outgrowth, while negative charge inhibits outgrowth [50].

There are many methods for measuring porosity and other scaffold properties. The permeability coefficient can be used to estimate pore size. A slice of the gel with known thickness is placed in a water column and subject to a known hydraulic pressure [26]. The water collection over unit time determines porosity. Scanning or transmission electron microscopy may also measure porosity, but the preparation procedure may affect pore size, introducing an artifact into the system. Therefore, electron microscopy under physiological conditions or in combination with other methods may offer a better

alternative to minimize artifacts introduced by sample preparation procedures. In addition, hydrogels may swell while under culture conditions because of fluid uptake. Therefore, characterization of any hydrogel should include measurement of fluid uptake and formulation adjustment, as this may affect *osmolarity* of the extracellular fluid. In addition, the *stability* of a scaffold is vital to consistent culture conditions, whether for short term cultures or cultures designed to support cells for weeks or months. Scaffolds can be affected by enzymatic degradation or mere culture erosion over time. This can be used as an advantage, however, as neurite outgrowth of photoencapsulated cells within polyethylene glycol has been shown to be controllable by varying the degradation rate [52].

The method for gelation is important in choosing scaffolds for 3-D culture, especially for those cultures in which cells are entrapped or "cast" at the same time as scaffold gelation. Many different methods are possible, perhaps with temperature phase transition based methods being the most common. Extreme heat or cold; however, should be avoided, as proteolytic processes and immediate early genes may be activated, and this transient insult may affect cell behavior. Other gelation methods apply, changes in pH transition, ionic strength, or photo crosslinking, and may be considered based on applicability for particular applications. Gelation methods should be chosen with caution because of potential toxicity from unpolymerized monomers, change in osmotic pressure during polymerization, heat production, or free radical production.

Matrigel™ – A 3-D Extracellular Matrix Containing Hydrogel Scaffold

An appropriate microenvironment for 3-D culture maintains relevant physiological conditions for long-term experiments. Besides adequately diffusing nutrients and wastes, the environment for neural cell cultures must also support cell attachment, neurite outgrowth and functional synapse formation. Previously described 3-D neural culture models incorporate scaffolds of collagen [53], agarose [54-55] and fibrin [14] in an attempt to meet these concerns with varying levels of success. One successful model contains a hydrogel scaffold comprised of bioactive extracellular matrix (ECM) components closely mimicking the *in vivo* environment. Matrigel™ matrix, a reconstituted basement membrane derived from the Engelbreth-Holm-Swarm mouse sarcoma, includes constituents found in the developing or mature brain such as laminin, hyaluronan, and proteoglycans, and facilitates 3-D neural network development through ECM-related [56] and other cytokine-mediated [57-58] interactions. Matrigel™ has also been shown to promote neurite outgrowth [59-60].

ECM molecules play an influential role in the morphological and electrophysiological function of neural networks by inducing intracellular signaling through secondary-messenger pathways [61-63]. ECM molecules *in vivo* can both induce axonal growth through interaction with neurotrophins and nerve growth factors [64-65] or inhibit neurite outgrowth [66-67]. In addition, "nonspecific" adhesive interactions of neurons with Matrigel™ components may also influence network formation via transmembrane signal transduction. Given the pertinent ECM characteristics, the molecular structure and composition of Matrigel™ provides an excellent alternative to an *in vivo* environment.

SU-8/SU-8 2000 Cytocompatibility

In recording the electrophysiological activities of our 3-D dissociated neural cultures a MEMS based device, 3-D multi-electrode array, was used. One material that is used in the manufacturing of these high-aspect ratio MEMS structures is SU-8, a negative, near-UV photoresist. Both as a structural material, as well as an insulation material for MEMS based devices, SU-8 has great potential for many biological applications [68-70]. Two types of SU-8, the original formulation using gamma-butyrolactone as the solvent [68-69], and the more recent SU-8 formulations using cyclopentenone as a solvent (SU-8 2000) exist [70]. Exposed SU-8/SU-8 2000 photoresists are thermally and chemically stable due to their aromatic functionality and highly cross-linked matrix [69-72].This stability makes them ideal for the fabrication of high-aspect ratio MEMS based systems such as 3-D microelectrode culture systems.

Long-term cytocompatibility is needed in 3-D microelectrode systems with SU-8 or SU-8 2000 as a fabrication material [73-74]. Many current systems do not incorporate an appreciable amount of SU-8 within their devices, limiting its potential use. For example, Ayanda Biosystem's MEAs contain only a 5μm insulation layer [75-80]. SU-8-based devices have been used for both dissociated cultures, as well as slice cultures. For example, in a microfluidic device made partially out of SU-8, chick embryonic motoneurons were viable for up to 48 hours [73]. In another study, electrophysiological activity was detected in neuronal cultures for 45-60 days within SU-8 containing MEAs, but no quantitative viability assessment was performed [81]. Neuroblastoma cells cultured on thick SU-8 2000 structures showed poor cell adhesion [82]. Several other

studies have used 5μm insulation layer SU-8-containing structures to monitor electrophysiological activity in slice preparations, but again, viability as a function of materials in the devices was not evaluated [75-78, 80].

Toxicity of thick SU-8 2000 coatings with neuronal cell types has not been extensively studied, however non-neuronal biocompatibility of cured SU-8 has been investigated. For example, Voskerician, et al., 2003 implanted SU-8 within stainless steel cages subcutaneously in rodents to evaluate the material's biological interaction. However, these samples manifested an insignificant response relative to the control [74]. On the other hand, Weisenberg et al. found SU-8 to be thrombogenic [83]. SU-8 exhibited cytotoxicity in cultured mouse fibroblasts, yet minimal negative responses were are found in rabbit muscle [72]. Others have also observed that untreated SU-8 is incompatible with mammalian cells, yet following HNO_3 and ethanolamine treatments, HeLa cells (an immortal cell line) maintained viability up to 4 days *in* vitro on hydrophilized SU-8 surfaces [84]. Therefore, the cytocompatibility of SU-8 / SU-8 2000 has not yet been established, likely due to differential cell responses, culture environments, fabrication modes, material processing, and/or exposure to surface area.

Furthermore, the previous biocompatibility studies of SU-8 have focused on the original SU-8 formulation. However, the biocompatibility of the SU-8 2000 series [70] (MicroChem Corporation, Newton, MA) warrants investigation since it offers several processing advantages over the original SU-8 formulation, including improved wetting, faster drying, and clean edge bead removal without the need for an intermediate bake step. Improvements in the biocompatibility of SU-8 2000 would not only improve cell

viability, but potentially also the overall quality of data obtained using MEAs that use SU-8 2000 as a key fabrication material.

Multi-Electrode Arrays (MEAs)

If we successfully imitate the *in vivo* neural environment with a cytocompatible *in vitro* environment, then we can obtain relevant electrophysiological data with multi-electrode arrays (MEAs). MEAs consist of an array of 2-D or 3-D microfabricated voltage probes to electrically interface with neuronal somata and processes. This array forms an extracellular interface to stimulate and record potential changes across a neuronal network simultaneously. MEA electrodes typically appose with cells within 10-100 nm, which helps high signal to noise ratio recording, providing a clear spatiotemporal "picture" of the neural network activity [85]. An MEA acquired "picture" depends on the electrical properties of the cellular signal sources, cell/tissue-electrode contact, the microelectrodes, the insulated substrate, and external hardware connected to the electrodes [86].

MEAs have evolved over the years to increase utility for several neurological applications. While *in vitro* MEAs were developed by Thomas et al. [87], Gross [88], and Pine [89], *in vivo* 3-D multi-electrode probes were developed by the Michigan Probes [90] and Utah Array [91] groups. Commercial *in vitro* 2-D MEA devices are available from Multichannel Systems (www.multichannelsystems.com), Ayanda Biosystems (www.ayanda-biosys.com), and Panasonic MED (www.med64.com). 3-D *in vitro* MEAs, in which electrodes extend approximately 50 μm from the surface in a cone shape, have also become available [77]. The 3-D MEAs overcome many of the

limitations of 2-D MEAs. For example, 3-D electrodes penetrate tissue slices, avoiding the outer layer of dead and injured cells, and permit better cell contact [92]. According to [93], if a 3-D MEA electrode intercepts a high-density neuronal dendritic tree, it can record the sum of very small field potentials originating from the dendritic tree, traditionally undetectable by the patch clamp method. Furthermore, 3-D cone-shaped electrodes possess nearly twice the surface area of comparable planer electrodes. This increased surface area reduces electrode impedances by 50% and doubles the recorded signal amplitudes, thereby increasing the signal-to-noise ratio [77].

Since its development, MEA technology has been used to study neural network electrophysiological activity in dissociated spinal cord [79], cortical [94], hippocampal, acute retina [95-96], and cardiac myocyte cultures [97]. These studies have led to valuable insights into network correlation in learning and memory, visual perception [98-99], spontaneous activity emergence and dynamics [100-106], and neural regeneration [107].

MEA technology not only enables new studies and insights, it also presents a comparatively favorable network alternative to single cell screening or whole animal behavioral testing for drug analyses. For example, MEAs do not contaminate or destroy neural circuitry nor obscure microscopic access to tissue like the patch-clamp and intracellular micro-electrodes [108]. MEAs also allow for multi-site recording, a chemically controlled sterile environment with no need for toxic potential-sensitive dyes [109]. MEAs allow continuous non-terminal *ex vivo* assaying of network activity at relatively high spatio-temporal resolutions without the *in vivo* confounds of anesthesia and uncontrolled sensory input [8-9, 85, 100, 102, 104, 110-113]. These functions make

MEAs a high-throughput tool with relatively reduced cost and labor when compared to *in vivo* and other *in vitro* techniques [114-115].

However, MEA electrodes are limited by their small microelectrode surface areas. Small surface areas raise selectivity, but also relatively increase impedance resulting in thermal electrode noise [92]. Furthermore, the extracellular MEA electrodes results in smaller-than-actual amplitudes of recorded electrophysiological activity, since the electrodes never penetrate the cellular signal source. Additionally, the spatial resolution confines of the current sixty electrode MEA design (as compared to a higher electrode per unit area design), rarely achieve single-cell resolution of detected activity [77].

Despite these limitations, our study used 3-D *in vitro* MEAs due to its potential advantages in recording in 3-D environments. These potential advantages include increased sensitivity of recordings, reduced impedance, decreased damage to neurons, exclusion of *in vivo* interferences, better control of the cellular environment, relative cost effectiveness, and a relatively simplistic set-up. However, to optimize the application of 3-D MEAs to neural cultures, neurons must adhere to the MEA surface.

Neural Adhesion to MEAs Through Surface Treatments

To achieve MEA recordings, neurons must adhere to MEA electrodes. However, MEAs are covered with a hydrophobic insulation that resists aqueous wetting and macromolecular adsorption, two key factors in neuronal adhesion [116-117]. Without adhesion, physical gaps form between the active neurons and the MEA electrodes. These gaps allow current to dissipate and weaken MEA recordings. Hydrophilizing the MEA

surface and physisorbing specific cell-adhesive peptides and proteins can increase MEA cell adhesiveness and thereby improve MEA recordings.

Physisorption utilizes van der Waals or electrostatic forces to hold proteins to the MEA surface [116, 118-119]. Physisorption of poly-lysine, a polypeptide with pendant e-amine groups, forms an approximately 15Å thick, positively charged, hydrophilic monolayer of randomly coiled molecules under media pH conditions, creating an adhesive polar linkage between the MEA surface, and neurons [120]. Poly-D-lysine is an excellent candidate for ensuring long-term adhesions because mammalian neural proteases cannot enzymatically degrade it. Processes to promote poly-D-lysine adherence includes cleaning and activating MEA surfaces with sonication, UV exposure, and the use of gaseous plasma functionalization [116]. Functionalization with the gaseous plasma technique has been shown to increase poly-lysine adhesion by adding oxygen-rich, hydrophilic, adhesive chemical functional groups to the surface [121].

ECM proteins (present in Matrigel^{TM}) may also improve long-term adhesion of the 3-D culture to the MEA [122]. One of these proteins, laminin, enhances culture adhesion. While some coatings on MEA electrodes sacrifice signal quality for adhesion [116], coatings of poly-D-lysine, laminin, and the 3-D Matrigel^{TM}-based cell culture did not significantly increase electrode impedance in our studies. Lastly, to prevent the 3-D culture from detaching due to reduction in adhesion over time, an immobilizing Nylon grid-based construct was placed on top of the 3-D culture in our studies.

The addition of oxygen rich functional groups, poly-D-lysine, and laminin renders the MEA surface more hydrophilic, protein adhesive, and cell adhesive. The Nylon grid-based construct further immobilized the 3-D cultures. After these modifications, 3-D

cultures exhibited increased long-term culture adhesion to the MEA surface without detracting from recording signal quality.

The Recording of Neural Network Electrophysiological Activity Using MEAs

In neural networks, electrophysiological activity spreads from cell to cell via synaptic connections. Ionic currents flow along the cell bodies between intracellular and extracellular fluid. The distribution of ionic current corresponds to varying extracellular voltage gradients spatially and temporally [86]. With respect to a grounded reference electrode, MEA electrodes record extracellular voltage fluctuations from parts of single cells, such as dendrites, axon hillocks, or soma, generally within a 30 µm radius [86]. MEAs record both slow field potential and fast action potential signals. Fast action potentials are temperature-sensitive below 30ºC and decrease to a small value at room temperature [86, 123]; therefore, the experiments presented in this thesis were all conducted at 37 ºC.

The underlying physics of the recording of an action potential involves current flowing into the axon hillock, representing a current point sink, which activates a neuron action potential [124-125]. In recording these potentials, detected voltage decreases as the distance from the current point sink to the electrode increases, according to the equation $V = I\rho/4\pi r$. In this equation, r is the distance between the current point sink and electrode; ρ is the resistivity of the culture medium; I is the current during a neuronal action potential; and V is the detected concomitant voltage [123]. Given the extracellular nature of MEA recordings, r is generally large, and given these recordings take place in

cell culture media which has low resistivity ρ; voltages V recorded via MEAs have low signal magnitudes.

Given that the signals of MEA recordings are small in magnitude, the signal-to-noise ratio must be sufficiently large for useful data acquisition [115]. Impedances of across-the-electrode and electrode-to-earth paths determine the signal-to-noise ratio. These impedances also determine the recorded signal shape and magnitude [126]. Ideally, when a neuronal soma is closely apposed on an electrode, the capacitive coupling produces a replica of the shape of the intracellular action potential. However, a gap of approximately 100 nm generally exists between tissue and electrodes, resulting in sub-optimal cell-to-electrode sealing causing the MEA electrodes to record a negative voltage profile with respect to time [89, 93]. As the gap between the cell and the electrode increases, the signal-to-noise ratio decreases.

Using MEAs to record electrophysiological activity presents two additional challenges. First, current MEA designs are not adapted for the detection and measurement of sub-threshold synaptic potentials [123]. Second, high-density cultures with many neuronal processes or somas over the electrodes limit physical isolation of the MEA electrode interactions to specific neurons [123]. However, the multi-cellular components of an MEA recorded signal can be mathematically resolved into the individual component voltage shapes from each neuron with respect to time [127].

MEAs successfully capture an accurate representation of the general trend of electrophysiological activities within a culture while simultaneously recording small magnitude signals from numerous electrodes at varied distances. Thus, MEAs enable tracking of the electrophysiological activity changes in a 3-D culture model.

The Development of Electrophysiological Activity in Dissociated Neural Networks

The mechanical and enzymatic dissociation of neurons from rat embryo cortices causes the loss of many of the original cellular processes and synaptic connections. However, dissociated cortical neurons form neurite-driven interconnections within a few hours of plating [5, 94]. The development of spontaneous synchronous activity accompanies the extensive neurite outgrowth and, thus, the development of synaptic contacts in dissociated neural cultures [5, 9, 113, 128-131]. Within approximately 3 days *in vitro* (DIV), the cortical neurons spontaneously establish an electrophysiologically active network [128-129]. Within this period, individual neurons emit rare and irregular spikes or bursts of action potentials, indicating the possibility of immature synapse formation [129, 132-133]. Early activity has been shown to be responsive to currents generated via NMDA, AMPA, $GABA_a$, and fast-sodium ionotropic receptors, although no signals actually propagate, indicating early receptor expression, but incomplete/immature synapse formation [129]. At approximately 4 DIV, synapses tend to grow stronger as neuronal cultures begin to exhibit signal propagation. Between 5 to 16 DIV, the cultures continue to exhibit a more organized firing pattern. Regular sequences of synchronized bursts, or population bursts, occur almost simultaneously across all the MEA electrodes, in addition to isolated spikes [5, 94]. As the cultures age cross-network population bursts propagate more quickly [129]. The quick burst propagation indicates an overshoot phase of *in vitro* network structural development, in which synaptic connection strength and number of neurites both increase [128, 130, 132]. After approximately 30 DIV, the networks exhibit elaborate temporal patterns of

synchronized population bursts [9, 94, 129]. This maturation phase relates to activity-dependent processes [134] and homeostatic plasticity [135]. This stage is also indicative of a decline in the number of synapses or modulation of synaptic efficacy. Thus, from the initial build-up of electrophysiological activity, neuronal cells communicate and synchronize their firing of spikes and bursts to obtain a cooperative pattern of population bursts. This development of neural network activity depends on the types of neurons and the cell density when plated [113].

Synaptogenesis in Neural Networks

Synaptogenesis, the formation of synapses, occurs throughout an organism's entire lifespan and depends on many factors [136-138]. Importantly, the rate of synaptogenesis depends on cellular density in culture. Higher density cultures not only exhibit a higher rate of synaptogenesis, but also a greater number of synapses than lower density cultures. These high-density cultures exhibit GABA and glutamate release, an indicator of synaptogenesis, at 3-4 DIV, much earlier than lower density cultures [139]. Likewise, neuronal cultures have been shown to exhibit higher levels of bursting of action potentials when plated at a higher density of 2500 cells/mm^2 rather than when plated at a lower density of 600 cells/mm^2 as measured by MEAs [113]. Furthermore, higher density cultures exhibited population-based bursting at an earlier day *in vitro* (DIV), suggesting that plating density may also influence the rate of neuronal maturation [113].

Neuron-to-neuron distances and other factors also influence synaptogenesis. *In vitro*, how far neurites must travel to reach a synaptic target significantly affects the rate

of synapse formation [139]. Inter-neuronal distances are shorter in denser cultures, which increases the number of nearby potential synaptic contacts, enhancing neurite outgrowth and extension, in turn increasing the rate of synaptogenesis [139]. In addition to neuronal density, astroglial presence, neurotrophin concentrations, and soma size also influence synapse formation [139-142].

Pruning (purposeful loss of neurons and neurites) shows a mutualistic relationship between synaptic transmission and neuronal death. Although the connection is unclear, synaptic activity directly correlates with cell death rate: increased synaptic activity shows an increase in the rate of neuronal death; conversely, suppressed synaptic transmission shows a reduction in neuronal death [143]. Synaptic plasticity leading to an increase in the number of synapses per neuron as well as the synaptic weights, tends to have a compensatory effect to this seeming loss of structure and function associated with the process of pruning [141]. For example, in the maturation of neonate mouse somatosensory cortex (layers II/III), a 35% reduction in neuronal density accompanies a five-fold increase in synaptic density. Whereas, initially immature brains are very dense in neurons but with less than 250 synapses per neuron, after maturation, the brains are less dense but with close to 5000 synapses per neuron, resulting in approximately a 20-fold increase in the ratio between synapses and neurons [142]. Therefore, the processes of synaptogenesis, synaptic plasticity, and pruning play an influential role in the process of development and aging.

Chemical Modulation of the Electrophysiological Activity of Dissociated Neural Networks

Chemical modulation can allow deeper understanding of the basis of neural electrophysiological activity. Chemical modulation of electrophysiological activity *in vitro* consists of bath application of a chemical to a dissociated neural culture such that all neuronal receptors are exposed to a similar concentration of the chemical. Often times, chemicals used in such type of experiments are drugs and neurotransmitters. In contrast to bath application of neurotransmitters *in vitro*, *in vivo* concentrations of neurotransmitters vary from region to region within the neural network and localize primarily in the synaptic clefts. Likewise, the local concentration distribution of drugs will differ *in vivo* from *in vitro*; the latter will maintain a homogeneous concentration, while the former will experience higher chemical modulation in specific tissue regions. Thus, electrophysiological responses between *in vitro* and *in vivo* may differ, especially in the strength/amplitude of the response. Nevertheless, *in vitro* drug-testing provides a simple means to test the cellular and network level response to drug application, while *in vivo* testing provides a more realistic model of the physiological response. Together, such testing can help elucidate a drug's physiological mechanism of action.

Neurotransmitters used in the modulation of electrophysiological activity may be broadly classified as excitatory and inhibitory, although depending on the receptors certain neurotransmitter behavior may switch. Excitatory neurotransmitters includes glutamate and aspartate, amino acids that increase spike rates via stimulation at the synapses and, at high concentrations (~10 μM), disrupt native network interactions, resulting in irregular high-frequency spiking [111]. N-methyl-D-aspartic acid (NMDA),

an exogenous glutamate analog, potentiates synaptic excitation and increases burst amplitude and burst rate [144]. At high concentrations (>30 μM), NMDA may lead to fused bursting and high-frequency spiking, followed by excitotoxicity [144-145]. Norepinephrine and acetylcholine are primarily excitatory neuromodulators that enhance existing activity patterns (although these can be inhibitory as well, depending on the receptor).

Other neurotransmitterss are inhibitory. GABA and glycine are neurotransmitters which reduce spike and burst rates when applied in culture medium, via enhanced synaptic inhibition at 30 μM and approximately 60-100 μM respectively [144]. GABA only affects burst initiation, not synchronization [144]. Excitatory channel blockers of synaptic transmission, such as D-2-amino-5-phosphonovalerate (50μM, D-APV) and 6-cyano-7-nitroquinoxaline-2,3-dione (10μM, CNQX) suppress network electrophysiological activity by competitively antagonizing excitatory glutamatergic receptors, such as N-methyl-D-aspartic acid receptors (NMDA-R) and alpha-amino-3-hydroxy-5-methyl-4-isoxazolepropionic acid receptors (AMPA-R) [8, 93, 146].

Changing the extracellular concentration of certain ions, such as calcium, magnesium, potassium, and blocking intrinsic neuronal spiking mechanisms can also modulate network electrophysiological activity. Bursting on a cellular level is dependent on calcium entry and slow calcium-gated conductance changes. Lowering the extracellular calcium ion concentration eventually abolishes population bursting, even after initial sporadic bursting [100]. Magnesium ions not only partially block calcium entry into neurons, but also block the ionotropic component of NMDA-R receptors and suppress network electrophysiological activity. Therefore, lowering the extracellular

magnesium ion concentration in mature cultures indirectly activates NMDA-receptors, increasing population bursting [147]. Potassium ion concentration also changes cellular dynamics: an increase in extracellular potassium ion concentration results in an increase in burst rates via depolarization [148-149]. Network activity modulation can also occur by blocking intrinsic neuronal spiking mechanisms. For example, a 1 μM solution of tetrodotoxin can halt spontaneous electrophysiological activity by blocking sodium channels [5, 93, 129, 149].

Studying excitatory and inhibitory chemical modulation, in *in vitro* cultures can help characterize the cultures and their activity, and can potentially allow high-throughput pharmaceutical experimentation in a more controlled manner. It is easier *in vitro* to analyze single physiological aspects at longer periods, as opposed to animal behavior *in vivo* models or *in vitro* brain slices. Besides chemical changes, these cultures can also model mechanical changes, such as applied stress and strain, and so can be useful in the study of traumatic neural injuries.

Traumatic Neural Injury

Physical suprathreshold insults can cause traumatic neuronal injury. In conjunction with secondary events, these primary insults can cause persistent neuronal dysfunction and death both acutely (during the first few hours following injury) and chronically (a prolonged phase of neurodegeneration that can last up to one year post-injury) [150].

Knowing the injury tolerance of cells can help design therapeutic treatments for traumatic neuronal injury [151]. Injury tolerance cannot be accurately defined by cell

death because cells can experience significant functional deficits without death [152-153]. In fact, functional changes can occur prior to any morphological damage; for example, a model of optic nerve stretch shows electrophysiological changes at a lower stretch level than morphological changes [154]. Furthermore, effects of the primary injury (mechanical event that lasts milliseconds only) are difficult to isolate from those of secondary events (that occur later) that can exacerbate cellular dysfunction. For example, neighboring cells of injured ones become more at risk to damage from secondary events than those further apart, defining an injury penumbra [155]. For these reasons, a single threshold for cellular dysfunction is challenging to define.

Since all cells are not affected in the same way, injury thresholds are likely non-linear [151]. Differences in mechanical properties, cell type and morphology, cellular states (e.g., metabolic, receptor expression), and tissue architecture (i.e. cell orientation, cell-cell and cell-matrix interactions) all play a part in differential injury responses [33, 156]. Likewise, neurons are differentially susceptible to different modes and types of physical loading. For example, injury-related calcium influx and membrane permeability increases indicate that neurons are more susceptible to biaxial stretch than uniaxial stretch, possibly due to the distribution of local strains [157]. Similarly, differences exist between cortical impact and impact acceleration models (open vs. closed head injuries) in local stress and strain distributions, leading to permeability differences between cell populations [158-165]. Further work should correlate local cellular level stresses and strains with bulk tissue-level mechanical insults.

In vitro models are relevant for the study of acute events following trauma because in *in vitro* models this window lasting only a few seconds is more accessible for

study than *in vivo* [166]. However, *in vitro* models lack many secondary interactions provided from systemic complexity, over time losing their relevance with *in vivo* models. By administering uniform loading to isolated neural components *in vitro*, cellular response and dysfunction thresholds to different mechanical loading parameters such as strains and strain rates can be measured [167]. While it is still unknown what strains and stresses are delivered on a cell-by-cell basis, as anticipated from the viscoelastic nature of biological tissue, *in vitro* models have demonstrated that injury responses depend on the magnitude and the rate of loading [30, 168-170].

One of the consequences of traumatic loading to cells, is the disruption of the plasma membrane. The plasma membrane is the selective barrier and boundary of the cell, playing crucial roles in both neuronal structure and function. Transient or chronic disruption causes neuronal dysfunction and possibly death. Used in many models of traumatic neural injury, uptake of a cell-impermeant dye added to culture media or cerebrospinal fluid serves as a permeability marker for membrane disruptions [157, 169, 171-173]. Use of variously sized permeability markers can help measure the approximate size of non-specific pores or tears from disruption [171, 173-175]. The size of tears and the resealing time increase with increasing strain and strain rate [169].

Disruption of the plasma membrane allows ions such as Ca^{2+} to diffuse down their concentration gradients, disrupting ionic homeostasis, action potential firing, and synaptic function [175-178]. Ca^{2+} influx after CNS injury has been correlated with many damaging downstream events: excitotoxicity caused by the release of excitatory amino acid neurotransmitters such as glutamate; axonal conduction impairment; necrosis caused by proteolytic calpain activation which leads to cytoskeletal breakdown; apoptosis caused

by endonuclease activation and mitochondrial damage [179-183]; [151]. Whereas, few studies have evaluated aspects of electrophysiological changes in individual cells *in vitro* following mild/moderate traumatic injury [177-178]; even fewer have investigated the overall changes in endogenous network activity following insult [30].

Thus, the primary insult invariably leads to secondary events including efflux of intracellular components such as lactate dehydrogenase [168, 184], influx of extracellular contents such as Ca^{2+} [168, 185-186], conduction block [187], aberrant cell signaling [188], protease activation [189], reactive oxygen species activity [180], and phospholipase activation [180, 190]. Other consequences include alterations in cellular morphology [171, 174, 191], alterations in gene expression as in c-fos and c-jun [180, 192], induction of cell death processes owing the aforementioned glutamate induced excitotoxicity through the over activation of NMDA and AMPA receptors that result in sodium and calcium influx [177-178, 193] and delayed cell death [151, 166, 168-169, 194-197]. These and other events, such as invasion of blood-borne cells into the injured area, hemorrhage, ischemia, tissue deformation, and swelling of brain tissue, manifest at different times. Initiation of secondary events affects cellular electrophysiological and biochemical functionality, and compounded with cell-to-cell alterations, can ultimately yield neural network level changes, which may be neurodegenerative or neuroprotective in nature [167]. The complexity of the series of events after the primary insult makes the study of traumatic injury very challenging. A first step in this direction is to understand what happens during the primary insult as addressed in the third aim of this thesis.

Synchronized Bursts

Synaptic interaction among the large numbers of cells within the network results in the firing of solitary action potentials (spikes) or the firing of spikes in repeated successions for extended periods (bursts). Both can be coincident or synchronized [198]. Compared to single spikes, bursts consistently effect the release of neurotransmitters, forming a possibly more reliable neural communication code [199]. Therefore, bursting is thought to encode the processing and storing of sensory, motor, and cognitive information [200]. Correlated network-wide bursting has been observed transiently during development [201-203], some stages of sleep [204], and pathological conditions resembling epilepsy [205]. Changes in synaptic efficacy [206] and long-term potentiation [207] in the cortex also depend on high frequency bursting of spikes.

Several other characteristics of spontaneous synchronous activity of dissociated neural cultures have been studied, delving into the location [103], spread [94], origin [103], post-burst recovery of spontaneous bursts [101], prediction of bursts [208]. It has been found that culture-wide spontaneous bursts, initiated from various sites in the dissociated culture, occur in a variety of patterns [103]. Results of network sectioning suggested that a synchronized burst would spread to the entire culture by sparse excitatory connectivity mediated by chemical synapses, not gap junctions and/or diffusible factors [5]. Prediction of an upcoming network burst was shown to be possible by observing a set of neurons in culture, in which the firing rates increased tens of milliseconds before the peak of a culture-wide burst [208]. On the contrary, observation of varied locations of spontaneous burst origins, suggest that no single “pacemaker” cell drives the network to burst [103]. A period of post-bursting network depression and a

positive-correlation between burst duration and the preceding interval between bursts suggest that recovery parameters, such as replenishing neurotransmitter vesicles after the previous burst, modulate the proceeding burst duration [101]. This also implies the existence of a "burst refractory period." The burst refractory period may control how quickly a burst can be re-initiated. Given their increased temporal reliability and greater network-wide chemical influence, synchronized bursts may be integral to understanding how neural networks process and store sensory, motor, and cognitive information [209].

Inhibitory Neurons / GABAergic Neurons in Dissociated Cortical Cultures

Neurotransmitters affect synchronized bursts. One of these, gamma amino butyric acid (GABA) is a major inhibitory neurotransmitter in the adult cortex, although excitatory in immature networks [210-212]. *In vitro* the number of GABAergic neurons vary in response to altered levels of activity in neuronal networks [149, 213-215]. GABA's role in maintaining synchronous network activity, further implied as suppression of spiking activity, is concomitant with a decrease in GABA neurotransmission [149, 216].

The Microelectrode/Electrolyte Interface in the MEA-Neural-Culture System

In the MEA-neural-culture system, the extracellular electrolyte rich solution interacts electrochemically with the microelectrode surface to make neural recordings possible. MEAs transduce bioelectric potential signals carried by electrolyte/ionic currents to electronic signals and vice versa. Neurons send these bioelectric signals into the MEA electrodes via capacitive field interactions, inputing these signals into high-

impedance amplifier circuits. These circuits amplify the signals and record them as microvolt fluctuations. No charge transfer occurs from the neurons to the electrodes in this process [92].

A potential difference forms between the electrode metal and its dissolved cations, which accumulate on the electrode's surface at equilibrium with the excess concomitantly released electronic charge on the electrode's surface. This capacitative space between an electrode's electronic charge and the dissolved cationic charge constitutes a space charge layer. The cations range in concentration from some maximum closest to the metal electrode surface to some minimum farther from the charged electrode surface. A hydration sheath of oriented water molecules forms near the surface of the metal electrode. Lining the electrode, the first set of water molecules form the inner Helmholtz plane, while the next layer of hydrated cations outward from the electrode form the outer Helmholtz plane.

Three mathematical models, the Helmholtz-Perrin model, the Gouy-Chapman model, and the Stern model, describe the capacitive electro-chemical behavior at the electrode/electrolyte interface in neural recording scenarios. The Stern model additively combines the Helmholtz-Perrin and Gouy-Chapman models to account for both the dependence of capacitance on potential at lower voltages and the capacitance plateaus at higher voltages [217]. It yields an expression for the interface capacitance per unit area, C_I, (in F/m^2) as follows:

$$\frac{1}{C_I} = \frac{1}{C_H} + \frac{1}{C_D} = \frac{d_{OHP}}{\varepsilon_0 \varepsilon_r} + \frac{L_D \cosh(zV_0 / 2V_t)}{\varepsilon_0 \varepsilon_r}.$$

C_H represents the linearly dependant capacitance per unit area on voltage in the stuck-ion space-charge layer up to the outer Helmholtz plane from the Helmholtz-Perrin model and

C_D represents the exponentially dependent capacitance per unit area in the diffuse space charge layer beyond the outer Helmholtz plane from the Gouy-Chapman model; d_{OHP} denotes the distance from the electrode to the outer Helmholtz plane, which is also the location of the physical transition from C_H to C_D; ε_0 and ε_r represent the dielectric permittivity of free space and the relative dielectric permittivity of the medium between the two plates, respectively; L_D stands for the Debye length or the distance over which the potential decays "*e*"-fold; *z* designates the charge of the ion in question, while V_0 and V_t express the potential at the electrode and the thermal voltage, respectively.

While magnitude of C_H remains stable, the C_D increases at higher ionic solute concentrations or applied potentials because the diffuse space charge region becomes more compact. The C_I obtained reflects the real capacitance in biological applications involving MEA electrodes. Overall, MEA electrodes tend to behave in a completely capacitive manner in neural recording applications [92]. Therefore, the Stern model sufficiently explains the microelectrode/electrolyte interface involved.

Defined Media for Neuronal-Astrocytic Neural Cultures

In order to obtain consistent high-yield data, the culture needs controlled media that optimizes viability of neuronal cells. Serum-containing media is not as well characterized as serum-free defined media, yet contains many essential components. However, *in vitro* neural networks that grow in undefined serum-based media result in low neural culture viability at low cell density [127, 148]. Serum-based media also promotes the growth of astrocytes. The excess astrocyte growth may interfere with MEA electrode-to-neuron coupling [127]. Culture conditioned media is an option for some

culture conditions, yet consistency in composition needs to be verified. To avoid these complications, a feasible alternative to serum-based cell-culture media is a combination of an optimized B27 supplement and a basal medium (Neurobasal, by Gibco) containing defined amounts of nutrients. At low plating densities, this defined medium [218] maintains less than one percent of astrocytes in the cell culture population while allowing several weeks of greater than 90% primary hippocampal neuronal viability [127, 148]. The addition of G-5 supplement with defined components helps maintain the presence of astrocytes in culture under controlled conditions [219]. The use of defined media in neural experimentation has allowed another level of control thereby minimizing the variable of undefined physiological components.

Conclusion

A 3-D dissociated neural culture system has comparative advantages over *in vivo* systems and 2-D *in vitro* systems. A culture system used in this research work comprised of cells embedded in a Matrigel^{TM} scaffold over a processed SU-8 2000 MEA interface, so that cells in culture existed in a close imitation of the *in vivo* environment in close apposition to a cytocompatible recording surface. The use of 3-D *in vitro* MEAs to collect data instead of other devices, such as the patch clamp allows for distinct advantages, including simultaneous multi-location recording in 3-D environments with minimized impedence. However, 3-D cultures *in vitro* need to adhere well to the MEAs in order to record electrophysiological activity of neural network. Surface treatments effectuating physisorption and functionalization allow for better neural adhesion to the MEAs. Despite the obstacles of small signal magnitude to recording simultaneously at numerous electrodes, MEAs can capture an accurate representation of electrophysiological activity within the culture over weeks. Developing networks exhibit both synaptogenesis and pruning as they mature. These networks can be chemically modulated, a useful tool in drug analysis. Chemicals affect synchronized network bursts, which are thought to be responsible for the processing and storage of sensory, motor, and cognitive information. Moreover, networks can be modified or injured mechanically. Mechanical injury affects cell membrane permeability, resulting in altered ion and neurotransmitter fluxes, such as those of GABA, a neurotransmitter that inhibits network-activity. MEA recordings are possible due to electronic and ionic interactions at the microelectrode/electrolyte interface in the MEA-neural-culture system. This environment must have a defined media to enhance neuronal viability under controlled

conditions during recording. With several factors optimized, a 3-D culture model should prove to be a powerful tool in a variety of neurological experiments.

References

1. Kaech, S., H. Brinkhaus, and A. Matus, *Volatile anesthetics block actin-based motility in dendritic spines.* Proceedings Of The National Academy Of Sciences Of The United States Of America, 1999. **96**(18): p. 10433-10437.
2. Hockberger, P.E., D.K. Racker, and J.C. Houk, *Culturing Neural Networks*, in *Enabling Technologies for Cultured Neural Networks*, M.T.M. Stenger D.A., Editor. 1994, Academic Press: San Diego.
3. Mattson, M.P. and B. Rychlik, *Comparison of rates of neuronal development and survival in human and rat cerebral cortical cell cultures.* Mechanisms Of Ageing And Development, 1991. **60**(2): p. 171-187.
4. Mattson, M.P., et al., *beta-Amyloid peptides destabilize calcium homeostasis and render human cortical neurons vulnerable to excitotoxicity.* The Journal Of Neuroscience: The Official Journal Of The Society For Neuroscience, 1992. **12**(2): p. 376-389.
5. Giugliano, M., et al., *Emerging Network Activity in Dissociated Cultures of Neocortex: Novel Electrophysiological Protocols and Mathematical Modeling*, in *Advances in Network Electrophysiology Using Multi-Electrode Arrays*, B.M. Taketani M., Editor. 2006, Springer Science+Business Media, Inc: New York. p. 243-273.
6. Guthrie, P.B., D.E. Brenneman, and E.A. Neale, *Morphological and biochemical differences expressed in separate dissociated cell cultures of dorsal and ventral halves of the mouse spinal cord.* Brain Research, 1987. **420**(2): p. 313-323.
7. Dichter, M.A., *Rat cortical neurons in cell culture: Culture methods, cell morphology, electrophysiology, and synapse formation.* Brain Research, 1978. **149**(2): p. 279-293.
8. Corner, M., et al., *Physiological effects of sustained blockade of excitatory synaptic transmission on spontaneously active developing neuronal networks—an inquiry into the reciprocal linkage between intrinsic biorhythms and neuroplasticity in early ontogeny.* Neuroscience and biobehavioral reviews, 2002. **26**(2): p. 127-185.
9. Marom, S., et al., *Development, learning and memory in large random networks of cortical neurons: lessons beyond anatomy.* Quarterly Reviews of Biophysics, 2002. **35**(1): p. 63-87.
10. Jimbo, Y., et al., *The dynamics of a neuronal culture of dissociated cortical neurons of neonatal rats.* Biological Cybernetics, 2000. **83**(1): p. 1-20.
11. Morefield, S.I., et al., *Drug evaluations using neuronal networks cultured on microelectrode arrays.* Biosensors and Bioelectronics, 2000. **15**(7-8): p. 383-396.
12. Cukierman, E., et al., *Taking Cell-Matrix Adhesions to the Third Dimension.* Science, 2001. **294**(5547): p. 1708.
13. Hindié, M., et al., *Interactions of B16F10 melanoma cells aggregated on a cellulose substrate.* Journal of Cellular Biochemistry, 2006. **99**(1): p. 96-104.
14. Willerth, S.M., et al., *Optimization of fibrin scaffolds for differentiation of murine embryonic stem cells into neural lineage cells.* Biomaterials, 2006. **27**(36): p. 5990-6003.

15. Friedl, P., K.S. Zänker, and E.-B. Bröcker, *Cell migration strategies in 3-D extracellular matrix: Differences in morphology, cell matrix interactions, and integrin function.* Microscopy Research and Technique, 1998. **43**(5): p. 369-378.
16. Birgersdotter, A., R. Sandberg, and I. Ernberg, *Gene expression perturbation in vitro--A growing case for three-dimensional (3D) culture systems.* Seminars in Cancer Biology, 2005. **15**(5): p. 405-412.
17. Liu, H., J. Lin, and K. Roy, *Effect of 3D scaffold and dynamic culture condition on the global gene expression profile of mouse embryonic stem cells.* Biomaterials, 2006. **27**(36): p. 5978-5989.
18. Chun, T.-H., et al., *A Pericellular Collagenase Directs the 3-Dimensional Development of White Adipose Tissue.* Cell, 2006. **125**(3): p. 577-591.
19. Pedersen, J.A. and M.A. Swartz, *Mechanobiology in the third dimension.* Annals Of Biomedical Engineering, 2005. **33**(11): p. 1469-1490.
20. Behravesh, E., et al., *Comparison of genotoxic damage in monolayer cell cultures and three-dimensional tissue-like cell assemblies.* Advances in Space Research, 2005. **35**(2): p. 260-267.
21. Smalley, K.S.M., M. Lioni, and M. Herlyn, *Life Isn't Flat: Taking Cancer Biology to the Next Dimension.* In Vitro Cellular & Developmental Biology - Animal, 2006. **42**(8 & 9): p. 242-247.
22. Hoffman, R., *To do tissue culture in two or three dimensions? That is the question.* Stem Cells, 1993. **11**(2).
23. Schmeichel, K.L. and M.J. Bissell, *Modeling tissue-specific signaling and organ function in three dimensions.* J Cell Sci, 2003. **116**(Pt 12): p. 2377-88.
24. Cukierman, E., R. Pankov, and K. Yamada, *Cell interactions with three-dimensional matrices.* Current opinion in cell biology, 2002. **14**(5): p. 633-640.
25. Fawcett, J.W., R.A. Barker, and S.B. Dunnett, *Dopaminergic neuronal survival and the effects of bFGF in explant, three dimensional and monolayer cultures of embryonic rat ventral mesencephalon.* Exp Brain Res, 1995. **106**(2): p. 275-82.
26. Bellamkonda, R., et al., *Hydrogel-based three-dimensional matrix of neural cells.* Journal of biomedical materials research, 1995. **29**(5): p. 663-671.
27. Blackshaw, S., et al., *Promotion of regeneration and axon growth following injury in an invertebrate nervous system by the use of three-dimensional collagen gels.* Proceedings of the Royal Society B: Biological Sciences, 1997. **264**(1382): p. 657.
28. Choi, H., L. Won, and A. Heller, *Dopaminergic neurons grown in three-dimensional reaggregate culture for periods of up to one year.* Journal Of Neuroscience Methods, 1993. **46**(3): p. 233.
29. Horie, H. and Y. Akahori, *Three-dimensional cell aggregation enhances growth-promoting activity of NGF in adult DRG.* Neuroreport, 1994. **6**(1): p. 37.
30. Prado, G., et al., *Mechanical trauma induces immediate changes in neuronal network activity.* Journal of Neural Engineering, 2005. **2**(4): p. 148-158.
31. O'Connor, S., et al., *Primary neural precursor cell expansion, differentiation and cytosolic Ca2+ response in three-dimensional collagen gel.* Journal Of Neuroscience Methods, 2000. **102**(2): p. 187-195.
32. Peretz, H., et al., *Superior survival and durability of neurons and astrocytes on 3-dimensional aragonite biomatrices.* Tissue Engineering, 2007. **13**(3): p. 461-472.

33. Cullen, D. and M. LaPlaca, *Neuronal response to high rate shear deformation depends on heterogeneity of the local strain field.* Journal of neurotrauma, 2006. **23**(9): p. 1304-1319.
34. Hulspas, R., et al., *In VitroCell Density-Dependent Clonal Growth of EGF-Responsive Murine Neural Progenitor Cells under Serum-Free Conditions.* Experimental Neurology, 1997. **148**(1): p. 147-156.
35. Coates, P., et al., *Utilization of three-dimensional culture for early morphometric and electrophysiological analyses of solitary cerebellar neurons.* Dev Neurosci, 1992. **14**: p. 35-43.
36. Coates, P. and R. Nathan, *Feasibility of electrical recordings from unconnected vertebrate CNS neurons cultured in a three-dimensional extracellular matrix.* Journal Of Neuroscience Methods, 1987. **20**(3): p. 203.
37. O'Shaughnessy, T., H. Lin, and W. Ma, *Functional synapse formation among rat cortical neurons grown on three-dimensional collagen gels.* Neuroscience letters, 2003. **340**(3): p. 169-172.
38. Cullen, D., M. Lessing, and M. LaPlaca, *Collagen-dependent neurite outgrowth and response to dynamic deformation in three-dimensional neuronal cultures.* Annals Of Biomedical Engineering, 2007. **35**(5): p. 835-846.
39. O'Connor, S., et al., *Survival and neurite outgrowth of rat cortical neurons in three-dimensional agarose and collagen gel matrices.* Neuroscience letters, 2001. **304**(3): p. 189-193.
40. Woerly, S., G. Plant, and A. Harvey, *Neural tissue engineering: from polymer to biohybrid organs.* Biomaterials, 1996. **17**(3): p. 301-310.
41. Pautot, S., C. Wyart, and E.Y. Isacoff, *Colloid-guided assembly of oriented 3D neuronal networks.* Nat Meth, 2008. **5**(8): p. 735-740.
42. Cullen, D., et al., *Microfluidic engineered high cell density three-dimensional neural cultures.* J. Neural Eng, 2007. **4**(2): p. 159-172.
43. Drury, J.L. and D.J. Mooney, *Hydrogels for tissue engineering: scaffold design variables and applications.* Biomaterials, 2003. **24**(24): p. 4337-4351.
44. Li, G.N., et al., *Genomic and Morphological Changes of Neuroblastoma Cells in Response to Three-Dimensional Matrices.* Tissue Engineering, 2007. **13**(5): p. 1035-1047.
45. Dewitt, D.D., et al., *Collagen I-Matrigel Scaffolds for Enhanced Schwann Cell Survival and Control of Three-Dimensional Cell Morphology.* Tissue Engineering Part A, 2009. **15**(10): p. 2785-2793.
46. Brown, S., *Introduction*, in *Cell-Culture Test Methods: ASTM Special Technical Publication 810*, B. SA, Editor. 1983, ASTM: Philadelphia. p. 2-3.
47. Lontz, J., M. Nadijcka, and H. R., *Assessment of Biocompaitibility of orofacial materials and devices by culturing with human excised donor tissues*, in *Cell-Culture Test Methods: ASTM Special Technical Publication 810*, B. SA, Editor. 1983, ASTM: Philadelphia. p. 77-87.
48. Crompton, K.E., et al., *Polylysine-functionalised thermoresponsive chitosan hydrogel for neural tissue engineering.* Biomaterials, 2007. **28**(3): p. 441-449.
49. Borkenhagen, M., et al., *Three-dimensional extracellular matrix engineering in the nervous system.* Journal of biomedical materials research, 1998. **40**(3): p. 392-400.

50. Dillon, G.P., et al., *The influence of physical structure and charge on neurite extension in a 3D hydrogel scaffold.* Journal of Biomaterials Science, Polymer Edition, 1998. **9**: p. 1049-1069.
51. Liu, Q., et al., *Preparation of macroporous poly(2-hydroxyethyl methacrylate) hydrogels by enhanced phase separation.* Biomaterials, 2000. **21**(21): p. 2163-2169.
52. Mahoney, M.J. and K.S. Anseth, *Three-dimensional growth and function of neural tissue in degradable polyethylene glycol hydrogels.* Biomaterials, 2006. **27**(10): p. 2265-2274.
53. O'Connor, S., et al., *Immobilization of neural cells in three-dimensional matrices for biosensor applications.* Biosensors and Bioelectronics, 2000. **14**(10-11): p. 871-881.
54. Luo, Y. and M. Shoichet, *A photolabile hydrogel for guided three-dimensional cell growth and migration.* Nature materials, 2004. **3**(4): p. 249-253.
55. Yu, X., G. Dillon, and R. Bellamkonda, *A laminin and nerve growth factor-laden three-dimensional scaffold for enhanced neurite extension.* Tissue Engineering, 1999. **5**(4): p. 291-304.
56. Kleinman, H., et al., *Basement membrane complexes with biological activity.* Biochemistry, 1986. **25**(2): p. 312-318.
57. Vukicevic, S., et al., *Identification of multiple active growth factors in basement membrane Matrigel suggests caution in interpretation of cellular activity related to extracellular matrix components.* Experimental cell research, 1992. **202**(1): p. 1-8.
58. Vukicevic, S., et al., *Reconstituted basement membrane (Matrigel) promotes the survival and influences the growth of murine tumors.* International Journal of Cancer, 1992. **50**(5).
59. Wells, M.R., et al., *Gel Matrix Vehicles for Growth Factor Application in Nerve Gap Injuries Repaired with Tubes: A Comparison of Biomatrix, Collagen, and Methylcellulose.* Experimental Neurology, 1997. **146**(2): p. 395-402.
60. Madison, R., et al., *Increased rate of peripheral nerve regeneration using bioresorbable nerve guides and a laminin-containing gel.* Experimental Neurology, 1985. **88**(3): p. 767-772.
61. Schwartz, M., M. Schaller, and M. Ginsberg, *Integrins: emerging paradigms of signal transduction.* Annual review of cell and developmental biology, 1995. **11**(1): p. 549-599.
62. Xiao, Z., et al., *Tenascin-R is a functional modulator of sodium channel ß subunits.* Journal of Biological Chemistry, 1999. **274**(37): p. 26511-26517.
63. Bixby, J. and P. Jhabvala, *Extracellular matrix molecules and cell adhesion molecules induce neurites through different mechanisms.* Journal of Cell Biology, 1990. **111**(6): p. 2725-2732.
64. Hari, A., et al., *Neurotrophins and extracellular matrix molecules modulate sensory axon outgrowth.* International Journal of Developmental Neuroscience, 2004. **22**(2): p. 113-117.
65. Dodd, J. and T. Jessell, *Axon guidance and the patterning of neuronal projections in vertebrates.* Science, 1988. **242**(4879): p. 692-699.

66. Yamaguchi, Y., *Heparan sulfate proteoglycans in the nervous system: their diverse roles in neurogenesis, axon guidance, and synaptogenesis.* Seminars in cell & developmental biology, 2001. **12**(2): p. 99-106.
67. Ard, M. and R. Bunge, *Heparan sulfate proteoglycan and laminin immunoreactivity on cultured astrocytes: relationship to differentiation and neurite growth.* Journal of Neuroscience, 1988. **8**(8): p. 2844-2858.
68. Gelorme, J., R. Cox, and S. Gutierrez, *Photoresist composition and printed circuit boards and packages made therewith*, U.S. Patent, Editor. 1989.
69. Shaw, J., et al., *Negative photoresists for optical lithography.* IBM Journal of Research and Development, 1997. **41**(1): p. 81-94.
70. Shaw, M., et al., *Improving the process capability of SU-8.* Microsystem Technologies, 2003. **10**(1): p. 1-6.
71. Lorenz, H., et al., *High-aspect-ratio, ultrathick, negative-tone near-UV photoresist and its applications for MEMS.* Sensors and actuators A, 1998. **64**: p. 33-39.
72. Kotzar, G., et al., *Evaluation of MEMS materials of construction for implantable medical devices.* Biomaterials, 2002. **23**(13): p. 2737-2750.
73. Heuschkel, M., et al., *Buried microchannels in photopolymer for delivering of solutions to neurons in a network.* Sensors & Actuators: B. Chemical, 1998. **48**(1-3): p. 356-361.
74. Voskerician, G., et al., *Biocompatibility and biofouling of MEMS drug delivery devices.* Biomaterials, 2003. **24**(11): p. 1959-1967.
75. Gholmieh, G., et al., *A biosensor for detecting changes in cognitive processing based on nonlinear systems analysis.* Biosensors and Bioelectronics, 2001. **16**(7-8): p. 491-501.
76. Gholmieh, G., et al., *Custom-designed high-density conformal planar multielectrode arrays for brain slice electrophysiology.* Journal Of Neuroscience Methods, 2006. **152**(1-2): p. 116-129.
77. Heuschkel, M., et al., *A three-dimensional multi-electrode array for multi-site stimulation and recording in acute brain slices.* Journal Of Neuroscience Methods, 2002. **114**(2): p. 135-148.
78. Tscherter, A., et al., *Spatiotemporal characterization of rhythmic activity in rat spinal cord slice cultures.* European Journal of Neuroscience, 2001. **14**(2): p. 179-190.
79. Streit, J., et al., *The generation of rhythmic activity in dissociated cultures of rat spinal cord.* European Journal of Neuroscience, 2001. **14**(2): p. 191-202.
80. Wirth, C. and H. Luscher, *Spatiotemporal evolution of excitation and inhibition in the rat barrel cortex investigated with multielectrode arrays.* Journal of neurophysiology, 2004. **91**(4): p. 1635-1647.
81. Berdondini, L., et al., *A microelectrode array (MEA) integrated with clustering structures for investigating in vitro neurodynamics in confined interconnected sub-populations of neurons.* Sensors & Actuators: B. Chemical, 2006. **114**(1): p. 530-541.
82. Wu, Z., Y. Zhao, and W. Kisaalita, *A packed Cytodex microbead array for three-dimensional cell-based biosensing.* Biosensors and Bioelectronics, 2006. **22**(5): p. 685-693.

83. Weisenberg, B. and D. Mooradian, *Hemocompatibility of materials used in microelectromechanical systems: Platelet adhesion and morphology in vitro.* Journal of biomedical materials research, 2002. **60**(2).
84. Wang, Z., et al. *A simple hydrophilic treatment of SU-8 surfaces for cell culturing and cell patterning*. in *9th International Conference on Miniaturized Systems for Chemistry and Life Sciences*. 2005. Boston, MA.
85. Curtis, A., C. Wilkinson, and L. Breckenridge, *Living Nerve Nets*, in *Enabling Technologies for Cultured Neural Networks*, M.T.M. Stenger D.A., Editor. 1994, Academic Press: New York. p. 99-120.
86. Fejtl, M., et al., *On micro-electrode array revival: its development, sophistication of recording, and stimulation*, in *Advances in Network Electrophysiology Using Multi-Electrode Arrays*, B.M. Taketani M., Editor. 2006, Springer Science+Business Media Inc: New York. p. 24-37.
87. Thomas Jr, C., et al., *A miniature microelectrode array to monitor the bioelectric activity of cultured cells.* Experimental cell research, 1972. **74**(1): p. 61.
88. Gross, G., *Simultaneous single unit recording in vitro with a photoetched laser deinsulated gold multimicroelectrode surface.* IEEE Transactions on Biomedical Engineering, 1979. **26**(5): p. 273-279.
89. Pine, J., *Recording action potentials from cultured neurons with extracellular microcircuit electrodes.* Journal Of Neuroscience Methods, 1980. **2**(1): p. 19-31.
90. Hoogerwerf, A. and K. Wise, *A three-dimensional microelectrode array for chronic neural recording.* IEEE Transactions on Biomedical Engineering, 1994. **41**(12): p. 1136-1146.
91. Maynard, E., C. Nordhausen, and R. Normann, *The Utah intracortical electrode array: A recording structure for potential brain-computer interfaces.* Electroencephalography and clinical Neurophysiology, 1997. **102**(3): p. 228-239.
92. Kovacs, G.T.A., *Introduction to the Theory, Design, and Modeling of Thin-Film Microelectrodes for Neural Interfaces*, in *Enabling Technologies for Cultured Neural Networks*, M.T.M. Stenger D.A., Editor. 1994, Academic Press: New York. p. 121-165.
93. Heuschkel, M., et al., *Development of 3-D multi-electrode arrays for use with acture tissue slices*, in *Advances in Network Electrophysiology Using Multi-Electrode Arrays*, T. M. and B. M., Editors. 2006, Springer Science + Business Media: New York. p. 69-111.
94. Maeda, E., H. Robinson, and A. Kawana, *The mechanisms of generation and propagation of synchronized bursting in developing networks of cortical neurons.* Journal of Neuroscience, 1995. **15**(10): p. 6834-6845.
95. Hämmerle, H., et al., *Extracellular recording in neuronal networks with substrate integrated microelectrode arrays.* Biosensors & Bioelectronics, 1994. **9**(9-10): p. 691.
96. Meister, M., J. Pine, and D. Baylor, *Multi-neuronal signals from the retina: acquisition and analysis.* Journal Of Neuroscience Methods, 1994. **51**(1): p. 95-106.
97. Israel, D., et al., *An array of microelectrodes to stimulate and record from cardiac cells in culture.* American Journal of Physiology- Heart and Circulatory Physiology, 1984. **247**(4): p. 669-674.

98. Puchalla, J., et al., *Redundancy in the population code of the retina.* Neuron, 2005. **46**(3): p. 493-504.
99. Demas, J., S. Eglen, and R. Wong, *Developmental loss of synchronous spontaneous activity in the mouse retina is independent of visual experience.* Journal of Neuroscience, 2003. **23**(7): p. 2851.
100. Canepari, M., et al., *Experimental analysis of neuronal dynamics in cultured cortical networks and transitions between different patterns of activity.* Biological Cybernetics, 1997. **77**(2): p. 153-162.
101. Opitz, T., A.D. De Lima, and T. Voigt, *Spontaneous development of synchronous oscillatory activity during maturation of cortical networks in vitro.* Journal of neurophysiology, 2002. **88**(5): p. 2196-2206.
102. Voigt, T., H. Baier, and A. Lima, *Synchronization of neuronal activity promotes survival of individual rat neocortical neurons in early development.* European Journal of Neuroscience, 1997. **9**(5): p. 990-999.
103. Maeda, E., et al., *Modification of parallel activity elicited by propagating bursts in developing networks of rat cortical neurones.* European Journal of Neuroscience, 1998. **10**(2): p. 488-496.
104. van Pelt, J., et al., *Dynamics and plasticity in developing neuronal networks in vitro.* Progress in brain research, 2005. **147**: p. 173.
105. Beggs, J.M. and D. Plenz, *Neuronal avalanches in neocortical circuits.* Journal of Neuroscience, 2003. **23**(35): p. 11167-11177.
106. Wagenaar, D.A., Z. Nadasdy, and S.M. Potter, *Persistent dynamic attractors in activity patterns of cultured neuronal networks.* Physical Review E, 2006. **73**(5): p. 51907.
107. Hofmann, F., et al., *Functional re-establishment of the perforant pathway in organotypic co-cultures on microelectrode arrays.* Brain Research, 2004. **1017**(1-2): p. 184-196.
108. Standen, N., P. Gray, and M. Whitake, *Microelectrode Techniques, The Plymouth Workshop Handbook.* 1987: Company of Biologists.
109. Grinvald, A., et al., *In-vivo optical imaging of cortical architecture and dynamics.* Modern techniques in neuroscience research, 2001.
110. Jimbo, Y., H.P. Robinson, and A. Kawana, *Strengthening of synchronized activity by tetanic stimulation in cortical cultures: application of planar electrode arrays.* IEEE Transactions On Bio-Medical Engineering, 1998. **45**(11): p. 1297-1304.
111. Corner, M. and G. Ramakers, *Spontaneous firing as an epigenetic factor in brain development: physiological consequences of chronic tetrodotoxin and picrotoxin exposure on cultured rat neocortex neurons.* Developmental brain research, 1992. **65**(1): p. 57-64.
112. Gross, G. and J. Kowalski, *Origins of Activity Patterns in Self-Organizing Neuronal Networks in Vitro.* Journal of Intelligent Material Systems and Structures, 1999. **10**(7): p. 558.
113. Wagenaar, D., J. Pine, and S. Potter, *An extremely rich repertoire of bursting patterns during the development of cortical cultures.* BMC neuroscience, 2006. **7**(1): p. 11.

114. Stett, A., et al., *Biological application of microelectrode arrays in drug discovery and basic research.* Analytical and bioanalytical chemistry, 2003. **377**(3): p. 486-495.
115. Whitson, J., et al., *Multi-Electrode Arrays: Enhancing Traditional Methods and Enabling Network Physiology.* 2006.
116. Chang, J.C. and B.C. Wheeler, *Patterning technologies for structuring neuronal networks on MEAs*, in *Advances in Network Electrophysiology Using Multi-Electrode Arrays*, T. M. and B. M., Editors. 2006, Springer Science + Business Media: New York. p. 153-189.
117. Hickman, J. and D.A. Stenger, *Culturing Neural Networks*, in *Enabling Technologies for Cultured Neural Networks*, S. D.A. and M. T.M., Editors. 1994, Academic Press: San Deigo. p. 510-76.
118. Lom, B., K. Healy, and P. Hockberger, *A versatile technique for patterning biomolecules onto glass coverslips.* Journal Of Neuroscience Methods, 1993. **50**(3): p. 385-397.
119. Sadana, A., *Protein adsorption and inactivation on surfaces. Influence of heterogeneities.* Chemical Reviews, 1992. **92**(8): p. 1799-1818.
120. Stenger, D. and J. Hickman, *Lithographic definition of neuronal microcircuits*, in *Enabling Technologies for Cultured Neural Networks*, D. Stenger and T. McKenna, Editors. 1994. p. 77–98.
121. Ward, W., et al., *A new amperometric glucose microsensor: in vitro and short-term in vivo evaluation.* Biosensors and Bioelectronics, 2002. **17**(3): p. 181-189.
122. Bledi, Y., A. Domb, and M. Linial, *Culturing neuronal cells on surfaces coated by a novel polyethyleneimine-based polymer.* Brain Research Protocols, 2000. **5**(3): p. 282-289.
123. Pine, J., *A History of MEA Development*, in *Advances in Network Electrophysiology Using Multi-Electrode Arrays*, B.M. Taketani M., Editor. 2006, Springer Science + Business Media, Inc.: New York. p. 3-23.
124. Stuart, G. and B. Sakmann, *Active propagation of somatic action potentials into neocortical pyramidal cell dendrites.* Nature, 1994. **367**(6458): p. 69-72.
125. Claverol-Tinture, E. and J. Pine, *Extracellular potentials in low-density dissociated neuronal cultures.* Journal Of Neuroscience Methods, 2002. **117**(1): p. 13-21.
126. Connolly, P., et al., *An extracellular microelectrode array for monitoring electrogenic cells in culture.* Biosensors & Bioelectronics, 1990. **5**(3): p. 223-234.
127. Wheeler, B. and G. Brewer, *Multineuron patterning and recording*, in *Enabling Technologies for Cultured Neural Networks. Academic Press, San Diego*, M.T.M. Stenger D.A., Editor. 1994, Academic Press: San Diego. p. 167–185.
128. Nakanishi, K., et al., *Recurrent subthreshold electrical activities of rat neocortical neurons progress during long-term culture.* Neuroscience letters, 2001. **304**(1-2): p. 85-88.
129. Kamioka, H., et al., *Spontaneous periodic synchronized bursting during formation of mature patterns of connections in cortical cultures.* Neuroscience letters, 1996. **206**(2-3): p. 109-112.
130. Muramoto, K., et al., *Frequency of synchronous oscillations of neuronal activity increases during development and is correlated to the number of synapses in*

cultured cortical neuron networks. Neuroscience letters, 1993. **163**(2): p. 163-165.
131. Ichikawa, M., et al., *Formation and maturation of synapses in primary cultures of rat cerebral cortical cells: an electron microscopic study.* Neuroscience research, 1993. **16**(2): p. 95-103.
132. Nakanishi, K. and F. Kukita, *Functional synapses in synchronized bursting of neocortical neurons in culture.* Brain Research, 1998. **795**(1-2): p. 137-146.
133. Tsodyks, M., A. Uziel, and H. Markram, *Synchrony Generation in Recurrent Networks with Frequency-Dependent Synapses.* Soc Neuroscience, 2000. **20**(1): p. 50-54.
134. Van Huizen, F., H. Romijn, and M. Corner, *Indications for a critical period for synapse elimination in developing rat cerebral cortex cultures.* Brain Research, 1987. **428**(1): p. 1.
135. Turrigiano, G. and S. Nelson, *Homeostatic plasticity in the developing nervous system.* Nature Reviews Neuroscience, 2004. **5**(2): p. 97-107.
136. Eastwood, S., et al., *Synaptophysin protein and mRNA expression in the human hippocampal formation from birth to old age.* Hippocampus, 2006. **16**(8): p. 645.
137. Eastwood, S.L., et al., *Synaptophysin gene expression in human brain: A quantitative in situ hybridization and immunocytochemical study.* Neuroscience, 1994. **59**(4): p. 881-892.
138. Martin-Pena, A., et al., *Age-independent synaptogenesis by phosphoinositide 3 kinase.* Journal of Neuroscience, 2006. **26**(40): p. 10199.
139. Van Den Pol, A., et al., *Early synaptogenesis in vitro: role of axon target distance.* The Journal of Comparative Neurology, 1998. **399**(4).
140. Boehler, M., B. Wheeler, and G. Brewer, *Added astroglia promote greater synapse density and higher activity in neuronal networks.* Neuron glia biology, 2007. **3**(2): p. 127-140.
141. Waimey, K. and H. Cheng, *Axon Pruning and Synaptic Development: How Are They per-Plexin?* The Neuroscientist, 2006. **12**(5): p. 398.
142. Seeger, G., U. Gärtner, and T. Arendt, *Transgenic activation of Ras in neurons increases synapse formation in mouse neocortex.* Journal of Neural Transmission, 2005. **112**(6): p. 751-761.
143. Oppenheim, R., *Cell death during development of the nervous system.* Annual Review of Neuroscience, 1991. **14**(1): p. 453-501.
144. Gross, G., *Internal dynamics of randomized mammalian neuronal networks in culture.* Editors Stenger, DA, and McKenna TM, in Enabling Technologies for Cultured Neural Networks, Academic Press, San Diego, 1994: p. 277–317.
145. Choi, D.W., *Calcium and excitotoxic neuronal injury.* Ann N Y Acad Sci, 1994. **747**: p. 162-71.
146. Latham, P., et al., *Intrinsic dynamics in neuronal networks. II. Experiment.* Journal of neurophysiology, 2000. **83**(2): p. 828-835.
147. Robinson, H., et al., *Periodic synchronized bursting and intracellular calcium transients elicited by low magnesium in cultured cortical neurons.* Journal of neurophysiology, 1993. **70**(4): p. 1606-1616.

148. Cotman, C.W., D.H. Cribbs, and J. Kahle, *Toward Establishing Neural Networks in Culture*, in *Enabling Technologies for Cultured Neural Networks*, M.T.M. Stenger D.A., Editor. 1994. p. 3-22.
149. Ramakers, G., et al., *Activity-dependent plasticity of inhibitory and excitatory amino acid transmitter systems in cultured rat cerebral cortex.* International journal of developmental neuroscience: the official journal of the International Society for Developmental Neuroscience, 1994. **12**(7): p. 611.
150. Smith, D., et al., *Progressive atrophy and neuron death for one year following brain trauma in the rat.* Journal of neurotrauma, 1997. **14**(10): p. 715-727.
151. LaPlaca, M., et al., *Susceptibility of neuronal membranes to mechanical injury and implications for repair.* Editor Gefen, A. in The Pathomechanics of Tissue Injury and Disease, and the Mechanophysiology of Healing, Research Signpost, Trivandrum, Kerala, India, 2009: p. 67-91.
152. Lewen, A., et al., *Behavioural and morphological outcome of mild cortical contusion trauma of the rat brain: influence of NMDA-receptor blockade.* Acta neurochirurgica, 1999. **141**(2): p. 193-202.
153. McIntosh, T., et al., *Traumatic brain injury in the rat: characterization of a lateral fluid-percussion model.* Neuroscience, 1989. **28**(1): p. 233.
154. Bain, A., R. Raghupathi, and D. Meaney, *Dynamic stretch correlates to both morphological abnormalities and electrophysiological impairment in a model of traumatic axonal injury.* Journal of neurotrauma, 2001. **18**(5): p. 499-511.
155. Lusardi, T., et al., *A device to study the initiation and propagation of calcium transients in cultured neurons after mechanical stretch.* Annals Of Biomedical Engineering, 2004. **32**(11): p. 1546-1559.
156. LaPlaca, M., et al., *High rate shear strain of three-dimensional neural cell cultures: a new in vitro traumatic brain injury model.* Journal of biomechanics, 2005. **38**(5): p. 1093-1105.
157. Geddes-Klein, D., K. Schiffman, and D. Meaney, *Mechanisms and consequences of neuronal stretch injury in vitro differ with the model of trauma.* Journal of neurotrauma, 2006. **23**(2): p. 193-204.
158. Margulies, S.S. and L.E. Thibault, *A proposed tolerance criterion for diffuse axonal injury in man.* J Biomech, 1992. **25**(8): p. 917-23.
159. Gennarelli, T.A., *Mechanisms of brain injury.* J Emerg Med, 1993. **11 Suppl 1**: p. 5-11.
160. Meaney, D.F., et al., *Biomechanical analysis of experimental diffuse axonal injury.* J Neurotrauma, 1995. **12**(4): p. 689-94.
161. Holbourne, A., *Mechanics of head injury.* Lancet, 1943. **2**: p. 438-41.
162. Sahay, K., et al., *Elastomechanical characterization of brain tissues.* Journal of biomechanics, 1992. **25**(3): p. 319-326.
163. Thibault, L.E. and T.A. Gennarelli, *Biomechanics of diffuse brain injuries.* Proc. 10th Int. Tech. Conf. on Experimental Safety Vehicles. DOT, NHTSA., 1989.
164. McLean, A.J. and R.W.G. Anderson, *Biomechanics of Closed Head Injury.* Head Injury, 1997.
165. LaPlaca, M., et al., *CNS injury biomechanics and experimental models.* Progress in brain research, 2007. **161**: p. 13.

166. Ellis, E., et al., *A new model for rapid stretch-induced injury of cells in culture: characterization of the model using astrocytes.* Journal of neurotrauma, 1995. **12**(3): p. 325-339.
167. Morrison III, B., et al., *In vitro central nervous system models of mechanically induced trauma: a review.* Journal of neurotrauma, 1998. **15**(11): p. 911-928.
168. LaPlaca, M., V. Lee, and L. Thibault, *An in vitro model of traumatic neuronal injury: loading rate-dependent changes in acute cytosolic calcium and lactate dehydrogenase release.* Journal of neurotrauma, 1997. **14**(6): p. 355-368.
169. Geddes, D., R. Cargill, and M. LaPlaca, *Mechanical stretch to neurons results in a strain rate and magnitude-dependent increase in plasma membrane permeability.* Journal of neurotrauma, 2003. **20**(10): p. 1039-1049.
170. Cullen, D., C. Simon, and M. LaPlaca, *Strain rate-dependent induction of reactive astrogliosis and cell death in three-dimensional neuronal–astrocytic co-cultures.* Brain Research, 2007. **1158**: p. 103-115.
171. Pettus, E., et al., *Traumatically induced altered membrane permeability: its relationship to traumatically induced reactive axonal change.* Journal of neurotrauma, 1994. **11**(5): p. 507-522.
172. Shi, R., *The dynamics of axolemmal disruption in guinea pig spinal cord following compression.* Journal of neurocytology, 2004. **33**(2): p. 203-211.
173. Shi, R., et al., *Control of membrane sealing in injured mammalian spinal cord axons.* Journal of Neurophysiology, 2000. **84**(4): p. 1763-1769.
174. Pettus, E. and J. Povlishock, *Characterization of a distinct set of intra-axonal ultrastructural changes associated with traumatically induced alteration in axolemmal permeability.* Brain Research, 1996. **722**(1-2): p. 1-11.
175. Shi, R. and J. Whitebone, *Conduction deficits and membrane disruption of spinal cord axons as a function of magnitude and rate of strain.* Journal of Neurophysiology, 2006. **95**(6): p. 3384-3390.
176. Galbraith, J., L. Thibault, and D. Matteson, *Mechanically induced depolarization in the squid giant axon to simple elongation.* J. Biomech. Eng, 1993. **115**: p. 13-22.
177. Goforth, P., E. Ellis, and L. Satin, *Enhancement of AMPA-mediated current after traumatic injury in cortical neurons.* Journal of Neuroscience, 1999. **19**(17): p. 7367-7374.
178. Zhang, L., et al., *Reduction of voltage-dependent Mg2+ blockade of NMDA current in mechanically injured neurons.* Science, 1996. **274**(5294): p. 1921.
179. Dumont, R., et al., *Acute Spinal Cord Injury, Part II: Contemporary Pharmacotherapy.* Clinical neuropharmacology, 2001. **24**(5): p. 265.
180. McIntosh, T., et al., *Review. The Dorothy Russell Memorial Lecture. The molecular and cellular sequelae of experimental traumatic brain injury: pathogenetic mechanisms.* Neuropathology and Applied Neurobiology, 1998. **24**(4): p. 251-267.
181. Rami, A., D. Ferger, and J. Krieglstein, *Blockade of calpain proteolytic activity rescues neurons from glutamate excitotoxicity.* Neuroscience research, 1997. **27**(1): p. 93-97.

182. Villa, P., et al., *Calpain inhibitors, but not caspase inhibitors, prevent actin proteolysis and DNA fragmentation during apoptosis.* Journal of Cell Science, 1998. **111**(6): p. 713-722.
183. Weber, J., *Calcium homeostasis following traumatic neuronal injury.* Current neurovascular research, 2004. **1**(2): p. 151.
184. Regan, R. and D. Choi, *The effect of NMDA, AMPA/kainate, and calcium channel antagonists on traumatic cortical neuronal injury in culture.* Brain Research, 1994. **633**(1-2): p. 236.
185. Floyd, C.L., et al., *Traumatic injury of cultured astrocytes alters inositol (1,4,5)-trisphosphate-mediated signaling.* Glia, 2001. **33**(1): p. 12-23.
186. Lusardi, T.A., et al., *Effect of acute calcium influx after mechanical stretch injury in vitro on the viability of hippocampal neurons.* J Neurotrauma, 2004. **21**(1): p. 61-72.
187. Shi, R. and R. Borgens, *Anatomical repair of nerve membranes in crushed mammalian spinal cord with polyethylene glycol.* Journal of neurocytology, 2000. **29**(9): p. 633-643.
188. Serbest, G., et al., *Mechanisms of cell death and neuroprotection by poloxamer 188 after mechanical trauma*. 2006, FASEB. p. 308-310.
189. Farkas, O., J. Lifshitz, and J. Povlishock, *Mechanoporation induced by diffuse traumatic brain injury: an irreversible or reversible response to injury?* Journal of Neuroscience, 2006. **26**(12): p. 3130-3140.
190. Chung, R., et al., *Glutamate induces rapid loss of axonal neurofilament proteins from cortical neurons in vitro.* Experimental Neurology, 2005. **193**(2): p. 481-488.
191. Stone, J., et al., *Impaired axonal transport and altered axolemmal permeability occur in distinct populations of damaged axons following traumatic brain injury.* Experimental Neurology, 2004. **190**(1): p. 59-69.
192. Raghupathi, R., T. McIntosh, and D. Smith, *Cellular responses to experimental brain injury.* Brain Pathology, 1995. **5**(4): p. 437-442.
193. Matsushita, Y., et al., *Real-time monitoring of glutamate following fluid percussion brain injury with hypoxia in the rat.* Journal of neurotrauma, 2000. **17**(2): p. 143-153.
194. Geddes, D. and R. Cargill, *An in vitro model of neural trauma: device characterization and calcium response to mechanical stretch.* Journal of biomechanical engineering, 2001. **123**: p. 247.
195. Katayama, Y., et al., *Massive increases in extracellular potassium and the indiscriminate release of glutamate following concussive brain injury.* Journal of neurosurgery, 1990. **73**(6): p. 889-900.
196. LaPlaca, M. and L. Thibault, *Dynamic mechanical deformation of neurons triggers an acute calcium response and cell injury involving the N-methyl-D-aspartate glutamate receptor.* Journal of neuroscience research, 1998. **52**(2).
197. Yoshino, A., et al., *Dynamic changes in local cerebral glucose utilization following cerebral conclusion in rats: evidence of a hyper-and subsequent hypometabolic state.* Brain Research, 1991. **561**(1): p. 106.

198. Van Huizen, F., H. Romijn, and A. Habets, *Synaptogenesis in rat cerebral cortex cultures is affected during chronic blockade of spontaneous bioelectric activity by tetradotoxin.* Brain research., 1985. **19**(1): p. 67-80.
199. Lisman, J., *Bursts as a unit of neural information: making unreliable synapses reliable.* Trends in neurosciences, 1997. **20**(1): p. 38-43.
200. Rieke, F., et al., *Spikes: exploring the neural code*. 1997, Cambridge Massachusettes: MIT Press.
201. Wong, R., M. Meister, and C. Shatz, *Transient period of correlated bursting activity during development of the mammalian retina.* Neuron(Cambridge, Mass.), 1993. **11**(5): p. 923-938.
202. Ben-Ari, Y., et al., *Giant synaptic potentials in immature rat CA3 hippocampal neurones.* The Journal of Physiology, 1989. **416**(1): p. 303-325.
203. Leinekugel, X., et al., *Correlated bursts of activity in the neonatal hippocampus in vivo.* Science, 2002. **296**(5575): p. 2049-2052.
204. Krahe, R. and F. Gabbiani, *Burst firing in sensory systems.* Nature Reviews Neuroscience, 2004. **5**(1): p. 13-23.
205. Furshpan, E. and D. Potter, *Seizure-like activity and cellular damage in rat hippocampal neurons in cell culture.* Neuron, 1989. **3**(2): p. 199-207.
206. Zucker, R., *Frequency dependent changes in excitatory synaptic efficacy*. Mechanisms of Epileptogenesis, 1988: p. 153–167.
207. Brown, T., et al., *Long-term synaptic potentiation.* Science, 1988. **242**(4879): p. 724-728.
208. Eytan, D. and S. Marom, *Dynamics and effective topology underlying synchronization in networks of cortical neurons.* Journal of Neuroscience, 2006. **26**(33): p. 8465.
209. Madhavan, R., Z. Chao, and S. Potter, *Plasticity of recurring spatiotemporal activity patterns in cortical networks.* Physical biology. **4**(3): p. 181.
210. LoTurco, J., et al., *GABA and glutamate depolarize cortical progenitor cells and inhibit DNA synthesis.* Neuron, 1995. **15**(6): p. 1287-1298.
211. Owens, D., X. Liu, and A. Kriegstein, *Changing properties of GABAA receptor-mediated signaling during early neocortical development.* Journal of neurophysiology, 1999. **82**(2): p. 570-583.
212. Snodgrass, S., et al., *Biochemical correlates of GABA function in rat cortical neurons in culture.* Brain Research, 1980. **190**(1): p. 123.
213. Hendry, S. and E. Jones, *Activity-dependent regulation of GABA expression in the visual cortex of adult monkeys.* Neuron, 1988. **1**(8): p. 701.
214. Benevento, L., B. Bakkum, and R. Cohen, *Gamma-aminobutyric acid and somatostatin immunoreactivity in the visual cortex of normal and dark-reared rats.* Brain Research, 1995. **689**(2): p. 172-182.
215. Micheva, K. and C. Beaulieu, *Neonatal sensory deprivation induces selective changes in the quantitative distribution of GABA-immunoreactive neurons in the rat barrel field cortex.* The Journal of Comparative Neurology, 1995. **361**(4).
216. Voigt, T., T. Opitz, and A. de Lima, *Synchronous oscillatory activity in immature cortical network is driven by GABAergic preplate neurons.* Journal of Neuroscience, 2001. **21**(22): p. 8895.

217. Bard, A. and L. Faulkner, *Electrochemical Methods: Fundamentals and Applications*. 1980, New York: Wiley.
218. Brewer, G., et al., *Optimized survival of hippocampal neurons in B27-supplemented Neurobasal™, a new serum-free medium combination.* Journal of neuroscience research, 1993. **35**(5): p. 567-576.
219. Ullian, E., et al., *Control of synapse number by glia.* Science, 2001. **291**(5504): p. 657-661.

CHAPTER 3

SU-8 2000 RENDERED CYTOCOMPATIBLE FOR NEURONAL BIOMEMS APPLICATIONS

Summary

Microfabrication advances have resulted in small, inexpensive, and precise devices for biological microelectromechanical systems (bioMEMS). SU-8 / SU-8 2000 is an attractive material for these applications because of the high-aspect ratio fabrication capability, dielectric properties, and thermochemical stability. Despite these advantages, the potential toxicity of SU-8 2000 may limit its use in cell-based applications. We show that <10% of primary neurons survived when cultured adjacent to or on top of untreated SU-8 2000. We evaluated the efficacy of various detoxification and surface treatments for SU-8 2000 in neuronal cultures after 7-21 days *in vitro*. Viability was improved to 45.8 ± 4.5 % (mean ± standard error of the mean) following 3-day heat treatment (150°C) under vacuum, while UV exposure and CO_2 supercritical extraction did not improve survival. Furthermore, parylene coating (25 μm), in combination with heat and sonication (in isopropanol) treatments effectively masked the SU-8 2000 and led to 86.4 ± 1.9 % viability. Glow discharge (oxygen plasma) treatment rendered the SU-8 2000 surface more hydrophilic and improved neuronal adhesion to the SU-8 surface. No organic leachants were detected by mass spectrometry before or after heat treatment or after sonication. However, XPS analysis revealed the presence of potentially neurotoxic elements, fluorine and antimony. Strategies to improve SU-8 2000 cytocompatibility to

primary neurons will allow longer culture times and have applications for cell-based microfabrication.[1]

Key words. neurons, microfabrication, MEMS, MEA, process optimization, toxicity

---

Portions of this chapter were published previously in a collaborative study:
V.N. Vernekar, D.K. Cullen, N. Fogleman, Y. Choi, A.J. García, M.G. Allen, G.J. Brewer, and M.C. LaPlaca, "SU-8 2000 Rendered Cytocompatible for Neuronal BioMEMS Applications," Journal of Biomedical Materials Research A 2009, 89: 138–151.[1]

Introduction

Microfabrication advances have resulted in small, inexpensive, and precise devices for biological microelectromechanical systems (bioMEMS) [1]. SU-8, a negative, near-UV photoresist, enables the manufacturing of high-aspect ratio thick MEMS structures [2-4]. The original SU-8 formulation used gamma-butyrolactone as the solvent [2-3], while the more recent SU-8 formulations, using cyclopentenone as a solvent, are referred to as SU-8 2000 [4]. Exposed SU-8/SU-8 2000 resists are thermally and chemically stable due to their aromatic functionality and highly cross-linked matrix [3-7], making them ideal for the fabrication of high-aspect ratio 3-D microelectrode culture systems. A 3-D microelectrode system made using SU-8 / SU-8 2000 requires cytocompatibility [8-9].

Cytocompatibility studies of SU-8 / SU-8 2000 to date have focused on the original SU-8 formulation using both neuronal and non-neuronal cells and tissues. In addition, many current systems in use do not incorporate an appreciable amount of SU-8 (e.g., 5μm insulation layer in Ayanda Biosystem's multielectrode arrays (MEAs)) [10-15], drastically reducing the potential toxic leachants. Neural applications include dissociated cultures, as well as slice cultures. For example, in a microfluidic device made partially out of SU-8, chick embryonic motoneurons were viable for up to 48 hours [8]. In another study, while electrophysiological activity was detected in neuronal cultures for 45-60 days within SU-8 containing MEAs, no quantitative viability assessment was performed [16]. Neuroblastoma cells cultured on thick SU-8 2000 structures showed poor cell adhesion [17]. Several other studies have used 5μm insulation layer SU-8-

containing structures to monitor electrophysiological activity in slice preparations, yet viability as a function of materials in the devices was not evaluated [10-11, 13, 15].

Because of the paucity of toxicity-related information for thick SU-8 2000 coatings with neuronal cell types, investigations on biocompatibility of cured SU-8 using non-neuronal cell types may be relevant in determining conditions that contribute to cell toxicity. For example, SU-8 implanted within stainless steel cages in a subcutaneous rodent model had less bio-fouling and similar numbers of leukocytes accumulate compared to controls, suggesting that SU-8 is biocompatible [9], but SU-8 has also been found to be thrombogenic [18]. SU-8 has been shown to be toxic to cultured mouse fibroblasts, yet caused no overt complications when implanted in rabbit muscle [6]. Others have also observed that untreated SU-8 is incompatible with mammalian cells, yet following HNO_3 and ethanolamine treatments HeLa cells preferred hydrophilized SU-8 surfaces compared to non-hydrophilized SU-8 at least up to 4 days *in vitro* [19]. Therefore, the cytocompatibility of SU-8 / SU-8 2000 has not yet been established, likely due to differential cell responses and culture environments, variations in fabrication, material processing, and/or exposure to surface area.

Cytocompatibility of the SU-8 2000 series (MicroChem Corporation, Newton, MA) warrants investigation since it offers several processing advantages over the original SU-8 formulation, including significantly improved wetting, faster drying, and clean edge bead removal without the need for an intermediate bake step [4]. In the present study we show that thick untreated SU-8 2000 substrates ($\geq$ 100 μm), which can be associated with high-aspect ratio structures, are not compatible with primary neuronal culture. We postulate that the poor cytocompatibility of SU-8 2000 resulted from two sources: 1)

toxic leaching from the SU-8 2000 components; and 2) poor sustained neuronal adhesion. This study is the first reported characterization of SU-8 2000 cytocompatibility for *in vitro* neurobiological applications and presents several preparatory treatments for improved compatibility with primary neurons, which may be applicable to improvement of both SU-8 and SU-8 2000 materials.

Materials and Methods

Fabrication of SU-8 2000 substrates

An empirically derived modification of SU-8 2000 substrate processing, based on manufacturer's recommended procedure (Nano SU-8 2000 Negative Tone Photoresist Formulations 2035-2100. Newton, Microchem) [20] was used to fabricate high-aspect ratio (20:1) thick micro structures (up to 700 μm thick) [21]. Similar adapted protocols have been used previously, with pre- and post-baking times and UV exposures in a range similar to that used here for obtaining thick high-aspect ratio structures from SU-8 2000 [22-25]. A 100 μm (or 300 μm) thick layer of SU-8 2000 (either SU-8 2025 or SU-8 2050) (MicroChem Corp., Newton, MA) was spin-coated at 500 rpm (CEE Model 100CB Spinner, Rolla, MO) on a glass substrate (Figure 3.1) and pre-baked (30 minutes for the 100 μm samples or 4 hours for the 300 μm samples) at 95°C to remove the solvent from the resist layer. The two thicknesses allowed the study of two representative members of the SU-8 2000 series. The SU-8 2000 substrates were subsequently exposed to UV light (1000 mJ for the 100 μm samples and 2000 mJ for 300 μm samples) through a checkerboard-patterned mask to initiate crosslinking of the exposed SU-8 2000 plateaus (OAI HYBRALIGN Series 500 system, Optical Associates, Inc. Mask Aligner, San Jose, CA). Following the UV exposure the SU-8 2000 substrates were post-baked on a hotplate at 95°C (30 minutes for the 100 μm samples or 40 minutes for the 300 μm samples), changing the linear oligomer to a crosslinked network structure. Both the pre- as well as post- baking followed the alternatively recommended ramp procedure for baking on hot plate by initially ramping the temperature from 65°C to 95°C in 10

minutes. The SU-8 2000 substrate was then developed using PGMEA (Propylene Glycol Monomethyl Ether Acetate, Rohm and Haas Electronic Materials, North Andover, MA), removing the uncrosslinked regions and resulting in SU-8 2000 plateaus separated by the checkerboard pattern. Individual 1 cm^2 x 100 μm (or 300 μm) thick SU-8 2000 plateau samples were separated manually using forceps. These were assayed as untreated samples and used for the various treatments described below.

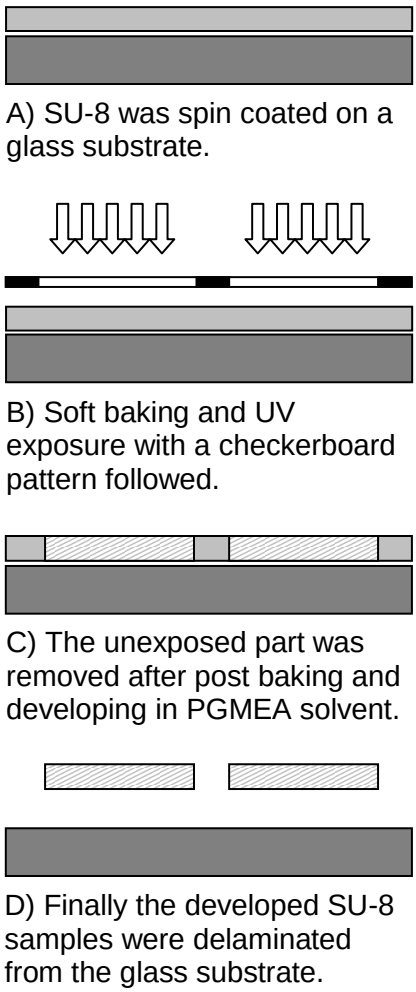

Figure 3.1. Microfabrication process for making SU-8 2000 samples. The different stages in the fabrication process include: spin coating, soft baking, UV exposure, post baking, developing in PGMEA, and finally delamination. Figure is not drawn to scale.

SU-8 2000 Treatments and Coating

Initially, the effect of exposure to SU-8 2000 on neuronal culture viability was determined by culturing cells adjacent to untreated samples and reused SU-8 2000 samples (used previously by us in cell culture for 34 days, to test the effect of long-term exposure to cell culture media on toxicity). SU-8 samples were processed for reuse by rinsing with 70% ethanol, and sterile de-ionized water. After drying, substrates were re-coated with poly-D-lysine. By placing cultures adjacent to the SU-8 2000 samples, we eliminated the variable of poor adhesion possibly contributing to the cell response. Next, the following treatments were employed to assess their ability to make SU-8 2000 more cytocompatible to neurons in culture adjacent to the SU-8 2000 samples: heating at 150°C for 3 days under vacuum (hard baking) (referred to as *H* hereafter), ultraviolet (UV) light exposure of 90 J/cm^2 (OAI HYBRALIGN Series 500 system, Optical Associates, Inc. Mask Aligner, San Jose, CA) (*UV*) and CO_2 supercritical extraction for 30 minutes (Autosamdri-815B, Tousimis Supercritical Dryer, Tousimis, Rockville, MD) (*CO_2*). The combination treatments tested were: *UV + CO_2, H + UV, H + CO_2, H + UV + CO_2*.

In addition, ultrasonication in isopropanol (Mettler Electronics model # 4.6, 85 W) (*S*) of *H* treated SU-8 2000 samples was performed for 0, 1, 3, or 15 minutes, followed by oxygen plasma treatment (EMS-100, Electron Microscopy Sciences, Hatfield, PA) and assessed for cytocompatibility. Finally, the effect of 30, 90, 180, 270 or 360 seconds glow discharge oxygen plasma treatments (*O_2*) or parylene coating (25 μm) (parylene C, poly(monochloro-p-xylylene), Cookson Electronics, Providence, RI; PDS 2010 LABCOATER, Specialty Coating Systems, Indianapolis, IN) (*P*) on the

cytocompatibility of *H + S* treated SU-8 2000 was also studied, in order to improve cell adhesion while testing for exposure to possible toxic leachants. The cultures tested in the experiments described here, therefore, were cultured on top of the SU-8 2000 samples.

Tissue culture treated polystyrene surfaces (Corning Inc., Corning, NY) or glass substrates (VWR Scientific, West Chester, PA) with or without a 25 μm parylene coat served as controls. All cell culture surfaces were coated with poly-D-lysine (100 μg/ml) before plating. Table 3.1 summarizes the experimental design for testing of the SU-8 2000 treatments. A subset of experiments was designated to simultaneously vary a number of conditions to identify a set of adequate conditions for further testing. Once treatment conditions suggested efficacy, a time series was evaluated with additional power obtained with group replication (e.g., Figures 3.4 and 3.6).

Table 3.1. Summary of the various SU-8 2000 treatments studied. The various bulk detoxification and surface treatments used are summarized. All culture surfaces were coated overnight with 100 µg/ml poly-D-lysine, n = number of replicates, DIV = days *in vitro*, Cort. = E17-18 primary cortical neurons, Hipp. = E17-18 primary hippocampal neurons, New = Untreated = new SU-8 2000 without any treatment mentioned in the table, Reused = SU-8 2000 without any treatment mentioned in this table but previously used in cell culture for 34 days, H = heating at 150°C for 3 days in vacuum, UV = UV light exposure of 90 J/cm^2, CO_2 supercritical extraction for 30 minutes, S = isopropanol sonication, P = parylene coating, O_2 = O_2 plasma treatment.

Treatments	n per Treatment	Cell Type	Plating Location with respect to SU-8	Plating Density (cells / mm^2)	# of SU-8 Samples per Culture, Sample Dimensions	Controls	Live/ Dead Time Point (DIV)	Results Figure #
New	4	Cort.	Adjacent	1000	4, 10 x 10 x 0.1 mm^3	Polystyrene, n=12	21	2
Reused	5							
H	4	Cort.	Adjacent	1000	4, 10 x 10 x 0.1 mm^3	Polystyrene, n=4	21	3
UV								
CO_2								
UV + CO_2								
H + UV								
H + CO_2								
H + UV + CO_2								
Untreated								
H	2	Hipp.	On top	500	2, 10 x 10 x 0.3 mm^3	Glass slip, n=2	7	4
H + S (1 min, 70% IPA)								
H + S (3 min, 70% IPA)								
H + S (15 min, 70% IPA)								
H + S (30 min)	5	Cort.	On top	1000	1, 10 x 10 x 0.1 mm^3	25 µm Parylene coated glass slip, n=5	7	5
H + S (30 min) + P (25 µm)								
H + S (1 min, 70% IPA) + O_2 (30, 90, 150 sec)	8 fields across one culture	Hipp.	On top	1000	1, 10 x 10 x 0.3 mm^3	Glass slip, n=2	7	6
H + S (1 min, 100% IPA) + O_2 (30 sec)								
H + O_2 (30 sec)								
H + S (1 min, 70% IPA)								
H								

Sterilization of SU-8 2000 Samples

SU-8 2000 samples were attached to polystyrene cell culture wells and sterilized with 70% ethanol under a laminar flow hood with ultraviolet light for 30 minutes, followed by rinsing in sterile filtered deionized (DI) water under UV light for 30 minutes, aspirating off the DI water, and exposing to 60 minutes of continued UV. SU-8 2000 samples that were attached to glass were sterilized by 45 minutes of UV exposure only**.** During sterilization the samples were placed at distances ≥ 65 cm from the laminar flow hood UV lamp (minimum distance of lamp from the working bottom surface of hood) with an intensity ≤ 0.6 J/cm^2.

Neuronal Cell Culture

Timed-pregnant Sasco Sprague-Dawley rats (Charles River, Wilmington, MA) were anesthetized using halothane (Halocarbon Laboratories, River Edge, NJ) at embryonic day 17-18 and decapitated. Fetuses were removed and placed in Hanks balanced salt solution (HBSS, Invitrogen). All procedures involving animals were approved by the Institutional Animal Care and Use Committee (IACUC) of the Georgia Institute of Technology or that of the Southern Illinois University, following NIH guidelines for the care and use of laboratory animals (NIH Publication # 85-23 Rev. 1985). Cerebral cortices and hippocampi were isolated and dissociated using pre-warmed trypsin (0.25%) + 1 mM EDTA (Invitrogen, Carlsbad, CA) for 10 min at 37ºC followed by deoxyribonuclease I (0.15 mg/mL, Sigma, St. Louis, MO) in HBSS (or papain, 2 mg/ml in Hibernate-calcium) (BrainBits LLC, Springfield, IL). The tissue was triturated with a flame-narrowed Pasteur pipette and centrifuged at 1000 rpm for 3 minutes and the

cells were resuspended in Neurobasal medium + 2% B-27 + 500 μM L-glutamine (Invitrogen, Carlsbad, CA). Cultures were plated in standard polystyrene 6 well plates (Corning Inc., Corning, NY) or 24 x 60 mm glass cover slips (VWR Scientific, West Chester, PA) both pretreated with 100 μg/ml poly-D-lysine (Sigma, St. Louis, MO). As summarized in Table 3.1, neurons were plated either adjacent to or directly on test biomaterials (e.g., SU-8 2000, glass controls, parylene coated glass controls), which were adhered to polystyrene wells or glass using polydimethylsiloxane (PDMS, Sylgard® 184 and 186 Silicone Elastomer Kit, Dow Corning Corporation, Midland, MI). Cortical cells were plated at a density of 1000 cells/mm^2; hippocampal cells were plated at 500 or 1000 cells/mm^2. These plating densities have been used previously for MEA studies and result in a cell density which permits recording at the electrodes while maintaining discernable cell-cell distances [26-27]. Cultures were incubated at 37°C and 5% CO_2-95% humidified air, and fed every 3-4 days *in vitro* (DIV) by replacing half the media with media pre-warmed to 37°C. Both embryonic cortical and hippocampal neurons were used in order to evaluate various SU-8 2000 treatments on two commonly used culture types, which allows the isolation of cells without causing irreversible damage of sheared axons and dendrites, as seen in adult tissue [28-30]. A culture time of one week was used to test acute effects of the SU-8 2000 (surface chemistry related) on the cultures that were plated on top of the SU-8 2000, while a 3 week culturing time point was used for assessing the chronic effects of SU-8 2000 leaching on cultures that were plated adjacent to the SU-8 2000. We used a sensitive and inexpensive *in vitro* testing method where the test material was directly exposed to the cell culture medium [31], and immobilized so as not to disturb the cell culture by floating or scratching it [32].

Live-Dead Staining for Assessing the Cytocompatibility of SU-8 2000 after Treatments

Fluorescent probes were used for distinguishing live and dead cells (LIVE/DEAD Viability/Cytotoxicity Kit; Molecular Probes, Eugene, OR) at 7 or 21 DIV. Cell cultures were incubated with 2 μM calcein AM (live cell probe) and 4 μM ethidium homodimer-1 (EthD-1) (dead cell probe) at 37° C for 30 minutes and rinsed in 0.1M Dulbecco's phosphate buffered saline (D-PBS, Invitrogen, Carlsbad, CA) before imaging.

Data Collection and Statistical Analysis

Fluorescent microscopy imaging was performed with either a Nikon Eclipse TE300 (Nikon Instruments Inc., Melville, NY), an Olympus BX51WI (Melville, NY), or a Zeiss 510 Laser Scanning Confocal Microscope (Carl Zeiss AG, Göttingen/Germany). Two to eight photomicrographs were taken per cell culture well for quantification. Image regions were randomly selected either by triangulation, or imaging at the four ends of a square and the center of the cultures. To prevent counting errors, all images were independently quantified twice (once by drawing a circle around each accounted cell), and only those corresponding counts that were within ±10% of each other were considered. Those counts that did not fit this criteria were recounted independently, and the process independently continued until consistently repeatable counts were obtained.

Cell culture data are presented as % viability and live cell density. Percent cell viability is the ratio of live over total *adherent* cells (live + dead) at the time of assaying, and not over *all* the cells that were originally present. This methodology does not take

into account cells that have been washed away from the surface during media changes and rinses. Comparisons between plating and final densities of cells on the different surfaces, therefore, would provide an estimate of the number of cells lost, assuming no proliferation. On the other hand, live cell density or live cells/mm^2 is the live cell count per area of substrate at the time of assaying. Data are presented as mean ± standard error of the mean. General linear model ANOVA was performed followed by Student-Newman-Keuls pairwise comparisons ($p < 0.05$ was considered significant).

Mass spectrometry, X-ray Photoelectron Spectroscopy (XPS) and Contact Angle Measurements

Mass spectrometry analysis was conducted to identify possible organic leachants from SU-8 2000 that could be toxic to the cells. Glass vials were rinsed with ethanol, DI water, and isopropanol and filled with ACS reagent grade isopropanol (2 mL). In one of the vials five SU-8 2000 samples (1cm x 1 cm x ~100μm) were added (*S*), while in another five SU-8 2000 samples from the same batch that were heat treated in a vacuum oven at 150°C for three days were added (*H + S*) while the third vial was used as a blank isopropanol control (*Blank S*). Vials were placed in an ultrasonication bath for 30 minutes, followed by removal of the solvent phase for analysis by mass spectrometry. Gas chromatography (J & W Column, DB-5, 30 m length, 0.25 mm I.D., J & W Scientific, Folsom, CA) was used to separate the potential leachants in the isopropanol solvent, followed by electron ionization mass spectrometry (VG 70SE, VG Instruments, Manchester, UK). Likewise, liquid chromatography (Agilent 1100 Series, Supelco C18, 100 mm length, 1 mm I.D., Agilent Technologies, Palo Alto, CA) was used to separate

the potential leachants, followed by electrospray mass spectrometry (Micromass Quattro LC, Manchester, UK). Separate samples were concentrated until completely dry, and reconstituted in 100 µl of isopropanol. Samples were injected onto a gas chromatography column followed by electron ionization mass spectrometry, as well as vaporized in a heated solids probe followed by electron ionization mass spectrometry, or reconstituted in 200 µl of water and subjected to liquid chromatgrophy followed by electrospray mass spectrometry.

The elemental composition analyses of the SU-8 2000 surfaces after various bulk detoxification and surface treatments were performed using XPS analysis (Surface Sciences Instruments Model SSX-100 Small Spot ESCA Spectrometer equipped with a monochromatized Al K-alpha X-ray source (1486.6 eV); Mountain View, CA). The operating pressure in the analysis chamber was maintained at 3.0×10^{-9} Torr or lower during the measurements. Each sample was scanned at 1-2 spots (100 µm diameter, X-ray spot size). For each spot, general survey scans (analyzer pass energy of 150 eV) were obtained for a sample from each of the above treatments followed by high resolution C1s and O1s scans (analyzer pass energy of 50 eV). The binding energies (BEs) were referenced to the C1s (C-H) peak at 285.0 eV, to compensate for the effects of charging. All treatments were done as described previously, except the oxygen plasma treatment, which was conducted in a Plasma Therm RIE 700 series reactive ion etcher (Plasma-Therm, Inc., Saint Petersburg, FL) at a pressure of 200 mTorr, O_2 flow of 100 standard cubic centimeters per minute O_2, 200 W power for one min.

The effect of oxygen plasma treatment on SU-8 2000 surface hydrophilicity was assessed by measuring contact angle. The ambient air-water-substrate contact angle

measurements (2 µl of deionized H_2O) were taken with a Rame-Hart 100-00 goniometer (Mountain Lakes, NJ) fitted with a digital camera and analyzed using in-house image analysis software. Table 3.2 summarizes the various analytical techniques used to study the different SU-8 2000 treatments.

Table 3.2. Summary of the analytical techniques used for assessing SU-8 2000 after various treatments. Mass spectrometry, X-ray photoelectron spectroscopy, and contact angle goniometry techniques were used for assessing SU-8 2000 after the various treatments. GC = gas chromatography, EIMS = electron ionization mass spectrometry, LC = liquid chromatography, ESMS = electro spray mass spectrometry, HPEIMS = heated probe electron ionization mass spectrometry, Blank S = 30 minutes blank isopropanol sonicated control, Untreated = new SU-8 2000 without any treatment, H = heating at 150 °C for 3 days in vacuum, S = sonication in isopropanol for 30 minutes, O_2 = O_2 plasma treatment for 1 minute, P = parylene coating of 25 µm.

Analytical Techniques	**Treatments**
Mass Spectrometry 1. GC + EIMS 2. LC + ESMS 3. Samples dried and reconstituted in 100 µl isopropanol + GC + EIMS 4. Samples dried and reconstituted in 100 µl isopropanol + HPEIMS 5. Samples dried and reconstituted in 200 µl water + LC + ESMS	Blank S S H + S
X-Ray Photoelectron Spectroscopy	Untreated H S H + S H + S + O_2 H + S + P H + S + P + O_2
Contact Angle Goniometry	Untreated O_2

Results

Assessment of Cell Viability Resulting from Exposure to Fresh and Reused SU-8 2000

At 21 DIV cortical neuronal cultures adjacent to SU-8 2000 samples had significantly lower viability than the plain polystyrene control groups (6.6 ± 6.6 % vs. 70.9 ± 3.7 %) (Figure 3.2), indicating that neurons die when cultured in media contacting SU-8 2000. Soaking SU-8 2000 substrates in culture medium at 37^{o}C during cortical neuronal culture improved neuronal survival in subsequent cultures; neuronal viability was improved (to 40.8 ± 5.5 %) in cultures growing adjacent to reused SU-8 2000, suggesting that toxic leachants may be removed from SU-8 2000 during prior cell culture period.

Assessment of Different Bulk Detoxification Treatments for SU-8 2000

At 21 DIV, with the exception of the heat treatment(*H*), all other treatments (*UV, CO_2, UV + CO_2, H + UV, H + CO_2, H + UV + CO_2*) resulted in neuronal viability in adjacent cultures significantly lower than control cultures (Figure 3.3). The heat treatment resulted in viability of 45.8 ± 4.5 % as compared to 61.1 ± 5 % in polystyrene controls. Neuronal viability following UV exposure (0.3 ± 0.3 %) and CO_2 supercritical extraction (0.1 ± 0.15 %) treatments was significantly less than untreated SU-8 2000 samples (6.6 ± 6.6 %). The measured cell densities for treatments and control groups at the end of the culturing period were lower than the cell densities at plating (500-1000 cells/mm^2) indicating cell loss after plating. The control viabilities in the range of 60-

70% at the time point tested are consistent with a previous report [33]. Comparisons between plating and final densities of cells on the different surfaces provide an estimate of the loss of cells from these materials, assuming no proliferation.

Heat plus ultrasonication in isopropanol for 15 minutes resulted in an increased density of live cells on SU-8 2000 beyond that obtained through heat treatment alone (Figure 3.4). The plating of cells in this experiment was on top of the SU-8 2000 samples, indicating that sonication over a period of time improves adhesion of the neurons to SU-8 2000 with consequent better survival, but with less effect on the ratio of live to total cells.

Assessment of Adhesive Surface Treatments for SU-8 2000

There was a significant improvement in live cell density (for cells cultured on top of the SU-8 2000 samples) on heat and sonication treated SU-8 2000 substrates following parylene coating (25 μm) (556.9 ± 68.3 live cells/mm^2) compared to uncoated (308.6 ± 81.1 live cells/mm^2), which was comparable with parylene-coated glass controls (626.2 ± 58.2 live cells/mm^2) (Figure 3.5). Oxygen plasma treatment improved live cell density and greatly increased neurite outgrowth for cells cultured on top of the SU-8 2000 samples (Figure 3.6). The relative benefit of the heat + sonication (*H*+*S*) treatments reported in Figure 3.4 as can be seen in Figure 3.6.

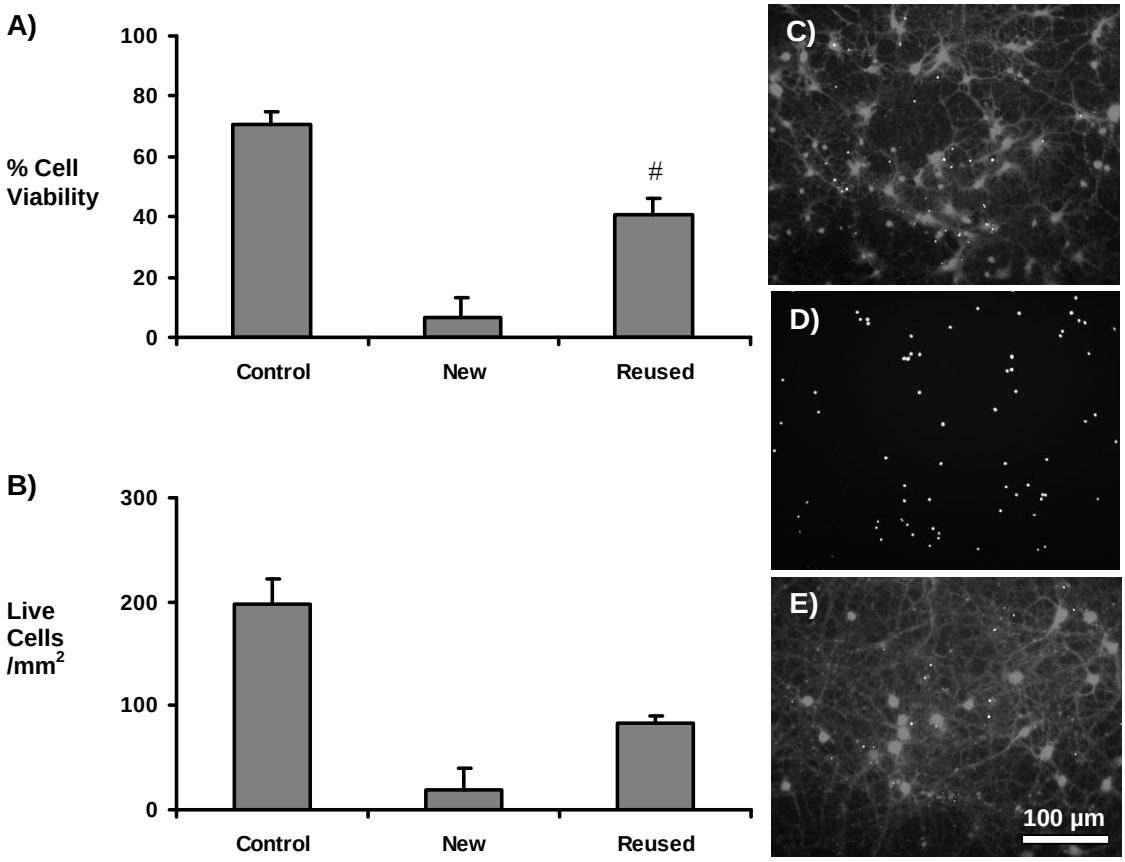

Figure 3.2. Assessment of cell viability of neural cultures plated adjacent to fresh and reused SU-8 2000 samples. Cellular response to SU-8 2000 exposure quantified as % cell viability (A), and live cells/mm^2 (B), with representative photomicrographs of neuronal cultures plated on polystyrene controls (*Control*, C), on polystyrene adjacent to new SU-8 2000 samples (*New*, D), and on polystyrene adjacent to reused SU-8 2000 samples (*Reused*, E) labeling live cells (gray) and dead cell nuclei (white). Neural cultures adjacent to SU-8 2000 samples that have been used previously in cell culture (*Reused*) have significantly higher viability than parallel cultures plated adjacent to new SU-8 2000 samples (*New*) (# $p<0.005$).

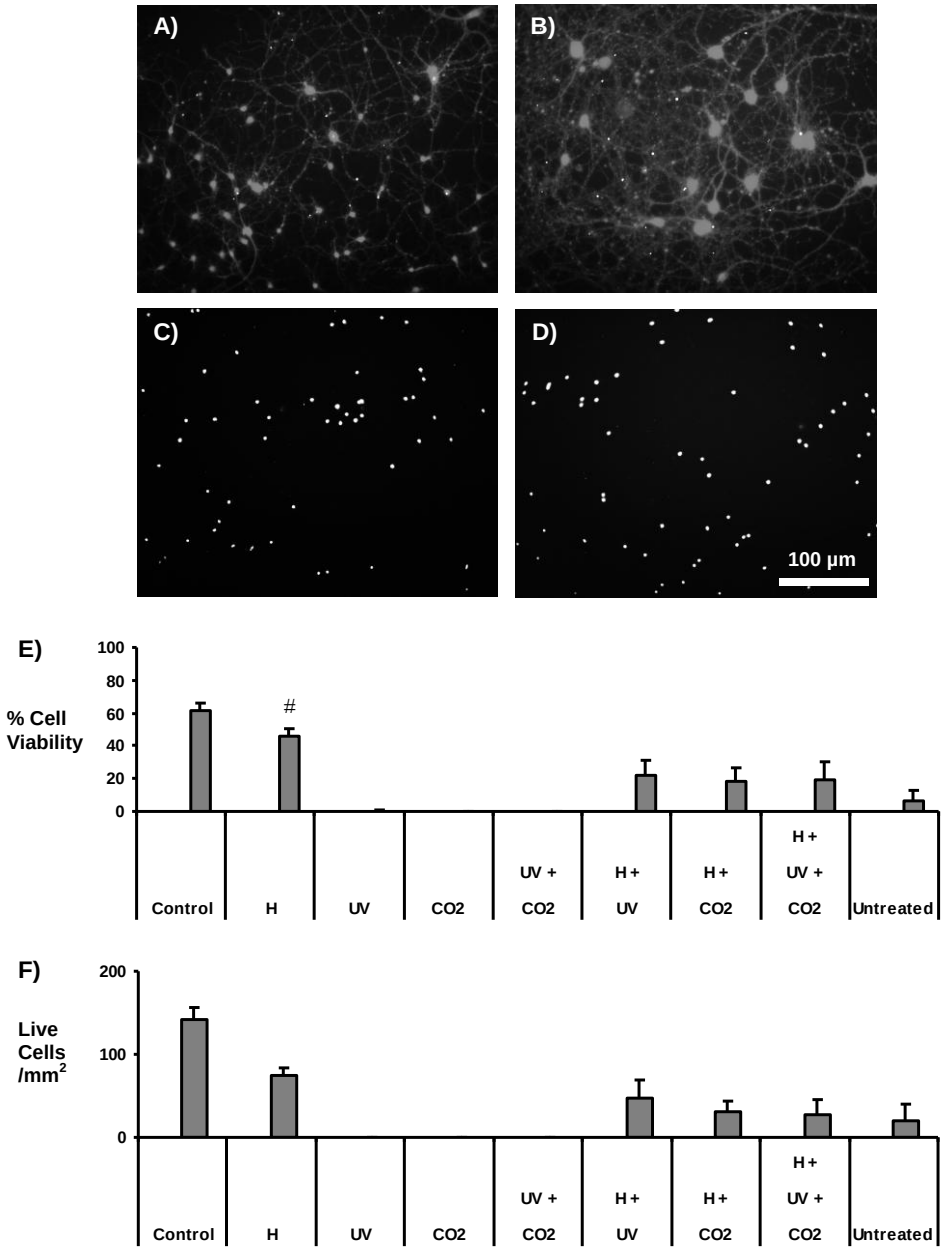

Figure 3.3. Assessment of different bulk treatments on SU-8 2000 samples for improving cytocompatibility with adjacent neuronal cultures. Representative photomicrographs of neuronal cultures plated on polystyrene controls (*Control*, A), on polystyrene adjacent to SU-8 2000 samples that were heat treated (*H*, B), on polystyrene adjacent to SU-8 2000 samples that were treated with UV exposure (*UV*, C), on polystyrene adjacent to SU-8 2000 samples that were treated with CO_2 under supercritical conditions (CO_2, D) labeling live cells (gray) and dead cell nuclei (white). The cellular response to these treatments and their combinations are quantified as % cell viability (E), and live cells/mm^2 (F). Cell viability following heat treatment (*H*) was significantly improved compared to the other detoxifying treatments (# $p<0.05$).

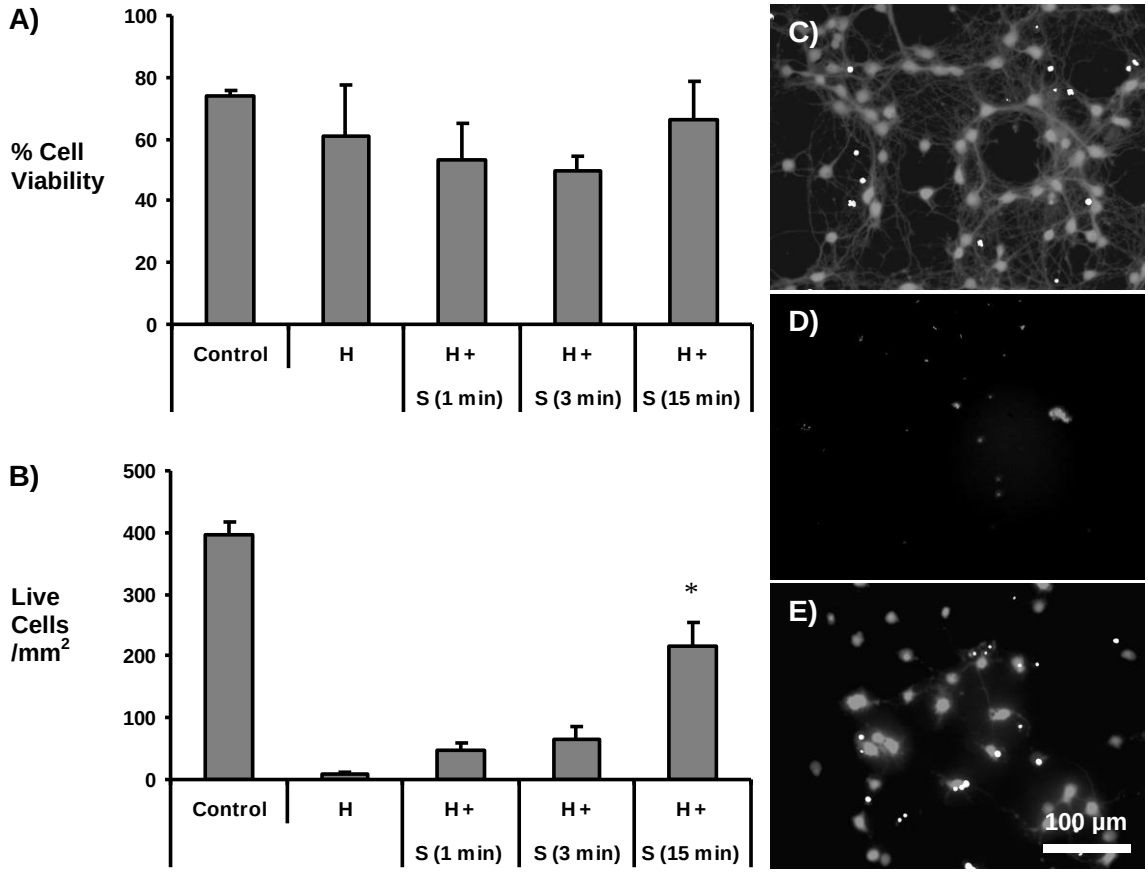

Figure 3.4. Assessment of sonication of SU-8 2000 in isopropanol for improving cytocompatibility with neuronal cultures. Neuronal cultures plated on top of SU-8 2000 after heat plus sonication treatments quantified as % cell viability (A), and live cells/mm^2 (B), with representative photomicrographs of neuronal cultures plated on glass controls (*Control*, C), on heat treated SU-8 2000 samples (*H*, D), on heat treated SU-8 2000 samples with 15 minutes of sonication in isopropanol (*H + S (15 min)*, E) labeling live cells (gray) and dead cell nuclei (white). Longer periods of sonication in isopropanol produced better live cell density in culture. Live cell density for the 15 min isopropanol sonication treatment in addition to the heat treatment (*H + S (15 min)*), was significantly higher than the live cell density following the other detoxifying treatments (* $p<0.0005$).

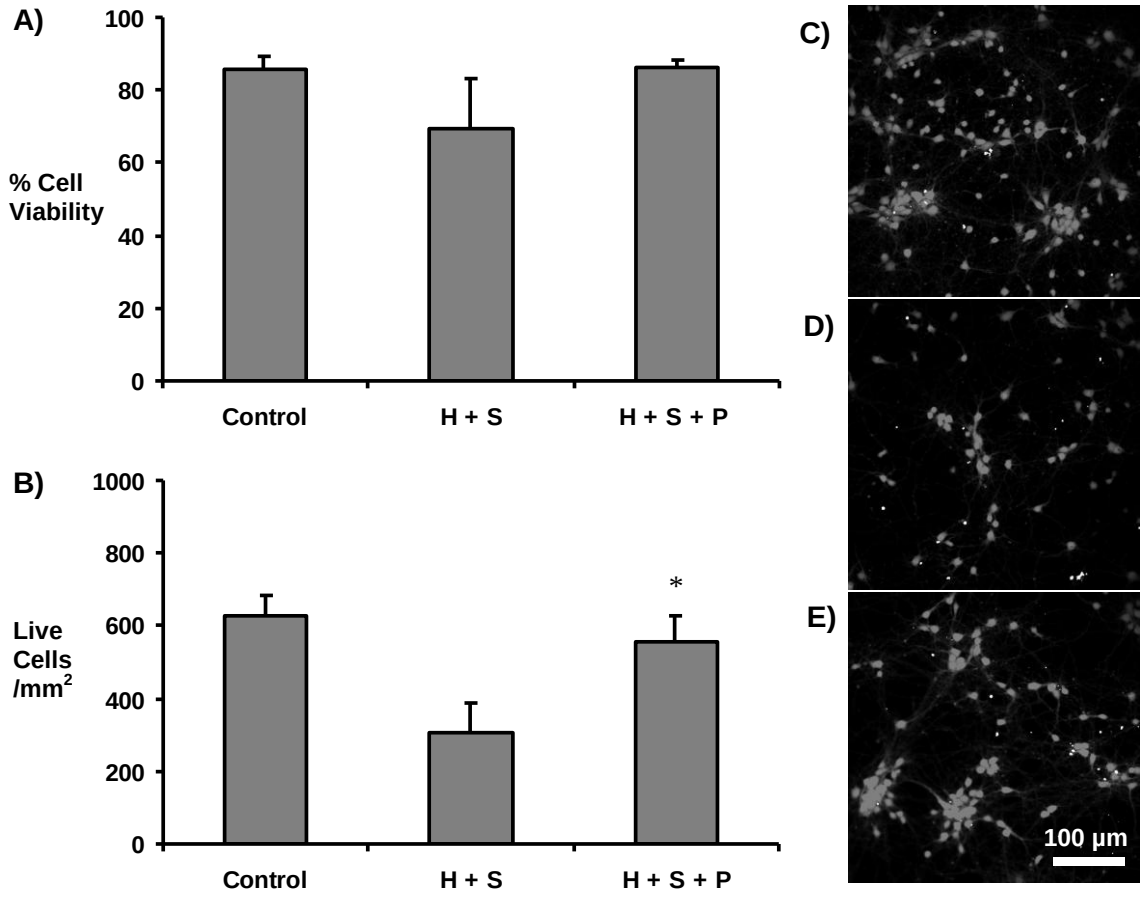

Figure 3.5. Assessment of parylene coating of SU-8 2000 samples for improving cytocompatibility with neuronal cultures. Neurons were plated on top of SU-8 2000 samples treated for 30 min by sonication in isopropanol following the heat treatment with or without parylene coating. Cellular responses are presented as % cell viability (A), and live cells/mm^2 (B), along with representative photomicrographs of neural cultures plated on parylene coated glass controls (*Control*, C), on heat treated plus isopropanol sonicated SU-8 2000 samples (*H + S*, D), on H + S treated SU-8 2000 samples followed by parlyene coating (*H + S + P*, E) labeling live cells (gray) and dead cell nuclei (white). Heat plus sonicated SU-8 2000 with parylene coating (*H + S + P*) resulted in significantly improved live cell density compared to just the heat plus sonicated SU-8 2000 samples (*H + S*), and was statistically indistinguishable from the control cultures (*Control*) (*$p<0.05$).

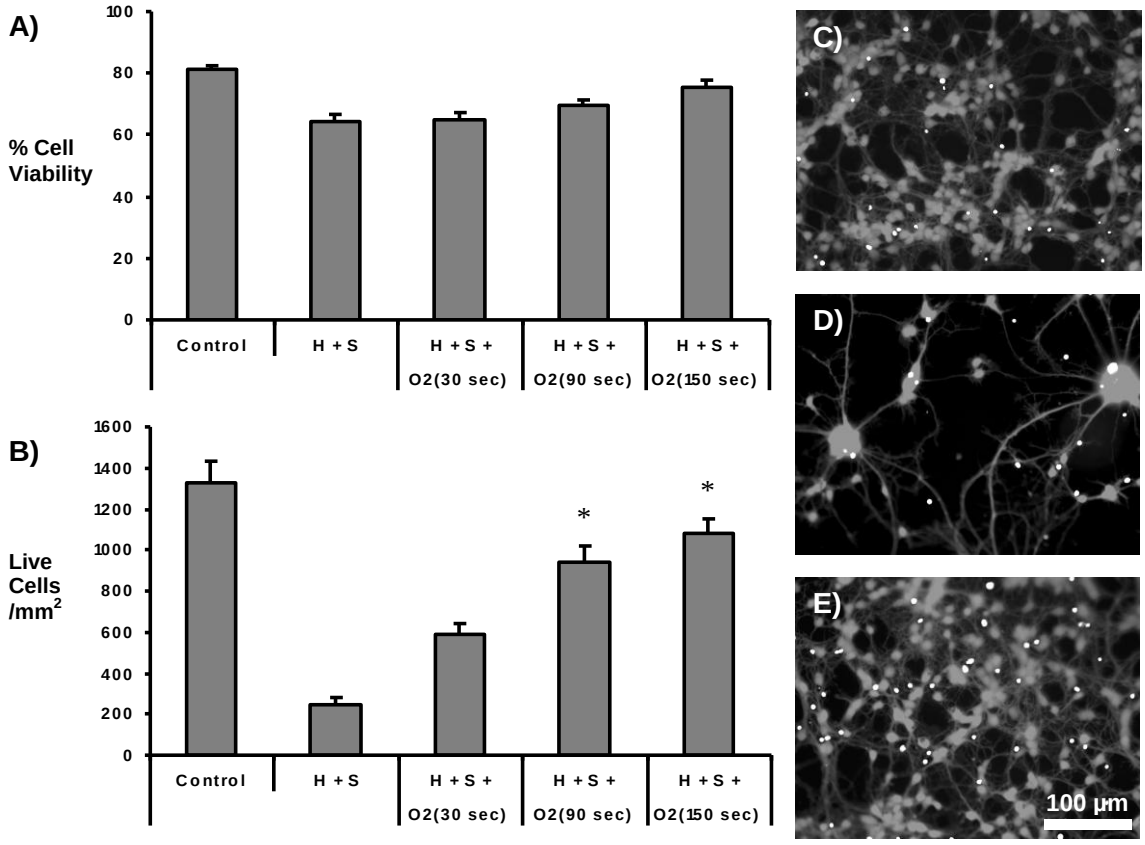

Figure 3.6. Assessment of different periods of glow discharge (oxygen plasma) treatment for improving cytocompatibility of SU-8 2000 samples. Neurons plated on top of heat plus isopropanol sonicated SU-8 2000 samples with or without glow discharge treatment were quantified as % cell viability (A), and live cells/mm^2 (B). Representative photomicrographs of neural cultures are shown on the right for cells plated on glass controls (*Control*, C), on heat plus isopropanol sonicated SU-8 2000 samples (*H + S*, D), on H + S treated SU-8 2000 samples with 150 seconds of glow discharge (*H + S + O_2 (150 sec)*, E) labeling live cells (gray) and dead cell nuclei (white). Live cell densities for the glow discharge treatments at 90 seconds (*H + S + O_2 (90 sec)*) and 150 seconds (*H + S + O_2 (150 sec)*) were significantly better than the other treatments but were statistically indistinguishable from each other (* $p<0.05$).

Mass Spectrometry, X-ray Photoelectron Spectroscopy (XPS) and Contact Angle Measurements

Mass spectrometry analyses of all the different treatments did not reveal the presence of organic-based leachants from the SU-8 2000. The chromatograms and mass spectrograms for each of the treatments were indistinguishable from controls for all treatments (data not shown). The large molecular weight sensitive mass spectrometry techniques we used were not tuned for the detection of metals, so although undetected, the presence of metallic leachants could not be ruled out.

In the absence of any surface treatment such as parylene coating or oxygen plasma treatment, XPS analysis showed that the SU-8 2000 bulk detoxification treatments do not change the oxygen to carbon (main elemental components of SU-8 2000) ratio in SU-8 2000, which was approximately 0.2. However, XPS analysis revealed the presence of fluorine. Analysis showed that after oxygen plasma treatment, the oxygen to carbon ratio of SU-8 2000 increased from approximately 0.2 to approximately 1.4, and fluorine and antimony were also detected. Parylene C coating on the SU-8 2000 resulted in an XPS spectra without oxygen peaks, but chlorine peaks were evident, as is characteristic of the parylene C molecular structure [34]. After oxygen plasma treatment of the parylene coated SU-8 2000 however, the oxygen to carbon ratio increased from 0.0 to approximately 0.4. The presence of silicon in the SU-8 2000 is attributed to contamination from the processing environment, such as previous materials used in the processing equipments, since it is not normally expected to be present in SU-8 / SU-8 2000 [2-4, 35-36]. Table 3.3 summarizes the XPS results.

Table 3.3. Assessment of the surface elemental composition of SU-8 2000 samples with the various treatments tested in this study using x-ray photoelectron spectroscopy. Most treatments did not affect the O/C ratio, however, the glow discharge (oxygen plasma) treatment significantly increased this ratio. Presence of fluorine as well as antimony was revealed in the SU-8 2000.

Treatments	**Elemental Composition**						**O%/C% Ratio**
	C %	**O %**	**F %**	**Si %**	**Sb %**	**Cl %**	
Untreated	82	16	2	0	0	0	*0.2*
H	78	17	1	5	0	0	*0.2*
S	66	14	20	0	0	0	*0.2*
H + S	83	17	0	0	0	0	*0.2*
H + S + O_2	37	54	2	0	8	0	*1.4*
H + S + P	86	0	0	0	0	14	*0.0*
H + S + P + O_2	67	29	0	0	0	5	*0.4*

Contact angle measurements were performed to study the effect of oxygen plasma treatments on the SU-8 2000 surface hydrophobic-hydrophilic character. The water contact angle was reduced from 72.9 ± 1.5 ° to 37.0 ± 2.3 ° after oxygen plasma treatment.

Thus, while mass spectrometry reduced the possibility of organic leachants from the SU-8 2000 after the heat treatment and during the isopropanol sonication, XPS analysis pointed to fluorine and antimony as candidate leachants from the SU-8 2000. Parylene coating resulted in the SU-8 2000 surface being masked of fluorine and antimony and any other potential leachants, while oxygen plasma treatment increased the oxygen groups on the SU-8 2000 surface, thereby making it more hydrophilic, as evidenced by the decreasing water contact angle measurements. While oxygen plasma appeared to expose low levels of fluorine (from a few nanometers below the SU-8 surface), the fluorine levels are only 10% of those detected after extraction by sonication

alone (presumably being washed away during the poly-D-lysine coating prior to cell culture). This suggests that oxygen plasma treatment (which slightly etches the surface) after heat and sonication treatments, simply exposes the remaining fluorine and antimony from depths below the SU-8 surface (which may not be sensed by the cells), in addition to removing any that was accessible to XPS after the sonication treatment alone.

Discussion

We found that SU-8 2000 is not cytocompatible with primary cortical or hippocampal neuronal cultures. While mass spectrometric analysis did not detect any organic leachants from the SU-8 2000, XPS analysis pointed to fluorine and antimony as candidate leachants from the SU-8 2000. The idea of toxic leaching is supported by poor viability of neuronal cultures plated adjacent to the SU-8 2000 samples. Both fluorine and antimony have the potential to be toxic and are present in the photo acid generator within the SU-8 2000 formulation [2, 35-38]. Heat treatment, isopropanol sonication, parylene coating, and oxygen plasma treatment improved SU-8 2000 cytocompatibility. Together these treatments improved viability and live cell density to equivalent levels of control grade glass or parylene coated glass, thus providing protocols to render SU-8 2000 more cytocompatible for biological applications with neurons.

As can be seen, the cell culture data for the different experiments conducted (Table 3.1) was analyzed and presented in the form of two parameters: percent cell viability and live cell density. Percent of viable cells (which accounts for the dead cells count) was particularly sensitive, in the adjacent cell culture experiments, to assess cell death as a result of toxic leaching. Whereas, the live cell density was sensitive, in cultures placed on top of the sample, to assess the number of viable cells that remained attached to the test biomaterial surfaces giving a measure of the material's cell adhesiveness.

When cells were cultured adjacent to (but not touching) SU-8 2000, they were exposed constantly to the SU-8 2000 through the cell culture media, a similar scenario to many BioMEMs applications. Decreased viability for cultures plated adjacent to SU-8

2000 samples indicated that SU-8 2000 contained one or more extractable substances toxic to neurons, in agreement with previous findings [6]. This tested the effect of gradual leaching that may occur from the SU-8 2000 into the cell culture media. Reusing the SU-8 2000 over two rounds of cell culture possibly aided in passive diffusion of these toxic agents from the SU-8 2000, thereby rendering it more cytocompatible. This provided an opportunity to detoxify SU-8 2000 through diffusive removal of leachants from the SU-8 2000. While we cannot rule out that protein adsorption at the surface of the SU-8-2000 occurred over the longer incubation periods, it is not likely to be substantial enough to prevent the diffusion of smaller molecular species such as fluorine and antimony, since the adsorbed protein is believed to not form more than a monolayer over the surface [39]. Furthermore, the poly-D-lysine may have formed a monolayer over the adsorbed protein layer, normalizing the effect of the protein layer on the cell culture. This is supported by the fact that the % cell viabilities as well as live cell density for new and reused controls were statistically indistinguishable from each other (data not shown). Control experiments demonstrated that the adhesive polydimethysiloxane (PDMS) used to attach the SU-8 2000 to the culture dishes had no adverse effects on cytocompatibility (data not shown).

XPS analysis revealed the presence of fluorine on the SU-8 2000 after the sonication treatment alone (20%), indicating that the sonication treatment assisted in extracting fluorine from at least a shallow depth in the SU-8 2000 substrate. Furthermore, minimal fluorine was detected after the heat treatment alone (~1%), indicating possible diffusive removal aided by heat. Finally, after heat followed by sonication treatment, no fluorine was detected, indicating that this treatment combination

resulted in the removal of fluorine from at least a shallow depth into the SU-8 2000 surface. This also explains the observation that after one minute of oxygen plasma treatment, which etches the SU-8 2000 surface by a few nanometers, low amounts of fluorine as well as antimony were detected, correlating with other studies [40]. While fluorine and antimony from the photo acid generator are potentially toxic to the cells [2, 35-38], cyclopentenone (the solvent used in the SU-8 2000 formulation, boiling point 130°C), and PGMEA (solvent used in developing SU-8 2000, boiling point 146°C) may also be toxic to neurons [4, 41-42].The heat and oxygen plasma treatments may remove residual levels of these solvents through faster diffusion and oxidation, respectively.

Sustained heating of SU-8 2000 for 3 days at 150°C under vacuum represents hard-baking of the material, which may enhance neuronal viability by three possible mechanisms: 1) by allowing for the crosslinking process of SU-8 2000 to reach completion as the photo-acid actively crosslinks the resist using thermal energy, effectively decreasing the void volume inside the polymer, increasing its viscosity, and thereby reducing the diffusion rates of the photocatalyzing acids as well as other species in the system, such as solvent molecules [3-4]; 2) by the faster diffusion of the toxic leachants out of the SU-8 2000 under high temperature and vacuum conditions; and 3) by making changes in the surface characteristics of the SU-8 2000. The mechanical properties of cured SU-8 films differ with the baking temperature and this difference was reduced when the baking temperature reached 150°C [43].

The improved cytocompatibility of SU-8 2000 after isopropanol ultrasonication treatment following the heat treatment may be partially due to the high solvating capability of isopropanol, along with the increased kinetic energy for diffusion provided

by ultrasonication, further helping in the removal of toxic leachants. The cured SU-8 2000 photoresist is highly crosslinked, resulting in a very low diffusion rate at the exposed surface under static conditions. Ultrasonication, not only may be increasing these diffusion rates, but also increasing turnover of the isopropanol solvating the leachants at the SU-8 2000 interface [5].

Parylene coating improves the live cell density on the SU-8 2000, presumably by providing a barrier to the diffusion of leachants. This is supported by the XPS data for parylene coated SU-8 2000 where fluorine and antimony peaks are absent. While parylene by itself cannot be used to make the high-aspect ratio MEMS structures, parylene coating may be useful especially for applications such as insulation on high-aspect ratio MEMS structures made out of SU-8 2000, because of ease in fabrication and its coating on SU-8 2000 enhances cell viability as compared to SU-8 2000 that is exposed to heat and sonication alone. Glow discharge treatment (oxygen plasma) was very effective in making SU-8 2000 more cytocompatible, consistent with the reported effects of wet chemical treatments [19, 44]. Such treatments essentially make the surface more hydrophilic by increasing oxygen species (as indicated both by the water contact angle and XPS measurements), allowing better cell adhesion. The oxygen plasma treatment is not only effective at creating oxygen rich groups, but also etches the surfaces, thereby removing possible toxic leachants as well as roughing the surface [1], which may improve cell attachment. While oxygen plasma treatment may have exposed new fluorine and antimony, the fluorine levels were much lower than those associated with sonication alone (2% as compared to 20%). Despite, these low levels of fluorine and the exposed antimony detected after the oxygen plasma treatment (which, probably

are washed away during the poly-D-lysine coating prior to cell culture), the concomitant neuronal survival and neurite outgrowth suggest that it is the large increase in oxygen (0.2 to 1.4 oxygen to carbon ratio), which may increase surface hydroxyl groups, contributing to better poly-lysine binding to the surface and improved cellular adhesion [45-46], leading to improved neuronal viability. In addition, since XPS probes up to a few nanometers below the surface contacted by the cells, the depth of the XPS probe is likely to be greater than the level sensed by cells.

We also observed that UV exposure exacerbated SU-8 2000 cytotoxicity, instead of reducing it, as expected. This suggests that the UV exposure possibly increases at least some of the toxic leachants. The excess of strong acids generated by the photo acid generator after UV exposure [43] may contribute to the enhanced cytotoxicity after UV flood exposure. The contribution of the UV used in sterilization to this toxicity is expected to be minimal because the UV dose from the biohazard hood UV lamp (used for sterilization, $\leq$ 0.6 J/cm^2) is much lower than that of the mask aligner (used for UV treatment, 90 J/cm^2) and because the distance of the samples from the UV lamp while sterilizing ($\geq$ 65 cm) is much greater than that of the UV source in the mask aligner (7 cm). The detection on SU-8 2000 by XPS of fluorine and antimony, both photo-acid generator associated elements, supports this conclusion. Likewise, CO_2 supercritical extraction also exacerbated toxicity of the SU-8 2000 rather than improving it. CO_2 treatment altered the physical characteristics of the SU-8 2000, resulting in sample warping.

The thick high-aspect ratio SU-8 2000 structures that we fabricated required longer pre-bake times to remove excess solvent for obtaining a similar solvent as a

thinner film, higher exposure energies to ensure that photo-acid generation with the UV was complete for the thick SU-8 structures, and longer post-bake times to allow for completion of the photo-crosslinking reaction, than recommended by the manufacturer (Nano SU-8 2000 Negative Tone Photoresist Formulations 2035-2100. Newton, Microchem, www.microchem.com/products/su_eight.htm); [20-25]. In order to get a vertical wall profile, especially in high-aspect ratio structures, the amount of UV exposure and heat energy were increased. Based on Fick's law of diffusion, the thicker the SU-8 2000 material, the tougher it would be to detoxify. Therefore, we have included the 3 day heat and the 30 min sonication times, which are long periods of times for diffusive removal. However, as discussed earlier, in practice as the thickness of the photoresist increases, its behavior with respect to processing conditions is different; different thickness of SU-8 2000 are obtained from different formulations of SU-8 2000, leading to fabrication procedures that are different for the different thicknesses in terms of the pre and post bake times, and exposure energies which do not necessarily scale linearly (Nano SU-8 2000 Negative Tone Photoresist Formulations 2035-2100. Newton, Microchem) ; [22, 47]. These differences can lead to the end materials with different amounts of possible toxic leaching materials, based on the cross-linking reaction progress and the cross-linking density. There are several varying processing parameters reported in the literature such as soft bake, exposure and post bake, which will contribute differently to the properties of the SU-8 [47] / SU-8 2000 [22] . The cytocompatibility of SU-8 / SU-8 2000 is directly related to the fabrication process and the processing environment and these protocol changes will require ongoing cytocompatibility

evaluation. The treatments examined here offer several options for thick, high-aspect ratio SU-8 2000 applications.

Conclusion

This study is the first characterization of SU-8 2000 cytotoxicity to neuronal cultures, potentially linking the poor SU-8 2000 cytotoxicity to components within the SU-8 2000, such as solvents and photo acid generator associated elements and the poor adhesive properties of SU-8 2000. Furthermore, this work demonstrates that post-processing strategies for making SU-8 2000 more cytocompatible should include a combination of heat and isopropanol sonication followed by surface treatments of either oxygen plasma or parylene coating. In combination, these results provide a methodology for increasing the potential for SU-8 2000 to be a primary microfabrication material for bioMEMS and other biomedical applications.

Acknowledgements

The authors acknowledge support from the NIBIB/NINDS (BRP EB000786) and the NSF (EEC-9731643). The authors thank Professor Brent Carter (School of Materials Science Engineering, Georgia Tech) and Dr. Amanda Walls (Department of Biomedical Engineering, Georgia Tech) for assistance in the XPS analysis, Mr. Cameron Sullards and Mr. David Bostwick (School of Chemistry and Biochemistry, Georgia Tech) for assistance in the mass spectrometry analyses, and Ms. Hillary Irons, Mr. Winston Pewin, and Ms. Jennifer Springman for editorial assistance.

References

1. Voldman, J., M. Gray, and M. Schmidt, *Microfabrication in biology and medicine.* Annual review of biomedical engineering, 1999. **1**(1): p. 401-425.
2. Gelorme, J., R. Cox, and S. Gutierrez, *Photoresist composition and printed circuit boards and packages made therewith*, U.S. Patent, Editor. 1989.
3. Shaw, J., et al., *Negative photoresists for optical lithography.* IBM Journal of Research and Development, 1997. **41**(1): p. 81-94.
4. Shaw, M., et al., *Improving the process capability of SU-8.* Microsystem Technologies, 2003. **10**(1): p. 1-6.
5. Lorenz, H., et al., *High-aspect-ratio, ultrathick, negative-tone near-UV photoresist and its applications for MEMS.* Sensors and actuators A, 1998. **64**: p. 33-39.
6. Kotzar, G., et al., *Evaluation of MEMS materials of construction for implantable medical devices.* Biomaterials, 2002. **23**(13): p. 2737-2750.
7. Song, Y., C. Kumar, and J. Hormes, *Fabrication of an SU-8 based microfluidic reactor on a PEEK substrate sealed by a'flexible semi-solid transfer'(FST) process.* Journal of Micromechanics and Microengineering, 2004. **14**(7): p. 932-940.
8. Heuschkel, M., et al., *Buried microchannels in photopolymer for delivering of solutions to neurons in a network.* Sensors & Actuators: B. Chemical, 1998. **48**(1-3): p. 356-361.
9. Voskerician, G., et al., *Biocompatibility and biofouling of MEMS drug delivery devices.* Biomaterials, 2003. **24**(11): p. 1959-1967.
10. Gholmieh, G., et al., *A biosensor for detecting changes in cognitive processing based on nonlinear systems analysis.* Biosensors and Bioelectronics, 2001. **16**(7-8): p. 491-501.
11. Gholmieh, G., et al., *Custom-designed high-density conformal planar multielectrode arrays for brain slice electrophysiology.* Journal Of Neuroscience Methods, 2006. **152**(1-2): p. 116-129.
12. Heuschkel, M., et al., *A three-dimensional multi-electrode array for multi-site stimulation and recording in acute brain slices.* Journal Of Neuroscience Methods, 2002. **114**(2): p. 135-148.
13. Tscherter, A., et al., *Spatiotemporal characterization of rhythmic activity in rat spinal cord slice cultures.* European Journal of Neuroscience, 2001. **14**(2): p. 179-190.
14. Streit, J., et al., *The generation of rhythmic activity in dissociated cultures of rat spinal cord.* European Journal of Neuroscience, 2001. **14**(2): p. 191-202.
15. Wirth, C. and H. Luscher, *Spatiotemporal evolution of excitation and inhibition in the rat barrel cortex investigated with multielectrode arrays.* Journal of neurophysiology, 2004. **91**(4): p. 1635-1647.
16. Berdondini, L., et al., *A microelectrode array (MEA) integrated with clustering structures for investigating in vitro neurodynamics in confined interconnected sub-populations of neurons.* Sensors & Actuators: B. Chemical, 2006. **114**(1): p. 530-541.

17. Wu, Z., Y. Zhao, and W. Kisaalita, *Interfacing SH-SY5Y human neuroblastoma cells with SU-8 microstructures.* Colloids and Surfaces B: Biointerfaces, 2006. **52**(1): p. 14-21.
18. Weisenberg, B. and D. Mooradian, *Hemocompatibility of materials used in microelectromechanical systems: Platelet adhesion and morphology in vitro.* Journal of biomedical materials research, 2002. **60**(2).
19. Wang, Z., et al. *A simple hydrophilic treatment of SU-8 surfaces for cell culturing and cell patterning*. in *9th International Conference on Miniaturized Systems for Chemistry and Life Sciences*. 2005. Boston, MA.
20. *Nano SU-8 2000 Negative Tone Photoresist Formulations 2035-2100. www.microchem.com/products/su_eight.htm*, Microchem: Newton.
21. Choi, Y., et al., *Three dimensional MEMS microfluidic perfusion system for thick brain slice cultures.* Biomedical Microdevices, 2007. **9**(1): p. 7-13.
22. Barber, R., et al., *Optimisation of SU-8 processing parameters for deep X-ray lithography.* Microsystem Technologies, 2005. **11**(4): p. 303-310.
23. Ho, C., et al., *Ultrathick SU-8 mold formation and removal, and its application to the fabrication of LIGA-like micromotors with embedded roots.* Sensors & Actuators: A. Physical, 2002. **102**(1-2): p. 130-138.
24. Lin, C., et al., *A new fabrication process for ultra-thick microfluidic microstructures utilizing SU-8 photoresist.* Journal of Micromechanics and Microengineering, 2002. **12**(5): p. 590-597.
25. Bogdanov, A. and S. Peredkov, *Use of SU-8 photoresist for very high aspect ratio x-ray lithography.* Microelectronic Engineering, 2000. **53**(1-4): p. 493-496.
26. Wagenaar, D., J. Pine, and S. Potter, *An extremely rich repertoire of bursting patterns during the development of cortical cultures.* BMC neuroscience, 2006. **7**(1): p. 11.
27. Voigt, T., H. Baier, and A. Lima, *Synchronization of neuronal activity promotes survival of individual rat neocortical neurons in early development.* European Journal of Neuroscience, 1997. **9**(5): p. 990-999.
28. Gross, G. and J. Kowalski, *Origins of Activity Patterns in Self-Organizing Neuronal Networks in Vitro.* Journal of Intelligent Material Systems and Structures, 1999. **10**(7): p. 558.
29. Brewer, G., et al., *Optimized survival of hippocampal neurons in B27-supplemented Neurobasal™, a new serum-free medium combination.* Journal of neuroscience research, 1993. **35**(5): p. 567-576.
30. Brewer, G., *Isolation and culture of adult rat hippocampal neurons.* Journal Of Neuroscience Methods, 1997. **71**(2): p. 143-155.
31. Brown, S., *Introduction*, in *Cell-Culture Test Methods: ASTM Special Technical Publication 810*, B. SA, Editor. 1983, ASTM: Philadelphia. p. 2-3.
32. Lontz, J., M. Nadijcka, and H. R., *Assessment of Biocompaitibility of orofacial materials and devices by culturing with human excised donor tissues*, in *Cell-Culture Test Methods: ASTM Special Technical Publication 810*, B. SA, Editor. 1983, ASTM: Philadelphia. p. 77-87.
33. Lesuisse, C. and L. Martin, *Long-term culture of mouse cortical neurons as a model for neuronal development, aging, and death.* Journal of neurobiology, 2002. **51**(1).

34. Beche, E., et al., *XPS and AES characterization of SiNx: H layers deposited by PECVD on Parylene C. Effects of thermal treatments on Parylene C surfaces and Parylene C SiN x: H interlayers.* Thin Solid Films, 1995. **258**(1-2): p. 143-150.
35. Johnson, D., D. Nawrocki, and R. Ruhmann, *Improving the Process Capability of SU-8, Part III.* Journal of Photopolymer Science and Technology, 2002. **15**(5): p. 749-756.
36. Dentinger P, K.K., Simison KL, *Photoimageable Composition*. 2005.
37. Aktary, M., et al., *High-resolution pattern generation using the epoxy novolak SU-8 2000 resist by electron beam lithography.* Journal of Vacuum Science & Technology B: Microelectronics and Nanometer Structures, 2003. **21**(4): p. L5.
38. Yang, H., et al., *Investigation into antimony pentafluoride-based catalyst in preparing organo-fluorine compounds.* Journal of Molecular Catalysis. A, Chemical, 2005. **233**(1-2): p. 99-104.
39. Horbet, T., et al., *Biology, Biochemistry, and Medicine: Some Background Concepts*, in *Biomaterial Science: An introduction to materials in medicine*, B. Ratner, et al., Editors. 1996, Academic Press: San Diego. p. 133-141.
40. Zhang, J., et al., *Argon plasma modification of SU-8 for very high aspect ratio and dense copper electroforming.* Journal of the Electrochemical Society, 2005. **152**: p. C716.
41. Musiek, E., et al., *Cyclopentenone isoprostanes are novel bioactive products of lipid oxidation which enhance neurodegeneration.* Journal of neurochemistry, 2006. **97**(5): p. 1301.
42. Kirman, C., et al., *Using physiologically-based pharmacokinetic modeling to address nonlinear kinetics and changes in rodent physiology and metabolism due to aging and adaptation in deriving reference values for propylene glycol methyl ether and propylene glycol methyl ether acetate.* An International Journal, 2005. **25**(2): p. 271-284.
43. Feng, R. and R. Farris, *Influence of processing conditions on the thermal and mechanical properties of SU8 negative photoresist coatings.* Journal of Micromechanics and Microengineering, 2003. **13**(1): p. 80-88.
44. Nordstrom, M., et al., *Rendering SU-8 hydrophilic to facilitate use in micro channel fabrication.* Journal of Micromechanics and Microengineering, 2004. **14**(12): p. 1614-1617.
45. Curtis, A., et al., *Adhesion of cells to polystyrene surfaces.* Journal of Cell Biology, 1983. **97**(5): p. 1500-1506.
46. Keselowsky, B., D. Collard, and A. Garc a, *Surface chemistry modulates focal adhesion composition and signaling through changes in integrin binding.* Biomaterials, 2004. **25**(28): p. 5947-5954.
47. Zhang, J., et al., *Polymerization optimization of SU-8 photoresist and its applications in microfluidic systems and MEMS.* Journal of Micromechanics and Microengineering, 2001. **11**(1): p. 20-26.

CHAPTER 4

DEVELOPMENT OF SPONTANEOUS NEURAL NETWORK ACTIVITY IN A 3-D NEURONAL-ASTROCYTIC CO-CULTURE MODEL

Summary

Neural-electronic interfaces within cell culture models allow the controlled study of specific components of neuronal electrophysiological behavior, such as understanding the spatial and temporal development of neural network activity. Since 3-D cultures may better mimic the *in vivo* environment than 2-D cultures, we have engineered 3-D culture models of neural tissue to study neural network-level properties. Since cell type, viability, connection patterns, and synaptic density in a neural network contribute to electrophysiological activity, we have characterized these 3-D cultures using both immunocytochemistry and 3-D multielectrode array (MEA) recordings. MEAs were oxygen plasma treated, followed by polylysine, and laminin coating before the plating of 3-D neuronal-astrocytic (2:1) co-cultures at 2500 cells/mm^3 in Matrigel™ matrix approximately 750 μm thick and at a protein concentration of 7.5 mg/mL. The spontaneous electrophysiological activity of the 3-D cultures was recorded daily, and the cultures were stained with either viability markers or markers to investigate the number of nuclei, neuronal maturation, and synapstic density at 4, 7, 10, and 14 days *in vitro*. The culturing conditions promoted considerable neurite outgrowth, complex 3-D network structure, and good neural viability for several weeks. Furthermore, these cultures displayed both spontaneous and evoked electrical field potentials and functional synaptic transmission as measured through culture-wide spike and burst rates. The spike and burst

rates increased rapidly during the first week in culture, reached a plateau during the second week, suggesting an adaptation or saturation of the network activity. A gradual drop in overall electrophysiological activity occurred in the third week suggesting pruning and/or culture degradation. This activity was verified to be of biological origin by studying the influence of agents that interfere with synaptic transmission and neuronal action potential firing. The neuronal and synaptic densities increased dramatically midway through the second week in culture as evidenced by an increase in neuronal MAP2 and synaptic marker expression. The period of rapid increases in electrophysiological activity (function) in the first week in culture did not coincide with the period of rapid increases in neuronal maturation markers (structure) which occurred in the latter-half of the second week in culture. It is postulated that in the first week, the cultures develop a highly excitatory character because most synapses that are developed are potentially excitatory in nature with neurons spontaneously firing action potentials without much inhibitory input. However, in the second week (as the number of synapses increases and neurons mature), inhibitory synapses increase, creating a homeostatically sustainable level of culture activity. Sensitivity of spike and burst rate response of these cultures to bicuculline methiodide (BMI) and gramicidin in 21 DIV 3-D cultures (both agents increase the culture electrophysiological activity) not only supported the biological origin of the electrically measured activity of these cultures, but these responses also suggest the hypothesized influence of inhibition on the culture activity, because BMI disinhibits (*reversibly removes the inhibitory synaptic influence*) and gramicidin causes poration. Overall, this work represents important contributions to methods in engineering

more physiologically-relevant 3-D neural tissue in culture and the understanding of its structure-function relationship.

Key words. three dimensional, 3-D culture, Matrigel™, neuron, astrocyte, neural network, multi electrode array, MEA, electrophysiology

Introduction

Neural network recordings from both *in vivo* and *in vitro* models have been used to understand neural plasticity, trauma, disease, age-related degeneration [1]; deafness, memory deficits, epilepsy [2-3]**;** and neuroprostheses [4]. *In vivo* animal models are complex and often confound data interpretation, while single-cell studies (both *in vivo* and *in vitro*) preclude extended network-level analysis. In contrast, *in vitro* cell culture models provide for a relatively controlled study environment and allow for simpler experimental manipulation at the network level.

In vitro neural network studies, which employ planar 2-D culture, may not accurately represent *in vivo* cellular and network level functions, because *in vivo* conditions are 3-D in nature. Therefore, a 3-D *in vitro* culture model may more closely mimic the microenvironment of *in vivo* neural networks. The presence of 3-D growth and interactions may be crucial because the matrix surrounding cells, as is typical of the 3-D *in vivo* environment, has been shown to affect cellular function for a variety of cell types [5-6], including neural cells [7-9]. There is evidence that 3-D culture conditions may better approximate the morphology, cytoarchitecture, gene expression, proliferation of neural tissue [6, 10-12], and organization and types of cell-cell and cell-matrix interactions, [13] than 2-D culture conditions.

We established a 3-D culture co-model of a neural network to closer approximate *in vivo* tissue, by harvesting embryonic cortical neurons and astrocytes of newborn rats and mixing them homogeneously within a 3-D hydrogel-based bioactive scaffold, Matrigel™. Matrigel™ matrix, a reconstituted basement membrane derived from the Engelbreth-Holm-Swarm mouse sarcoma, includes constituents of the extracellular

matrix found in the developing or mature brain such as laminin, hyaluronan, and proteoglycans, facilitating 3-D neural network development through the ECM-related [14] and other cytokine-mediated [15-16] interactions. Matrigel^{TM} has been shown to promote neurite outgrowth [17-18]. The cell culture model interfaced with an array of microelectrodes, where external electronics recorded the electrophysiological activity.

We studied the structural and functional development of the neural networks within this 3-D neural co-culture model using microscopic imaging and 3-D multi electrode array (MEA) based electrophysiological recording. MEA technology has been used to study neural electrophysiological activity in 2-D dissociated spinal cord [19], cortical [20], hippocampal, acute retina [21-22], and cardiac myocyte cultures [23]. However, few studies exist on the electrophysiological activity of 3-D dissociated neural culture [24]. The study published by Irons et al. in 2008, is probably the only study presenting electrophysiological activity recording from 3-D neural cultures; However, that study was done using the patch clamp technique and merely showed that the neurons in the 3-D cultures were electrophysiologically active; it did not characterize the 3-D network level activity and it's development with respect to time. Unlike the patch clamp technique, 3-D MEA technology allows simultaneous multi-location recording in 3-D environments. Here we tracked the spontaneous electrophysiological (functional) and structural changes involved in 3-D neural network development in culture with respect to days *in vitro* (DIV). We hypothesized that *in vitro* spontaneous electrophysiological activity of the cultured 3-D neural networks would directly correlate with neuronal and synaptic densities. Therefore, to investigate the dynamic electrophysiological capability based on the structural organization of a neural network, we compared field potential

based measurements of spike and burst rates over three weeks *in vitro* to markers of synaptic distribution and neuronal maturation. In addition, we compared the native spontaneous activity of the cultures to the activity during pharmacologically altered states to confirm the biological response, learn more about the nature of these 3-D neural networks developed *in vitro*, and to assess the possibility of using these networks for pharmacological and toxcicological testing. This model can be used to test various therapies such as single dose, time-release, mono- and combination drug therapies; drug-releasing devices; cell-based therapies such as stem cell delivery; study pathological conditions; characterize and validate tissue engineering strategies; characterize and validate neural implants for continuous monitoring, diagnostic, and therapeutic applications to the nervous system; or simply to understand the development of neural networks.

This work represents important contributions to engineering 3-D neural tissue in culture and understanding structure-function relationships of neural networks. We predict that such efforts will eventually contribute to developing hybrid-neural-interfaces that can diagnose, ameliorate, or even resolve human functional deficits resulting from damage, disease, or dysfunction in the nervous system.

Materials and Methods

The Multi-Electrode Arrays

Ayanda system 3-D MEAs and Multichannel Systems thin optical 2-D MEAs (control MEAs) were used in this study. More details about the control 2-D "Thin-MEAs," which have a bottom thickness of only 180 μm, and conductive leads made of optically transparent indium tin oxide are found in [25-26]. This subsection describes the details of the 3-D MEA.

The 3-D MEA biochip (Ayanda Biosystems, Lausanne, Switzerland) is a micro-fabricated glass chip, approximately 1.5 cm x 1.5 cm x 700μm, glued onto a printed circuit board (PCB, 4.9 cm x 4.9 cm), and covered with a glass ring culture chamber silicone-sealed to the PCB [27]. An aperture in the PCB defines an 8 mm-diameter circular area for placing a culture.

The 3-D MEA electrode arrangement is based on an 8x8-matrix of platinum-tipped, microelectrode hillocks (see Figure 4.1A), located centrally in the circular workspace. There are 59 functioning electrodes (corner electrodes are absent, and one electrode is a ground) (see Figure 4.1B). The electrodes are spaced at 200 μm (center-to-center distance), each with an approximate base area of 1600 μm^2 (40 μm x 40 μm), generating a total recording area of 1.96 mm^2 (1.4 mm x 1.4 mm). This matrix samples the electrophysiological activity of thousands of neurons within the culture space defined by an 8-mm diameter circular base area (See Figures 4.1C). The effective recording area for each 3-D microelectrode hillock lies between the lateral surface area of a cone (2809 μm^2) and a pyramid (3600 μm^2) with base and height dimensions of 40 μm each [27].

Platinum, the 3-D electrode material, results in noise levels of 14 to 17 μV [27]. The electrode noise is mainly due to thermal noise, U_{th}, defined by $U_{th} = (4kTRB)^{½}$, where k is the Boltzmann constant ($k = 1.3807 \cdot 10^{-23}$ $J \cdot K^{-1}$), T is the temperature, R is the global resistance of the electrode, and B is the electrode bandwidth [27].

A 5 μm thick SU-8 epoxy layer insulates the electrode lines reducing interfering capacitances between electrode leads and culture medium due to its low dielectric constant. Moreover, SU-8 epoxy is optically transparent, chemically stable, and observably non-toxic to cells at a 5 μm thickness. However, the PCB epoxy has significant material toxicity; therefore, a biocompatible silicone sealant isolates the PCB epoxy from the cell culture region on the MEA biochip (See Figure 4.1C) [27]. Figure 4.1 illustrates the features of the 3-D MEA.

Cleaning of the MEAs, Cell Culture Chamber Rings, Teflon-Based Culture Caps, and Nylon-Mesh Culture Inserts for Reuse

MEAs were reused until high noise increased to unacceptable levels (baseline signal continuously greater than 17.5 μV)[27]. The noise level is an indirect indicator of MEA biochip integrity and electrode quality; higher noise levels suggest that the MEA has sustained damage [27].

Additional custom-made cell culture chambers were prepared by pressing the clean, dry cell culture chamber rings made of silicone based elastomer (Sylgard 184 and 186, Dow Corning, Midland, MI; cross-sectional area = 2 cm^2) on oxygen plasma treated glass cover slips. Upon 3-D culture plating on MEAs, a nylon mesh (70-200 μm square pores) insert placed on top of the 3-D cultures prevented them from detaching from the

MEA electrodes (See Figure 4.1G). Finally, both MEA-based cultures and cultures in the custom-made cell culture chambers were sealed with O_2- and CO_2-permeable Teflon-based fluorinated ethylene propylene (Teflon-FEP, or FEP) membrane [28]. Impermeable to water, this sealing membrane maintained humidity, prevented evaporative losses, prevented osmolality shocks to culture, and reduced the risk of infection without the use of antibiotics and antimycotics (See Figure 4.1H).

To clean the MEAs and non MEA objects (cell culture chamber rings, teflon-based culture caps, and nylon-mesh culture inserts) of culturing components and other reagents used in cell culture assays, they were rinsed in DI water, followed by 70% ethanol, and again by DI water. The MEAs were subsequently treated with Trypsin-EDTA (Invitrogen, Carlsbad, CA) at room temperature for approximately 7 minutes and observed under a microscope while agitating using a pipette, rinsed with DI water afterwards. MEAs were treated with 3% BM solution (Biomed, Munich, Germany), while the non MEA objects were treated with acetone (VWR International, West Chester, PA); each treatment was performed at room temperature for 15 minutes. All objects were rinsed once again in DI water, then by 70% ethanol, followed by DI water. Non-MEA objects were dried in a oven at 50°C (VWR International, West Chester, PA), while MEAs air-dried. In cleaning, the various solvents were gently agitated over the MEA using a pipette to assist in cleaning, so that the surface of the MEA was not scratched.

Oxygen Plasma Treatment

After cleaning and drying, the MEAs and the glass cover slips (VWR International, West Chester, PA) used for the cell culture chambers were plasma treated

for 1 min using air glow discharge (EMS-100, Electron Microscopy Sciences, Hatfield, PA) at a pressure of 1 x 10^{-1} mbar with a discharge current of 25 mA, and a negative discharge polarity, to hydrophilize the generally hydrophobic MEA surface, improving its adhesiveness to the cell culture.

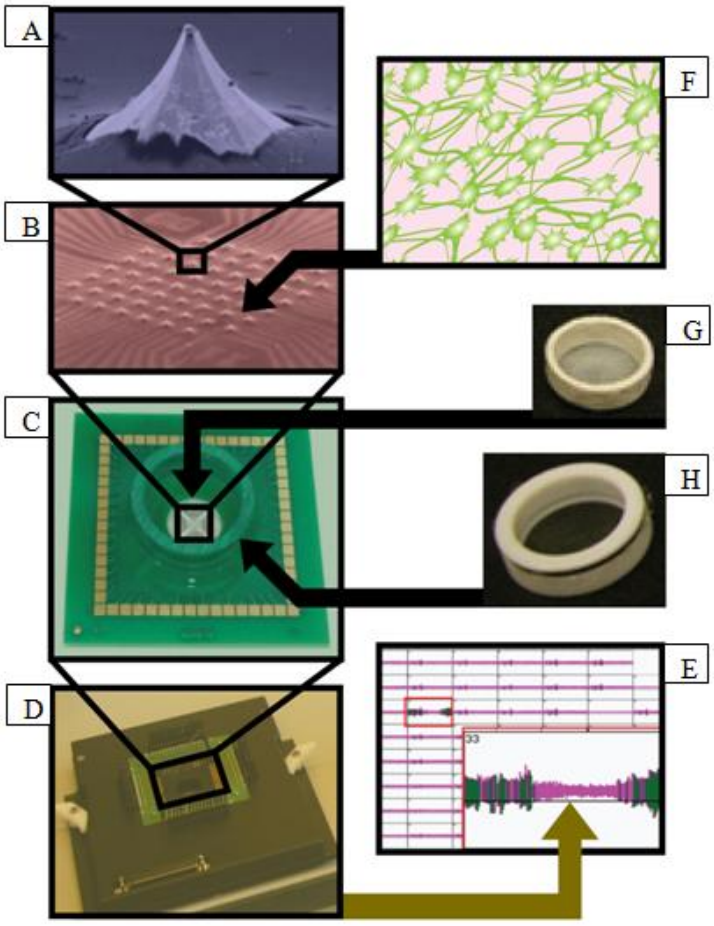

Figure 4.1. 3-D MEA based 3-D culture system for electrophysiological recording. Materials used in these experiments are shown: an enlarged view of a 3-D electrode (A), array of electrodes (B), MEA culture dish (C), Multichannel Systems preamplifier (D), and multichannel recording output snapshot showings spikes and bursts in green (E), a schematic of the 3-D neural culture (F), nylon mesh insert (G), and teflon cap (H).

Sterilization of the MEAs and Custom-Made Cell Culture Chambers

MEAs are not suited for autoclave sterilization because the different constituent materials have different thermal expansion coefficients, making them sensitive to high temperature changes. Therefore, oxygen plasma treated MEAs were sterilized with 70% ethanol inside a laminar flow hood under UV light for 30 minutes, then re-exposed to only UV light for another 30 minutes**,** and finally air-dried in the sterile hood for 15 minutes with activated laminar flow. During sterilization, the MEAs were at least 65 cm away from the UV lamp (minimum distance of lamp from the working bottom surface of hood) with intensity of at least 0.6 J/cm^2 in the laminar flow hood. The custom-made cell culture chambers were autoclaved (Tuttnauer Co. Ltd., Jerusalem, Israel) for 45 minutes.

MEA and Custom-Made Cell Culture Chamber Substrate Coatings to Promote Cell Adhesion

Dried, sterilized MEAs and custom-made cell culture chambers were incubated overnight in a cell culture incubator with a 100 µl drop of 100 µg/ml poly-D-lysine (MW > 300,000 Da; Sigma, St. Louis, MO) solution in DI water placed at the center of each culture substrate in order to form an adhesive coat of poly-D-lysine. Following incubation, the excess poly-D-lysine solution was removed and the culture substrates were rinsed once with sterile DI water, and left to air-dry. Subsequently, at the center of the culture substrates, a 60 µl drop was applied of 20 µg/ml laminin in Neurobasal medium (both from Invitrogen, Carlsbad, CA) and incubated overnight. Immediately prior to cell plating, the laminin solution was removed, the MEA surface was rinsed once with sterile calcium- and magnesium-free Hanks balanced salt solution (CMF-HBSS,

Invitrogen, Carlsbad, CA).

Isolation of Primary Cortical Neurons (Embryonic Day Eighteen) and Astrocytes (Postnatal Day One)

Harvesting of cells or tissue regions from whole tissue inherently involves some injury to the cells in the process of dissection or dissociation. We adopted various minimally invasive procedures to minimize tissue destruction during dissociation: we used mild mechanical and enzymatic treatments; kept tissue samples cold; avoided heat exposure, significant pH changes, and osmolality shocks; conducted dissections and dissociations quickly; used nutritionally optimal media; and avoided unnecessary handling.

For obtaining cortical tissue, timed-pregnant Sasco Sprague-Dawley rats (Charles River, Wilmington, MA) were anesthetized using isoflurane (Baxter Pharmaceutical Products Inc., Deerfield, IL) and decapitated at embryonic day 18 (E18). All subsequent steps were done under sterile conditions. The embryos were removed and placed in ice-cold (4°C) CMF-HBSS. All procedures involving animals were approved by the Institutional Animal Care and Use Committee (IACUC) of the Georgia Institute of Technology, following NIH guidelines for the care and use of laboratory animals (NIH Publication # 85-23, revised 1985).

The embryonic cerebral cortices, excluding the hippocampi, were isolated and dissociated using pre-warmed trypsin (0.25%) + 1 mM EDTA (Invitrogen, Carlsbad, CA) for approximately 10 min at 37ºC and followed by deoxyribonuclease I (0.15 mg/mL, Sigma, St. Louis, MO) in HBSS. Dissociated cells were centrifuged at 1000 rpm for 3

minutes and re-suspended in a defined plating medium (Neurobasal medium + 2% B-27 + 500 μM L-glutamine; Invitrogen, Carlsbad, CA). If necessary, cell clumps / pellet were further mechanically dissociated with approximately 5 passes through a 1 ml pipette tip [28] or a flame-narrowed and fire-polished Pasteur pipette [29]. Evaluating the exclusion of trypan blue (0.2%, Sigma) by the viable cells with a hemocytometer determined viable cell concentration.

Astrocytes were obtained separately from postnatal day 1 Sprague-Dawley cortices. Isolated cortices were minced, digested in trypsin (0.25% + 1mM EDTA) for 3-5 minutes at 37°C, followed by DNase I (0.15 mg/ml) treatment and gentle mechanical trituration. Cells were plated in DMEM/F12 with 10% fetal bovine serum. Mechanical agitation was used to detach less adherent cell types at 24 and 72 hours. For four weeks, the primary astrocyte culture (>95% type I astrocytes) was passaged upon reaching ~90% confluency. Plating for 3-D cultures was performed between passages 4-10.

3-D Primary Cortical Neural Cell Cultures

3-D neuronal-astrocytic co-cultures were plated at a 2:1, neuron:astrocyte ratio at a density of 2500 cells/mm^3 suspended in Matrigel™ matrix (up to 4000 μm thick; final concentration 7.5mg/mL). The 2:1 ratio would allow ample neurons in the culture to measure electrophysiological activity and relatively adequate supporting astrocytes. The 3-D cultures were plated over a circular area of an approximate diameter of 8 mm on either the pre-treated 3-D MEAs or on glass coverslips (VWR international, West Chester, PA) using a mixture of cells re-suspended in co-culture medium (Neurobasal medium + 2% B-27 + 500 μM L-glutamine + 1% G-5; Invitrogen, Carlsbad, CA) and

Matrigel^{TM} matrix (Catalog # 354263, BD Biosciences, San Jose, CA) at a total plating volume of 200 µl per 3-D culture (See Figure 4.1). After matrix gelation (30- 45 minutes incubation in a tissue culture incubator at 37°C, 5% CO_2, 95% Relative Humidity), 1 mL plating medium was gently added per culture well without disturbing the gel. Being careful not to disturb the 3-D culture, the medium was completely replaced at 24 hours and every other day thereafter with co-culture medium pre-warmed to 37°C. The co-culture medium contained glial growth-supporting G-5, essential for long-term culture health [30]. Good cell viability results from the selected 3-D plating density, permitting recording at the electrodes while maintaining discernable cell-cell distances. Use of embryonic cortical tissue, which is less developed and differentiated than adult tissue, allows the isolation of cells with minimal sheared axons and dendrites thus minimizing irreversible damage to the cells [31].

Experimental Design

The 3-D cultures were analyzed in 2 batches. The first batch consisted of 37 3-D co-cultures: 9 cultures on MEAs (6 on 3-D MEAs, and 3 on 2-D MEAs) and 28 cultures on glass cover slips. The second batch consisted of 23 3-D co-cultures: 3 cultures on 3-D MEAs and 20 cultures on glass cover slips. Electrophysiolgical activity was recorded for 5 minutes daily from MEA cultures for 24 days after allowing each culture approximately 5 minutes of equilibriation time on the preamplifier recording surface (maintained at 37°C).

Experiments assessing viability and phenotypic markers showed that 3-D cultures on MEAs had comparable live / dead cells and random distribution of cells in the 3-D

volume with neuronal and astrocytic processes in all directions with the 3-D cultures on the glass coverslips (n=3-4). Separate cultures on glass coverslips were stained with viability markers (n = 3) or fixed for immunocytochemistry (n = 4) to quantify nuclei, neurons, and synapses at 5, 8, 11, and 16 DIV. Of the cultures selected for immunocytochemistry, three cultures were stained with antibodies against MAP-2 (microtubule associated protein, a neuronal marker), synapsin (a pre-synaptic vesicular protein marker), and nucleic acid stain Hoechst. As a negative control, only secondary antibodies were added to the fourth culture. The cultures were then imaged under a confocal microscope. At 21 DIV, three MEA cultures were exposed to pharmacological/chemical treatments; the electrophysiological activity was recorded. In additional experimental runs, other immunocytochemical markers such as GFAP (glial fibrillary acidic protein, an astrocyte marker), TAU-5 (a microtubule associated protein, a neuronal marker), NF-M (neuro filament - medium, a neuronal marker), and NeuN (neuronal nuclii, a neuronal marker) were used.

Electrophysiological Recording from Cultures

The MEA 3-D cultures were maintained in a tissue culture incubator (37°C, 5% CO_2 and 95% RH) except during recording. Electrophysiological activity was recorded daily from the MEAs in random order at 37°C for 5 minutes inside a sterile laminar flow hood. The laminar flow was deactivated to prevent mechanical vibrations. To ensure long-term stability of recordings and low noise interference, the flow hood was electrically grounded, all electrical lights were switched off, and recording was done at the same time during the day when lab-activity was low.

Electrophysiological activity of the cultures was monitored by placing the 3-D culture containing MEAs in a Multi Channel Systems MEA60 preamplifier system (Multichannel Systems, Reulingten, Germany) interfaced with a computer carrying a Multi Channel Systems data acquisition card by MC Rack software (See Figure 4.1). Multi Channel Systems temperature controller TCO2 maintained the temperature of the preamplifier recording setup at 37°C. The MEA60 Preamplifier System, with surface-mounted technology, ensures low noise level of the complete amplifier chain (1200X amplification, 12-bit resolution, 10 to 3 kHz) at ± 3 μV, within the expected ± 14-17 μV noise level range of a 3-D MEA electrode [26-27]. At low noise interference, single units even in the lower range of 20 to 30 μV can be detected using the MEAs [27, 32]. Silicone- and gold-based "zebra connectors" ensured proper electrode contact of preamplifier pins with MEA pads. Noisy channels (that either had continuous baseline noise levels greater than ± 17.5 μV for the 3-D MEAs, or ± 20-30 μV for the 2-D MEAs, or in which acquired signal abruptly went out of a defined range of ± 1000 μV, or both) were not used for any analyses. Data were recorded with an amplifier gain of 1200, input voltage range of -4096 to 4095 mV, and a sampling frequency of 25 kHz. Data were filtered through a 200 Hz high pass filter to remove low frequency noise. Several gigabytes of raw-data were acquired within only minutes of recording, necessitating the use of high capacity data storage and processing systems.

Spike and Burst Detection Analysis

In our analysis, recordings from up to 59 channels per MEA were considered. At each viable channel, a 5 minute voltage fluctuation stream with respect to time was

analyzed. Neural activity present in these voltage fluctuations was then quantified in terms of spikes (individual deviations in voltage beyond a threshold) and bursts (clusters of spikes that fulfilled a minimum criteria).

MC Rack Software (Multichannel Systems, Reulingten, Germany) detected spikes with a simple algorithm that tagged a voltage trace whenever it exceeded a threshold of -17.5 µV (signal with a larger -ve voltage value) for the 3-D MEA data [27], or 3 times the standard deviation of the data stream for the 2-D MEA data (See Figure 4.1). Sources of noise are generally Johnson noise, diffuse neuronal activity, and power line-related (60 Hz) interference. False positives (overestimation of spikes) occurred when the waveform preceding or following an action potential had a large 'rebound' artifact exceeding the threshold. Likewise, when the same electrode detected multiple neurons, overlapping action potentials potentially obscured the raw voltage waveforms and caused false negatives (underestimation of spikes). Nevertheless, this method provides a consistent, non-biased criterion for data sampling and subsequent quantification of the network activity. From the extracted spike data, Neuroexplorer Software (Nex Technologies, MA) was used to obtain raster plots and count spikes/bursts.

Bursts were identified by a burst detector algorithm (NeuroExplorer user Manual and Reference, Revision 3.193, 2005); [33]. A spike was counted as 5 ms, based on 3.5 ms neuronal action potentials and propagation delays of approximately 1.5 ms. This estimation included the axonal delay and the synaptic release latency after presynaptic emission, irrespective of the spatial distance between cells [34]. A cluster of 4 spikes, a duration of 20ms (period for 4 action potentials), and an inter-burst interval of 10 ms (period for 2 action potentials) set the minimum requirement for bursts. Using Microsoft

Excel, average spike rates (spikes/second) and burst rates (bursts/minute) were calculated with respect to DIV for each replicate by adding the total number of spikes and bursts for all the viable channels and dividing by the total number of channels per replicate and the 5 minute recording period to give *average parameters per electrode*. Finally, statistical analysis was performed using one and/or two way ANOVA, followed by Tukey's pair-wise comparison (p-value <0.05). Such data analyses were performed for every replicate for each of the treatments tested, such as DIV, and chemical stimulation.

Imaging Analysis

For viability and immunocytochemical assays, at least 3 different regions (and up to 6) were imaged in z-stacks for each culture using a 10X, 20X, or a 40X objective lens on a Zeiss 510 Confocal Laser Scanning Microscope (Carl Zeiss AG, Göttingen, Germany). Image regions were randomly selected either by triangulation, or imaging at the four ends of a square and the center of the cultures. Cell plating density was approximately 2,500 cells/mm^3 with a 2:1 neuron to astrocyte ratio. This density changed with DIV potentially with astrocytic proliferation, cell migration, cell death, and remodeling of gel. Distinguishing individual neurons using automated image processing software was difficult due to the high packing density of neurons and neurites in 3-D. Therefore, images were manually analyzed using LSM Image Browser (Carl Zeiss AG, Göttingen, Germany). The software converted the z-stacks into 3-D reconstructions, in which viability or immunocytochemistry parameters were manually quantified and averaged with standard deviations, when appropriate. To prevent user bias, all images were independently quantified by two operators, and only those counts that were within

±10% of each operator's count were maintained. Those counts that did not fit this criterion were recounted independently, and the process continued until consistently repeatable counts were obtained. Statistical analysis was performed using one-way ANOVA followed by a post hoc test (p-value <0.05).

Assessment of Cell Viability

Cell viability was measured using fluorescent probes for distinguishing live and dead cells (LIVE/DEAD Viability/Cytotoxicity Kit; Molecular Probes, Eugene, OR) in separate cultures at 4, 7, 10, 15, and 23 DIV. Cell cultures were incubated with 2 μM calcein AM and 4 μM ethidium homodimer-1 at 37° C for 30 minutes and rinsed in 0.1M Dulbecco's phosphate buffered saline (D-PBS, Invitrogen, Carlsbad, CA) before 3-D confocal microscopic imaging. The percentage of viable cells per 3-D constructed image was determined from the number of live cells (fluorescing green by AM-cleavage) and the number of cells with compromised membranes (nuclei fluorescing red by EthD-1 intercalation in the DNA).

Immunocytochemistry

Immunostaining can help identify specific cellular proteins associated with a particular phenotype [35]; therefore, cultures were immunostained for specific markers at 4, 7, 10, 14, 15, and 21 DIV. Cultures were fixed in 3.7% formaldehyde (Fisher, Fairlawn, NJ) in phosphate buffered saline (PBS) at room temperature for 30-35 min, rinsed in PBS, and permeabilized using 0.3% Triton X100 (Kodak, Rochester, NY) + 4% goat serum (Invitrogen) in PBS for 20 minutes. After permeabilization, the cultures were

thoroughly rinsed with PBS, and primary antibodies (listed in next paragraph) were added (in PBS + 4% goat serum) at 18-24°C. After being maintained overnight, the cultures were thoroughly rinsed with PBS and secondary fluorophore-conjugated antibodies (Alexa Fluor-conjugated IgG: Alexa Fluor 488 goat anti-rabbit, 1:500; and Alexa Flour 546 goat anti-mouse, 1:500; Molecular probes, Eugene, OR) were added to the cultures (in PBS + 4% serum) at 18-24°C for 2 hours. The cultures were again rinsed with PBS, maintained moist, and imaged. Negative controls for staining were conducted with the same procedure, but without the primary antibodies.

Specifically, the cultures were immunostained using primary antibodies: 1) MAP-2 (mouse monoclonal antibody; MAB3418; 1:200; Chemicon); 2) tau-5 (MS247P, 1:200, NeoMarkers; Fremont, CA), a microtubule-associated protein expressed predominantly in neurons [36-40] 3) glial fibrillary acidic protein (GFAP) (AB5804, 1:400; MAB360, 1:400, Chemicon; Temecula, CA), an intermediate structural filament found in astrocytes [41]; and 4) synapsin I (A6442, 1:200, 51-5200, Invitrogen, Carlsbad, CA), a synaptic vesicle protein localized in presynaptic specializations [42]. Counterstaining for nuclei was performed using Hoechst 33258 (1:1000, Molecular Probes).

High-resolution confocal microscopy was utilized to quantify the number of neurons, astrocytes, and synapses. The numbers of MAP2-positive cell somata (a measure of mature neurons in culture), Hoechst-positive nuclei, and synapsin positive puncta (an *approximate indicator* of the number of *putative* synapses) were manually counted for each 3-D reconstructed confocal image z-stack. Following this, the neuronal density (#/mm^3) and synaptic density (#/mm^3) were calculated per 3-D reconstructed image. Our measure obtained by synapsin staining is only an *approximate indicator* of

the number of *putative* synapses because synapsin I is only one of the proteins present in the pre-synaptic vesicle regulating machinery at the synapses. Its presence does not prove a mature fully-functioning synapse. Likewise, at 400X magnification, one synapsin positive puncta may not directly correspond to one synapse.

Application of Bicuculline Methiodide (BMI) and Gramicidin

Bicuculline methiodide (BMI) and gramicidin were used to test the biological responsiveness of the dissociated 3-D co-cultures. To sense the influence of inhibitory synapses, specifically GABAergic synapses, we exposed 3-week-old cultures to 10μM, 50μM, and 200μM BMI, a $GABA_A$-receptor antagonist, at pH of 7.4. At the time of experimentation, 0.5mL of media was carefully removed from the top of the MEA culture dish (containing 1ml of media), and 0.5mL of the 2X concentration BMI was added and gently mixed using slow pipette aspirations. After approximately 5 minutes of exposure, the cultures were washed 2-6 times with complete co-culture medium changes and the medium was replaced. The electrophysiological activity before, during, and after application of BMI was recorded and the spike and burst rates from the recordings compared. Following the same procedure as BMI, testing was done for 0.01 and 1 μg/ml gramicidin, which forms transient pores in the neurons. This permeabilizing effect of gramicidin was also studied by imaging in the presence of calcein, a normally cell-impermeant dye, while also recording electrophysiological activity.

Results

3-D neural co-cultures consisting of 2:1, neurons:astrocytes in Matrigel^{TM} matrix were introduced to 3-D MEAs for microscopic and electrophysiological monitoring. Optimization was done for selection of the 3-D culture cell density (for improving viability), the Matrigel^{TM} type (for minimal presence of growth factors) and concentration (for improving mechanical stability of gel), the media type (to maintain defined conditions), the 3-D culture-to-substrate adhesion and immobilization procedure (for improving long term adhesion of cells for long-term electrophysiological recording), the electrophysiological activity recording procedure (to improve signal to noise ratio), and the immunocytochemistry procedure (to reduce nonspecific and increase specific immunostaining). The 3-D neural co-cultures contracted both horizontally (less than 10%) and vertically (between 50 to 90%) during the three week culturing period *in vitro*, similar to that reported for cells grown in 3-D collagen [43] and collagen glycosaminoglycan [44] matrices [24]. Concomitant to this contraction, network density and matrix opacity appeared to increase. Cells exhibited *in vivo*-like somatic morphologies with extensive process outgrowth, high viability, functional synaptic connections, and spontaneous electrophysiological properties as also observed previously in a similar 3-D culture model [24].

These cultures had nearly 100 % (97 ± 3 %) viability during the three week *in vitro* culturing period. Viability was based on the number of live and dead cells counted at the different time points assayed, and not based on the total cells originally plated. Live-dead staining in a confocal z-stack image projection of a 105 μm thick region of a 3-D co-culture on a 3-D MEA at 24 DIV in top view are seen in Figure 4.2A. While the

randomly distributed cells networked throughout the 3-D Matrigel™ matrix, they also formed clusters (between 100-200µm in diameter) suggesting remodeling as time progressed. The individual somata morphologies appeared spherical or ovoid with diameters of approximately 20 µm; cell processes extended in all directions, appearing fasciculated.

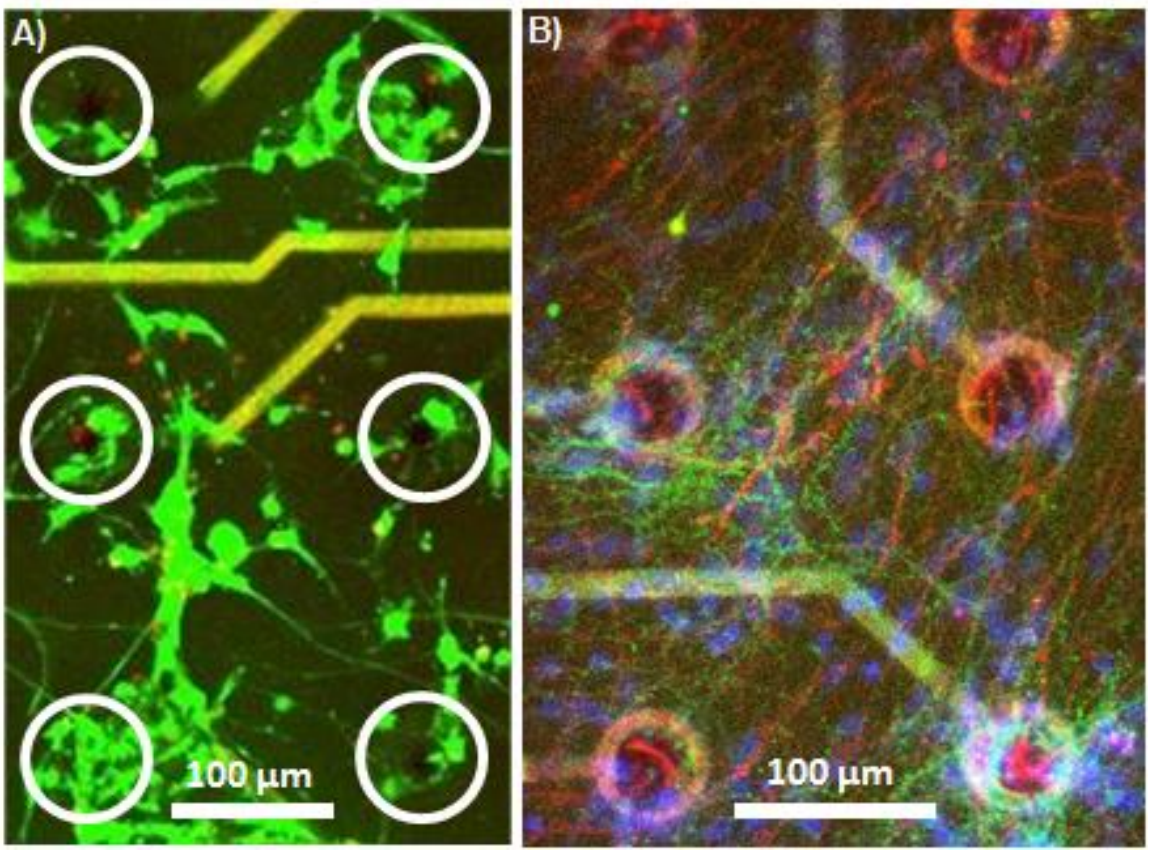

Figure 4.2. Live-dead staining (A) and immunocytochemical staining (B) in confocal z-stack image projections of co-cultures on 3-D MEAs at greater than 3 weeks in culture in top view. Live cells (fluorescing green by AM-cleavage) and dead cells with compromised membranes (nuclei fluorescing red by EthD-1 binding to DNA) could be distinguished. Image reveals that the co-cultures maintained significant viability at > 3 weeks in culture with cells in close apposition to the electrodes as hilighted by the white circles in A). In B), neurons, astrocytes, and cellular nuclei are seen immuno-stained green (Tau 5), red (GFAP), and blue (Hoechst), respectively. Note the close apposition of about 5-10 cells to the conical tower shaped electrodes appearing circular in top view. Electrodes are likely recording electrophysiological activity from multiple cells.

Figure 4.2B shows an immunocytochemical staining confocal z-stack image projection of a 80 μm-thick region of a culture on a 3-D MEA at 22 DIV in top view. Neurons, astrocytes, and cellular nuclei were immuno-stained green, red, and blue, respectively. As seen in the image, neurons and astrocytes randomly clustered on the conical towers of the 3-D MEA and throughout the 3-D culture. Each electrode is in contact with approximately 5-10 cells and several neurites, giving a "picture" of the potential number of signal sources from which each electrode could record.

Spontaneous network electrophysiological activity was successfully recorded from the 3-D co-cultures daily up to 24 DIV using both 3-D and 2-D MEAs. The spontaneous activity of the neural network without chemical manipulation, referred to as "native activity," ranged from individual spikes (amplitudes 25 to 250 μV) to bursts. Figure 4.3 show the evolution of this activity in terms of *average* spike rate (spikes/second) and burst rate (bursts/minute) *per electrode* with respect to DIV. Random spiking, as well as synchronized bursting activity occurred early in the 3-D cultures, from 2 DIV, indicating the concurrent development of functional synapses as cells in the culture formed networks. As a general trend, the spike and burst rates increased rapidly during the first week in culture, reached a plateau during the second week, suggesting an adaptation or saturation of the network activity, followed by a gradual drop in the third week, suggesting pruning and/or culture degradation. As can be seen in Figure 4.3, these electrophysiological parameters varied between cultures. Electrophysiological activity also varied for any single culture not only from day to day; but also on the same day (separate recordings spaced 2-12 hours apart, data not shown). The electrophysiological activity was also very sensitive to temperature: while

electrophysiologically active at 37°C, the cultures exhibited almost no activity at 25°C indicating a strong temperature dependence of the electrophysiological activity of these cultures (data not shown). The most general feature of neural network activity was burst synchronization. This was because most of the detected spikes occurring within bursts. Burst fusion leading to continual high-frequency spiking was also observed. Bursting presumably required either a minimum background spike activity or a sudden subthreshold fluctuation for "ignition" from a nonspiking state, since on some occasions cultures were previously silent.

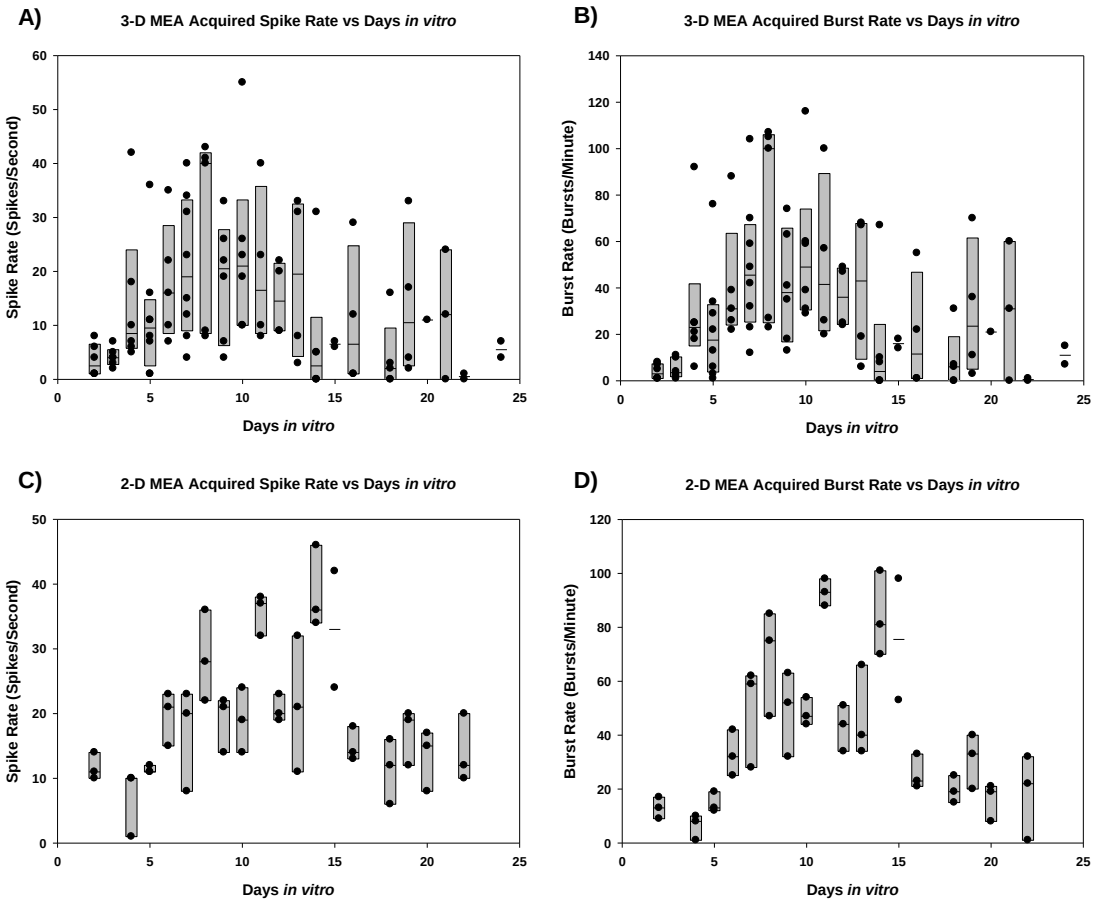

Figure 4.3. Spike and burst rate (*averaged per electrode*) distribution of 3-D neural co-cultures with respect to days *in vitro*, as recorded from 3-D MEA (A and B), and 2-D MEAs (C and D) respectively. The boxes show the 95% confidence interval, and the dark circles indicate the data points for each culture. As a common trend, the spike as well as the burst rate increased rapidly in the first week in culture, maximizing during the second week suggesting a form of a homeostatic process or saturation, followed by a gradual drop in the third week suggesting pruning or culture degradation. The burst rate distribution follows a similar trend as the spike rate distribution, mainly because a majority of spikes lie within bursts. The data appears to have a relatively lower variance during the first 5 days in culture, but the variance increases thereafter. While significant differences were observed both in the spike and burst rate analysis (with the burst analysis showing more significant differences), these are not shown, so that the general trend and data-spread can be appreciated.

The electrophysiological activity of the 3-D cultures responded to agents known to interfere with synaptic transmission (BMI) and neuronal action potential firing (gramicidin) (Figure 4.4). The data were analyzed in three successive segments: native network activity, the response to BMI or gramicidin, and response after 2-6 complete blank medium changes after the introduction of each of these chemicals. As a general trend, adding BMI and gramicidin (separately) to the 3-D cultures at 21 DIV, caused spike and burst rates to increase. Such increased intensity of spontaneous bursts after exposure to GABA antagonist BMI has been reported in other studies [45-46]. The addition of gramicidin appeared to increase cellular permeability in general, with calcein localization in regions the size of cellular vesicles and synaptic boutons (Figure 4.5). The two cultures studied showed varied electrophysiological response, although both cultures showed reduced baseline activity upon rinsing out the gramicidin (Figure 4.5).

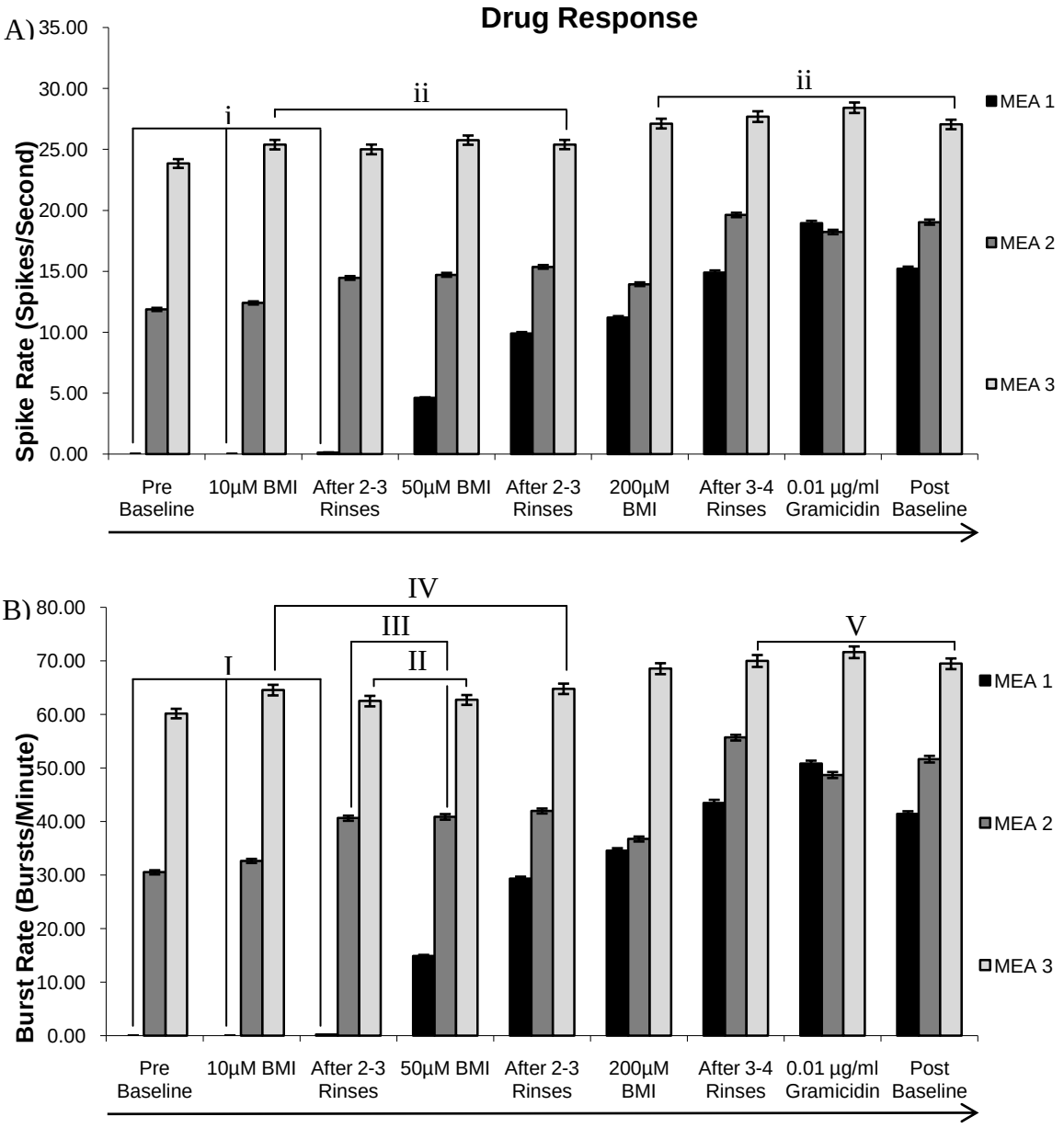

Figure 4.4. Changes in spike (A) and burst (B) rate (*averaged per electrode*) of 3-D neural co-cultures in response to BMI and gramicidin. BMI is a disinhibitor of neural activity, while gramicidin increases membrane porosity. At 21 DIV, as a general trend these drugs caused spike and burst rate increases, reflecting the drugs' expected neural response. The randomized network formation, different numbers of inhibitory synapses, and differing saturation limits for chemical excitation can partially explain the response variability between the cultures. Rinses did not completely reverse the pharmacological effect, indicating at least two possibilities: these drugs have low dissociation constants, and/or given the thickness and density of the cultures, the diffusion may be mass transport limited. Conditions in each MEA culture differed significantly ($P < 0.05$), except for the pairs or triplets indicated by Roman numerals for which the statistical test failed to show any differences.

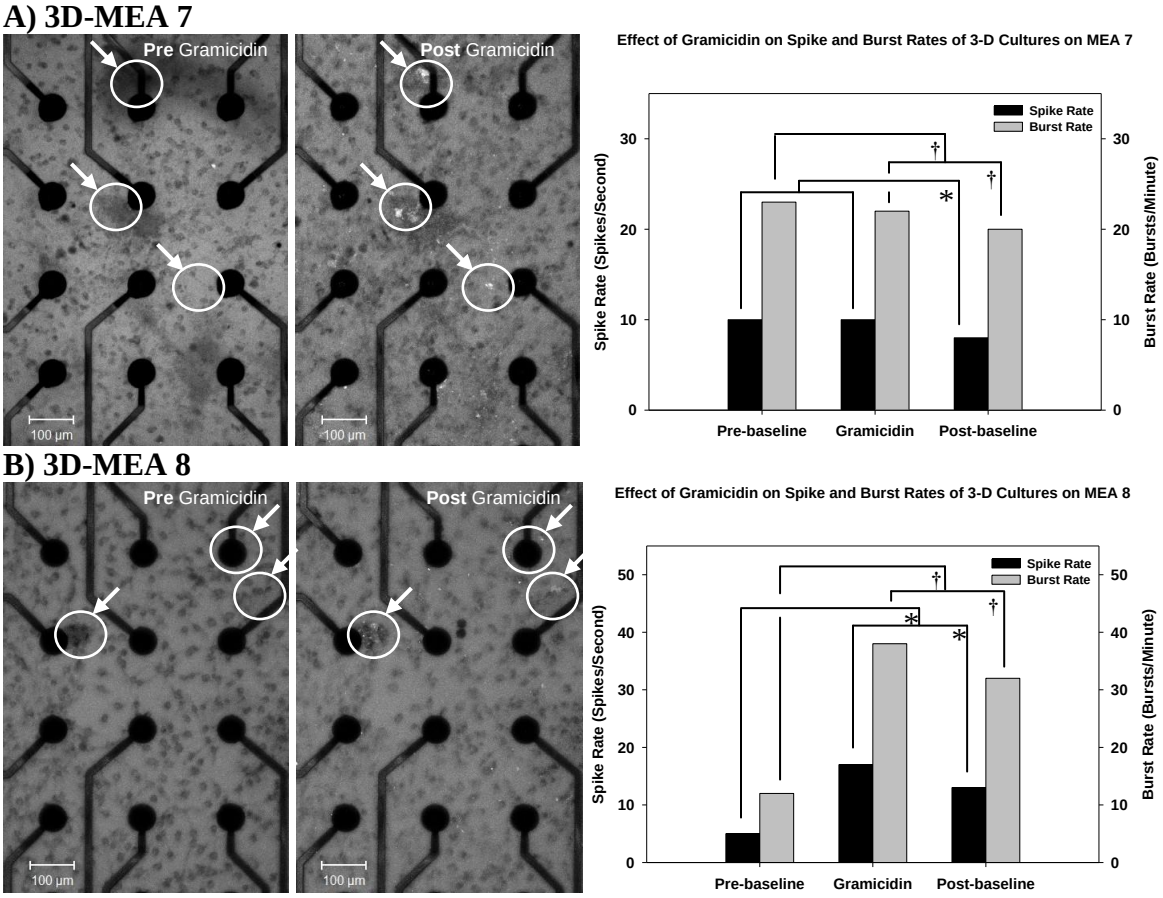

Figure 4.5. Addition of gramicidin to 3-D cultures resulted in slight increases in overall intra-cellular fluorescence in addition to large fluorescence increases in punctate regions the size of intracellular vesicles, indicating calcein uptake; and alterations in the electrophysiological activity of the cultures. 2-D projections of 20 µm thick z-stack images of 25 days *in vitro* 3-D cultures on MEAs 7 and 8 pre- and post-addition of 1µg/ml Gramicidin are shown in A) and B) respectively. Cellular areas indicated by white arrows show visible calcein uptake post addition of gramicidin indicating increased cellular permeability. These regions are of the size of cellular vesicles or synaptic boutons. The corresponding electrophysiological activity response of the two different cultures as expressed in the form of spike and burst rates is shown on the graphs on the left panel for MEAs 7 and 8 respectively. Error bars are not seen because standard deviations are negligible. Significant differences for spike rates (*) and burst rates (†) (*averaged per electrode*) are seen at $P<0.05$. The two cultures show different trends; whereas the culture on MEA 7 does not appear to be responsive to the addition of gramicidin, the activity on MEA 8 significantly increased upon gramicidin contact. However, upon rinsing electrophysiological activity reduced significantly for both the cultures as seen in the post-baseline activity. It is worthy to note that the culture for which gramicidin appeared to increase electrophysiological activity showed lower pre-baseline activity (indicative of higher intrinsic inhibition). Such type of testing methods combining microscopic and electrophysiological analysis can be used for testing the effects of drugs and trauma on neural tissue *in vitro*.

We observed evidence of synapse formation and neuronal maturation within the 3-D co-cultures with DIV. MAP-2ab, an immunomarker of neuronal maturation, identified neurons as they developed in culture, while a synapsin-1 antibody stained pre-synaptic terminals, which suggest synapse formation. Figure 4.6 shows that the synaptic density (the number of synapsin 1 positively stained puncta per unit volume) and the neuronal density (the number of MAP-2ab positive stained cell bodies per unit volume) increased dramatically midway through the second week in culture.

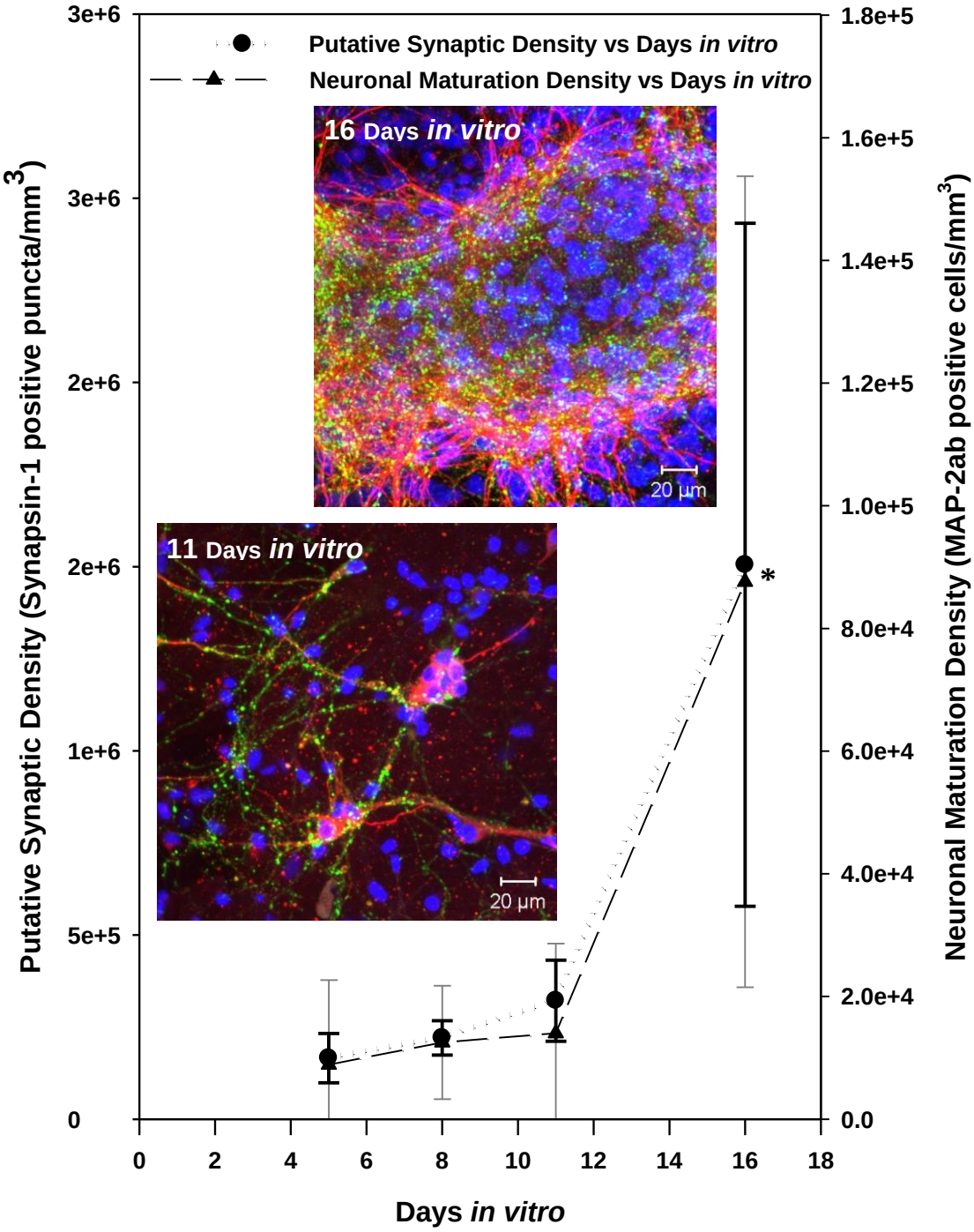

Figure 4.6. Neuronal network maturation and synaptic development with respect to days *in vitro*. The neuronal maturation density and the putative synaptic density increased in proportion slowly in the first one and a half weeks in culture, followed by a rapid increase in the second week. * indicates significant differences for both measures at 16 days *in vitro*, compared to previous time points, $P<0.05$. Insets show 3-D z-stack image projections of 11 and 16 days old cultures. Dramatic changes are seen in the neuronal maturation density (red MAP-2ab positive), synaptic density (green Synapsin 1 positive), and nuclear density (Blue Hoechst positive).

Discussion

3-D Culture Components and their Effects

We selected primary neurons for our 3-D co-cultures, because general transformed cell lines may have incomplete synapse formation, altered ion-channel expression, and abnormally low resting membrane potentials [47-49]. Passaged astrocytes were added to the 3-D co-cultures to serve as substrates for neurite outgrowth; to provide trophic factors and metabolic precursors; and to regulate neuromodulation, synaptic efficacy, and synapse numbers [30, 50]. The structural intactness depended on cell density, matrix concentration, and duration in culture. Low cell densities may diminish structural intactness by not providing adequate cell-to-cell contact and/or trophic support, but high cell densities may retard nutrient transport and waste removal by diffusion [51]. Low matrix concentration may also decrease mechanical stability. Cells were plated at a optimal cell density to ensure a healthy culture, potentially by providing the necessary cell-cell contact and trophic support. Initially, network development appeared uniform in all directions (weeks 1-2), but with the passage of time (weeks 2-3) the 3-D network was remodeled resulting in heterogenous cell densities and culture contraction potentially under the influence of process outgrowth, astrocytic activity etc. It is anticipated that the matrix was degraded and remodeled by astrocytic secretions of matrix metallo-proteinases, extracellular matrix components, and cell adhesive proteins [52-57]. Lipases and proteases released from dying cells and waste released during routine activities may also have contributed. Culture shrinkage may have likely resulted from the traction generated by cellular processes networking with each

other, a phenomenon similarly observed in 3-D collagen [43] and collagen glycosaminoglycan [44] matrix-based cultures. This contraction also probably increases the ratio between construct surface area and volume, allowing diffusion-based mass transport to support greater cell densities.

Structural Development of the 3-D Cultures

The cells in these dissociated cultures develop connectivity potentially in response to physiological stimulation from other cells, thereby self-organizing in to spontaneously active networks. Network formation involves dendritization, neurite extension, axonal and synaptic development, all of which are thought to be influenced by adhesive molecular distribution, trophic molecular distribution, molecular orientation, and contact guidance based on micro-, nano- and chemo-topography of the matrix and cell surfaces [58]; [59]; [60-65]. Additionally, it is suspected that glial cells in the 3-D cultures guide neurite growth cones to reach appropriate targets [66]. Large patterns of electrophysiological activity in the developing network could also affect neurite extension, synaptic development, and thus, connection patterns [67]; for example, contact or proximity interaction between two cells can allow electrophysiological activity from one cell to modify membrane activity in another, stimulating synapse formation [62].

Functional Development of the 3-D Cultures

The functional development of the 3-D networks was monitored by measuring the electrophysiological activity with respect to days *in vitro* (DIV) characterized by spike rate and burst rate, the total number of spikes with respect to the time of recording

(*averaged per electrode*) and the total number of spike-groups with respect to time (*averaged per electrode*), respectively. Our median maximum spike rate of 30-35 spikes/second per electrode and median maximum burst rate of 80-90 bursts/minute per electrode at around 10 DIV were higher than median spike rate of 4.5 (3.6-7.2) spikes/second and median burst rate of 20 (13-39) bursts/minute of 2-D dissociated neural culture as observed by [68]. These differences are potentially influenced by culture dimensionality, cell density, culture age, and media used, etc.

Throughout each of the MEA recordings, the electrophysiological activity abruptly transitioned from unsynchronized activity (potentially resembling natural activity) to synchronized activity (potentially resembling epileptic-like activity). This synchronization suggests that the cultures already have functional neuronal interconnectivity, which simply gets modulated potentially based on inhibitory and excitatory inputs from within the culture. Yet, the changes that occur at the structural level, resulting in these dynamic firing pattern switches are not known. Rapid synaptic modifications, such as abrupt synaptic weight changes, may be a possibility. Alternatively, locally changing field potentials (either intrinsic or stimulated) could alter the firing pattern between neurons.

Variation in the electrophysiological activity of cultures throughout the day suggests changes in the functional connectivity. At the neuronal level, these findings suggest that the output of one neuron potentially depends on its connections with other neurons, the functional synaptic inputs, and the electrophysiological state of the neuron at any given time [69].

Despite the randomized network organization, these 3-D co-cultures displayed bursts in electrophysiological activity similar to the neuronal avalanches (spontaneous spatiotemporal patterns of electrophysiological activity) observed in un-stimulated brain slices [70-71]. Bursts are a very common form of electrophysiological activity exhibited by neural networks; even micro-cultures containing only one or two neurons exhibit epileptic-like activity. Thus, burst communication can be a stimulus for individual neurons to order themselves into functional networks. Since bursts increase the likelihood of significant and reliable neurotransmitter release at the synapses over single spikes, they may be the main mode of neuronal communication.

As seen in Figure 4.3, the average spike and burst rates per electrode for all the cultures initially increased during the first week, maximized during the second week, and finally reduced during the third week in culture. The initial rise in network activity can be explained by rapid neurite outgrowth [72], and excitatory synaptic activity in the 3-D co-culture, because both processes will allow neurons in the network to influence one another. In the first week, it is likely that the neurons spontaneously fire action potentials without much inhibitory input, creating a highly excitatory culture. However, in the second week (as the number of synapses increases slowly and neurons mature, Figure 4.6), it is possible that inhibitory synapses increase, controlling the excitatory behavior of the culture to maintain a homeostatically sustainable level of activity. The highest recorded activity in the second week, followed by a fall in network activity in the third week (Figure 4.3) indicates the possible manifestation of several processes. A plausible explanation is that an initial overshoot of network structural development in the first week with a predominance of excitatory synapses results in increasing activity [73-74].

This increased activity, in turn, initiates homeostatic plasticity within the network through the changing of weights and types of synapses to maintain firing rates within limits, preventing hyper or hypo excitability in the second week in culture [75-76]. At the same time, synaptic pruning, part of the process of maturation of the cultures, may influence the spontaneous, synchronous electrophysiological activity of the cultures. AMPA receptor loss as a cause of reduced electrophysiological activity at later stages of the 3-D culture also merits study. For example, in Alzheimer's Disease, a decrease in the number of glutamatergic AMPA receptors causes a significant reduction in neuronal activity.

Data shown in Figure 4.4, which shows spike and burst rate (*averaged per electrode*) response to bicuculline methiodide (BMI) and gramicidin in 21 DIV 3-D cultures, supports the idea that intrinsic inhibition strongly influences the "native" electrophysiological activity of these cultures. The lower initial baseline, compared to the final baseline, for the three cultures indicates the intrinsic inhibition. With the addition of a disinhibitory drug, BMI, the electrophysiological activity increased for these relatively older and hence "mature" cultures (note that the variance for these data is very low and significant differences exist). Figure 4.4 provides evidence suggesting that pharmacological stimulation must be changing the electrophysiological state of the entire neural network via altering functional connectivity between individual neurons, such as modulating the inhibitory connections. Specifically, by blocking certain receptors functionally, we observe change in the electrophysiological response (in the form of changes in the spike and burst rates *averaged per electrode*). GABA receptors are ionotropic receptors for the neurotransmitter GABA, responsible for fast inhibitory

synaptic transmission in the CNS. When these receptors are blocked at the synapses with bicuculline, not only do spike rates increase indirectly via synaptic disinhibition, but synchronize into bursts, generating oscillatory burst patterns on all electrodes, consistent with previous reports [27, 77-82]. With low native burst activity, bicuculline increases the burst duration and rate as displayed by the 3-D co-culture on MEA 1 in Figure 4.4. On the other hand, a less dramatic response to bicuculline, as displayed by the 3-D co-culture on MEA 3 in Figure 4.4 indicates culture insensitivity, potentially because of a lower concentration of inhibitory GABA receptors at the synapses. In 2-D cultures, effects of bicuculline are reversible at low concentrations (Giugliano, Arsiero et al. 2006; Heuschkel, Wirth et al. 2006); however, in our 3-D co-cultures, most likely due to diffusion limitations, this reversibility is not seen after rinsing (via gentle repeated media changes), as the diffusion time constants are likely higher for 3-D systems. As seen in Figure 4.5, the electrophysiological activity increased with the addition of gramicidin, which forms transient pores in the neurons, thereby lowering the excitation threshold. With these experiments, we demonstrated the responsiveness of our cultures to chemical stimulation; however, more statistically robust results are required before comments on specific characteristics and trends can be made.

Both excitatory and inhibitory synaptic transmission must affect the cumulative spontaneous electrophysiological activity of the cultures. For example, an increase in GABAergic neurons would inhibit electrophysiological activity and vice versa; GABA levels *in vitro* have been shown to peak around 2-3 weeks in 2-D cultures [83]. These considerations may provide insight as to why the 3-D co-cultures displayed lower levels of "native" electrophysiological activity (potentially becoming increasingly inhibited)

between weeks 2 and 3 (see Figures 4.3, 4.4, and 4.5) [84-85]. Moreover, astrocytic proliferation, concurrent with neuronal loss with increasing DIV, could replace active neurons at the electrodes, thereby reducing the number of signal sources at the electrodes, and consequently the recorded signal.

In 2-D cultures, De Lima et al. have shown that the average density of all neurons peaks in the first week *in vitro* [86]. We observed that MAP-2ab staining peaked in the second week in our culture. We explain this increase by two processes: as the network develops, more MAP2-ab is expressed in the neurons (and more synapses are formed) giving an indication of the maturation of the neurons rather than an increase in the number of neurons; and the shrinking of the cultures with respect to DIV resulting in the neural network being packed in a smaller volume. The culture shrinking was estimated to be between 50-90% based on visual observations.

Based on previous studies on 2-D cultures, the onset and type of bursting is expected to depend on the density of the culture; denser cultures tend to burst earlier at higher frequencies, compared to sparse cultures [87]. Three-dimensionality may also contribute to a faster electrophysiological development by influencing cellular signaling, gene expression, as well as allowing more possibilities for cell to cell connections as denser 2-D cultures would do. Unlike in 2-D cultures, three dimensionality allows for cell-ECM contact in all directions over the complete cell membrane, implying that the number of ligand-receptor interactions at the cell surface in 3-D cultures may be orders of magnitude more than those at the cell surface in 2-D cultures, resulting in differential physiological activity. Figure 4.3 shows the presence of developing electrophysiological activity (both spikes and bursts) in 3-D co-cultures (2,500 cells/mm^3) at 2 DIV, while 2-D

cultures with a comparable 2-D density (2,500 cells/mm^2) from Wagenaar et al. 2006 begin spiking and bursting at 3 and 5 DIV, respectively. However, the general trend of increasing electrophysiological activity and its variance in the first two weeks in culture followed by a plateau effect as observed in our 3D co-cultures (Figure 4.3) is similar to that seen by Wagenaar et al. in 2006 with their 2-D cultures, suggesting the maintainance of similar neural functional characteristics between the two different culture configurations.

Electrophysiological activity in the cultures could be affected by changes in environmental conditions and long-term micro-movement of cells resulting from the growth, migration, and process-outgrowth of neurons and glia on the microelectrode surface. However, the changes from such factors are expected to be comparably distributed in all sister cultures at any recording time point, and; therefore, and not expected to significantly alter the analyses done in this study. Overall, we observed that the structural and electrophysiological (functional) characteristics of these 3-D cultures change with respect to DIV over a three week culturing period indicating the dynamic nature of these culture systems.

Experimental Challenges

The variability in the electrophysiological activity recordings between 3-D cultures made analyzing these data challenging. Variability may be explained by the formation of these networks from initially randomized cell organization. Yet, there is value in studying these cultures with a random architecture, because despite the randomness these cultures do evolve with repeatable trends in the gross behavioral

features and responses to physiologically relevant stimuli as measured in terms of the average spike and burst rates per electrode.

Several steps were taken to optimize the conditions for reproducibly obtaining high signal-to-noise ratio electrophysiological activity recordings from the cultures. To help maintain consistent MEA recordings from day-to-day, unstable environmental conditions had to be avoided, such as pH and osmolarity shifts and infections during recording [68]**.** These challenges were addressed by sealing the cultures with O_2-and CO_2^--permeable Teflon membranes [28]. Temperature was maintained constant at 37°C to prevent any pH changes and thermal noise drifts. Placing a nylon mesh insert on top of the 3-D cultures immobilized the 3-D cultures on the MEA electrodes allowing more stable recording of electrophysiological activity signals over the three week culturing period. Additionally, all electrophysiological recordings were conducted inside a UV sterilized laminar flow hood to reduce the likelihood of infections in the cultures. The laminar flow was deactivated to prevent mechanical vibrations, and the hood electrically grounded to ensure long-term stability of recordings and low noise interference. All power sources and the data acquisition computer unit were kept at least 1 meter away from the preamplifier recording set-up inside the hood to minimize noise interference. In addition, all electrical lights were switched off, and recording was done at the same time during the day when lab-activity was low to avoid any extraneous sources of noise.

In pilot runs, the MEAs often returned noisy signals. To counteract this, electric connectivity was increased by inserting conductive zebra strips with small cylinders of gold between the MEA contact pads and preamplifier contact pins, thus reducing signal noise. Other sources of signal noise included delamination of the platinum or insulation

of the MEA electrodes, which paired with capacitative coupling, resulted in good electrodes picking up noise from neighboring damaged electrodes. To limit noise bleeding, under-functioning electrodes (that either had continuous baseline noise levels greater than ± 17.5 μV for the 3-D MEAs, or ± 20-30 μV for the 2-D MEAs, or in which acquired signal abruptly went out of a defined range of ± 1000 μV, or both) were excluded from the recording. Likewise, channels were excluded that continuously fired for most of the recording period because these channels were not evenly distributed over the different cultures studied, nor across the different recording time-points. Therefore, excluding these channels prevented their disproportionate effect on the spike and burst rates measured, allowing us to see the trends followed by the majority of the channel recordings.

High cell density and challenges with microscopic imaging made determining the network connections responsible for the spike patterns generally impossible. The inverted confocal microscope objectives could not produce z-stacks of images of the 3-D cultures at greater than 400X magnifications through the MEAs because of their small working distances. Therefore, MEAs were imaged in an inverted position after media removal so that the objective lens could be positioned as close as possible to the 3-D cultures on the MEA electrodes. Alternatively, 2-D “Thin-MEAs” [25-26] with a thickness of only 180 μm and conductive leads made of optically transparent indium tin oxide were used in our study for both electrophysiological recording and immunocytochemical staining. The "Thin MEAs" could be imaged upright, with the objective approaching the bottom face of the MEA. By the same method, sister cultures on coverslip glass were used for direct microscopic imaging of the structural

development of the cultures. Fixed and stained 3-D neural network images under a microscope were used to quantify synapsin positive puncta development with respect to days *in vitro*. Yet, these analyses did not reveal aspects of functional connectivities such as the synaptic strength, or the excitatory or inhibitory character of the synapses quantified. Optical recording technologies such as voltage-sensitive dyes could measure intracellular calcium, intracellular pH, and voltage gradients throughout an entire cell and among cells in a network with excellent spatial resolution and provide information about the functional connectivity in the network [88]. However, voltage-sensitive dyes are often highly toxic, especially when excited at ultraviolet wavelengths, and ion-sensitive dyes respond slowly [89].

As a limitation, recording on 3-D MEAs occur in very small z-thicknesses (maximum ~ 40 μm) for all the electrodes, despite the substrate being nonplanar. However, we still conducted our experiments with these MEAs because none of the commercial MEAs for *in vitro* use can record from or stimulate throughout the volume of the 3-D neural cultures examined (~ 750 μm thick). Albeit less, the Ayanda 3-D MEAs that we used still offered some level of three-dimensionality in measurement. This indicates a need for the development of higher aspect ratio MEAs that can probe the neural activity over greater z-dimensions.

An alternative method, patch clamp, can be used to assess electrical properties of 3-D neuronal cultures either when cells are cultured atop a 3-D matrix [90-91] or by penetrating the 3-D culture [24]. However, MEAs are still advantageous because, unlike the invasive patch-clamp methods, MEAs do not contaminate or destroy neural circuitry or obscure microscopic access to tissue, but instead allow for continuous, non-terminal,

multi-site recording of network activity in a chemically controlled sterile environment at relatively high temporal and spatial resolutions [27, 92].

There are several challenges in analyzing the data acquired through multi channel systems such as MEA. Several techniques have been developed to analyze multiple channels of neuronal spike train data [93-95], yet the process of acquiring, managing, analyzing, and conveying the data has no standardized protocol. The analyses involve several variables and parameters at different levels. Our method of analysis does not resolve single-channel activity (activity recorded at each electrode) into its often multiple active unit components. While such resolution would be necessary for understanding the finer nuances of network dynamics, units tend to synchronize during bursts, so detection of major features of burst patterns like burst onset and duration is not obscured.

We did not classify bursts based on duration, due to high variance. However, such an analysis may reveal more information on electrophysiological activity patterns displayed by these cultures. Our burst counts are a function of our criteria, and so changing the burst criteria would give a different number of bursts, indicating that useful information may be filtered out based on the detection criteria. Another weakness in our analysis was that occasionally, weak bursting superimposed on tonic spiking at some electrodes make burst identification very difficult, and in some cases impossible, prompting the exclusion of those electrodes from analysis.

Some potential limitations while experimenting with 3-D cultures should also be noted. 3-D cultures typically are randomly oriented; therefore, tissue architecture is difficult to reproduce. Yet, the more *in vivo* like cell–cell and cell–matrix interactions, in contrast to the cell–glass / plastic interactions in 2-D cultures, warrant the use of 3-D

cultures compared to 2-D cultures [96]. Limitations are inherent even in the type of scaffolds used for 3-D culture. For example, despite the benefits of Matrigel^{TM} for a 3-D culture system, such as a biological origin and ECM protein composition, this scaffold type does not have controlled composition. Alternative biomimetic scaffolds with specific ligands cross linked to hydrogel backbones, such as methylcellulose [97] or agarose [98], may allow more control over the presentation of extracellular matrix ligands while continuing to provide the support necessary for neuronal function.

Despite limitations, the advantages of experimenting with 3-D cultures are great. These systems allow control over cellular parameters such as phenotype, ratio, and density. For example, since neurons and astrocytes were harvested separately and mixed in a controlled ratio in these cultures, this approach can be extended to include multiple cell types, such as microglia, oligodendrocytes etc, and the use of transgenic green fluorescent protein (GFP) positive and wild-type cell types, at different ratios for different experimental applications to address specific neurobiological questions.

Conclusion

A 3-D co-culturing system was developed using biological materials: neurons, astrocytes, Matrigel™ matrix, and synthetic materials: nylon mesh, Teflon membrane, and 3-D MEAs. 3-D neural culturing and analysis techniques were optimized. 3-D cultures were characterized electrophysiologically and morphologically with respect to days in culture for up to three weeks. This is the first investigation of the network-level electrophysiological activity of 3-D cultures. These cultures displayed functional synapse formation and both spontaneous and evoked electrical field potentials. The 3-D culture environment appeared to better promote the electrophysiological activity of these cultures as compared to a 2-D environment, as measured in terms of average spike and burst rates per electrode. This electrophysiological activity may be strongly influenced by the changing inhibitory synaptic character of these cultures. This work shows that physiologically relevant 3-D micro-environments can be created with control over cell density, cell types, and media conditions. This research work represents important contributions to the engineering of more physiologically-conformant 3-D neural tissue in culture and the understanding of its structure-function relationship. Applications range from testing drugs to treating pathologies such as traumatic injury, and characterizing and validating neural implants for continuous monitoring, diagnostic, and therapeutic applications to the nervous system. We predict that such efforts will eventually contribute to developing hybrid-neural-interfaces that can diagnose, improve, or resolve functional deficits in the nervous system that result from damage, disease, or dysfunction.

Acknowledgements

The authors would like to thank Brock Wester, Megan Springman, Winston Pewin, Tulika Raj, Nishil Patel, Angela Liu, Melody Keith, Willa Ni, and Rebekah Hamrick for technical and editorial assistance, and NIBIB/NINDS (BRP EB000786) for funding.

References

1. Heetderks, W. and F. Hambrecht, *Applied neural control in the 1990s.* Proceedings of the IEEE, 1988. **76**(9): p. 1115-1121.
2. Dalbasti, T., et al., *Multielectrode array for simultaneous recording of glucose, oxygen and electrocorticography from cerebral cortex in experimental focal epilepsy.* Biosensors and Bioelectronics, 1998. **13**(7-8): p. 881-888.
3. Marzella, P. and G. Clark, *Growth factors, auditory neurones and cochlear implants: a review.* Acta oto-laryngologica, 1999. **119**(4): p. 407-412.
4. Lauer, R., et al., *Applications of cortical signals to neuroprosthetic control: acritical review.* IEEE Transactions on Rehabilitation Engineering, 2000. **8**(2): p. 205-208.
5. Cukierman, E., et al., *Taking Cell-Matrix Adhesions to the Third Dimension.* Science, 2001. **294**(5547): p. 1708.
6. Schindler, M., et al., *Living in three dimensions: 3D nanostructured environments for cell culture and regenerative medicine.* Cell biochemistry and biophysics, 2006. **45**(2): p. 215-227.
7. Kiryushko, D., V. Berezin, and E. Bock, *Regulators of neurite outgrowth: role of cell adhesion molecules.* Annals of the New York Academy of Sciences, 2004. **1014**(1 Gastroenteropancreatic Neuroendocrine Tumor Disease Molecular and Cell Biological Aspects): p. 140-154.
8. Loers, G. and M. Schachner, *Recognition molecules and neural repair.* Journal of neurochemistry, 2007. **101**(4): p. 865.
9. Venstrom, K. and L. Reichardt, *Extracellular matrix. 2: Role of extracellular matrix molecules and their receptors in the nervous system.* The FASEB Journal, 1993. **7**(11): p. 996-1003.
10. Hoffman, R., *To do tissue culture in two or three dimensions? That is the question.* Stem Cells, 1993. **11**(2).
11. Fawcett, J.W., R.A. Barker, and S.B. Dunnett, *Dopaminergic neuronal survival and the effects of bFGF in explant, three dimensional and monolayer cultures of embryonic rat ventral mesencephalon.* Exp Brain Res, 1995. **106**(2): p. 275-82.
12. Smalley, K.S.M., M. Lioni, and M. Herlyn, *Life Isn't Flat: Taking Cancer Biology to the Next Dimension.* In Vitro Cellular & Developmental Biology - Animal, 2006. **42**(8 & 9): p. 242-247.
13. Schmeichel, K.L. and M.J. Bissell, *Modeling tissue-specific signaling and organ function in three dimensions.* J Cell Sci, 2003. **116**(Pt 12): p. 2377-88.
14. Kleinman, H., et al., *Basement membrane complexes with biological activity.* Biochemistry, 1986. **25**(2): p. 312-318.
15. Vukicevic, S., et al., *Identification of multiple active growth factors in basement membrane Matrigel suggests caution in interpretation of cellular activity related to extracellular matrix components.* Experimental cell research, 1992. **202**(1): p. 1-8.
16. Vukicevic, S., et al., *Reconstituted basement membrane (Matrigel) promotes the survival and influences the growth of murine tumors.* International Journal of Cancer, 1992. **50**(5).

17. Wells, M.R., et al., *Gel Matrix Vehicles for Growth Factor Application in Nerve Gap Injuries Repaired with Tubes: A Comparison of Biomatrix, Collagen, and Methylcellulose.* Experimental Neurology, 1997. **146**(2): p. 395-402.
18. Madison, R., et al., *Increased rate of peripheral nerve regeneration using bioresorbable nerve guides and a laminin-containing gel.* Experimental Neurology, 1985. **88**(3): p. 767-772.
19. Streit, J., et al., *The generation of rhythmic activity in dissociated cultures of rat spinal cord.* European Journal of Neuroscience, 2001. **14**(2): p. 191-202.
20. Maeda, E., H. Robinson, and A. Kawana, *The mechanisms of generation and propagation of synchronized bursting in developing networks of cortical neurons.* Journal of Neuroscience, 1995. **15**(10): p. 6834-6845.
21. Hämmerle, H., et al., *Extracellular recording in neuronal networks with substrate integrated microelectrode arrays.* Biosensors & Bioelectronics, 1994. **9**(9-10): p. 691.
22. Meister, M., J. Pine, and D. Baylor, *Multi-neuronal signals from the retina: acquisition and analysis.* Journal Of Neuroscience Methods, 1994. **51**(1): p. 95-106.
23. Israel, D., et al., *An array of microelectrodes to stimulate and record from cardiac cells in culture.* American Journal of Physiology- Heart and Circulatory Physiology, 1984. **247**(4): p. 669-674.
24. Irons, H., et al., *Three-dimensional neural constructs: a novel platform for neurophysiological investigation.* Journal of Neural Engineering, 2008. **5**(3): p. 333-341.
25. Kucera, J., et al., *Power-law behavior of beat-rate variability in monolayer cultures of neonatal rat ventricular myocytes*. 2000, Am Heart Assoc. p. 1140-1145.
26. Fejtl, M., et al., *On micro-electrode array revival: its development, sophistication of recording, and stimulation*, in *Advances in Network Electrophysiology Using Multi-Electrode Arrays*, B.M. Taketani M., Editor. 2006, Springer Science+Business Media Inc: New York. p. 24-37.
27. Heuschkel, M., et al., *Development of 3-D multi-electrode arrays for use with acture tissue slices*, in *Advances in Network Electrophysiology Using Multi-Electrode Arrays*, T. M. and B. M., Editors. 2006, Springer Science + Business Media: New York. p. 69-111.
28. Potter, S. and T. DeMarse, *A new approach to neural cell culture for long-term studies.* Journal Of Neuroscience Methods, 2001. **110**(1-2): p. 17-24.
29. Cullen, D. and M. LaPlaca, *Neuronal response to high rate shear deformation depends on heterogeneity of the local strain field.* Journal of neurotrauma, 2006. **23**(9): p. 1304-1319.
30. Ullian, E., et al., *Control of synapse number by glia.* Science, 2001. **291**(5504): p. 657-661.
31. Brewer, G., et al., *Optimized survival of hippocampal neurons in B27-supplemented Neurobasal™, a new serum-free medium combination.* Journal of neuroscience research, 1993. **35**(5): p. 567-576.

32. Granados-Fuentes, D., et al., *Olfactory bulb neurons express functional, entrainable circadian rhythms.* European Journal of Neuroscience, 2004. **19**(4): p. 898.
33. Legendy, C. and M. Salcman, *Bursts and recurrences of bursts in the spike trains of spontaneously active striate cortex neurons.* Journal of neurophysiology, 1985. **53**(4): p. 926-939.
34. Nakanishi, K. and F. Kukita, *Functional synapses in synchronized bursting of neocortical neurons in culture.* Brain Research, 1998. **795**(1-2): p. 137-146.
35. Valentino, K., J. Winter, and L. Reichardt, *Applications of monoclonal antibodies to neuroscience research.* Annual Review of Neuroscience, 1985. **8**(1): p. 199-232.
36. Binder, L., A. Frankfurter, and L. Rebhun, *The distribution of tau in the mammalian central nervous system.* Journal of Cell Biology, 1985. **101**(4): p. 1371-1378.
37. Vanier, M., et al., *Expression of specific tau exons in normal and tumoral pancreatic acinar cells.* Journal of Cell Science, 1998. **111**(10): p. 1419-1432.
38. Migheli, A., et al., *Light and electron microscope localization of the microtubule-associated tau protein in rat brain.* Journal of Neuroscience, 1988. **8**(6): p. 1846-1851.
39. Goedert, M., R. Crowther, and C. Garner, *Molecular characterization of microtubule-associated proteins tau and MAP2.* Trends in neurosciences, 1991. **14**(5): p. 193.
40. Shafit-Zagardo, B. and N. Kalcheva, *Making sense of the multiple MAP-2 transcripts and their role in the neuron.* Molecular neurobiology, 1998. **16**(2): p. 149-162.
41. Cullen, D., C. Simon, and M. LaPlaca, *Strain rate-dependent induction of reactive astrogliosis and cell death in three-dimensional neuronal–astrocytic co-cultures.* Brain Research, 2007. **1158**: p. 103-115.
42. Fletcher, T., et al., *The distribution of synapsin I and synaptophysin in hippocampal neurons developing in culture.* Journal of Neuroscience, 1991. **11**(6): p. 1617-1626.
43. Grinnell, F., et al., *Nested collagen matrices: a new model to study migration of human fibroblast populations in three dimensions.* Experimental cell research, 2006. **312**(1): p. 86-94.
44. Spilker, M., et al., *Contraction of collagen–glycosaminoglycan matrices by peripheral nerve cells in vitro.* Biomaterials, 2001. **22**(10): p. 1085-1093.
45. Corner, M., et al., *Physiological effects of sustained blockade of excitatory synaptic transmission on spontaneously active developing neuronal networks—an inquiry into the reciprocal linkage between intrinsic biorhythms and neuroplasticity in early ontogeny.* Neuroscience and biobehavioral reviews, 2002. **26**(2): p. 127-185.
46. de Lima, A., B. Lima, and T. Voigt, *Earliest spontaneous activity differentially regulates neocortical GABAergic interneuron subpopulations.* European Journal of Neuroscience, 2007. **25**(1): p. 1.
47. Pancrazio, J., et al., *Development and application of cell-based biosensors.* Annals Of Biomedical Engineering, 1999. **27**(6): p. 697-711.

48. Desai, A., et al., *Human neuroblastoma (SH-SY5Y) cell culture and differentiation in 3-D collagen hydrogels for cell-based biosensing.* Biosensors and Bioelectronics, 2006. **21**(8): p. 1483-1492.
49. Wu, Z., Y. Zhao, and W. Kisaalita, *A packed Cytodex microbead array for three-dimensional cell-based biosensing.* Biosensors and Bioelectronics, 2006. **22**(5): p. 685-693.
50. Tsacopoulos, M. and P. Magistretti, *Metabolic coupling between glia and neurons.* Journal of Neuroscience, 1996. **16**(3): p. 877-885.
51. Cullen, D., et al., *Microfluidic engineered high cell density three-dimensional neural cultures.* J. Neural Eng, 2007. **4**(2): p. 159-172.
52. Gottschall, P.E. and S. Deb, *Regulation of matrix metalloproteinase expressions in astrocytes, microglia and neurons.* Neuroimmunomodulation, 1996. **3**(2-3): p. 69-75.
53. Bellail, A.C., et al., *Microregional extracellular matrix heterogeneity in brain modulates glioma cell invasion.* Int J Biochem Cell Biol, 2004. **36**(6): p. 1046-1069.
54. Wells, G.M., et al., *Quantitation of matrix metalloproteinases in cultured rat astrocytes using the polymerase chain reaction with a multi-competitor cDNA standard.* Glia, 1996. **18**(4): p. 332-40.
55. Pedersen, J.A. and M.A. Swartz, *Mechanobiology in the third dimension.* Annals Of Biomedical Engineering, 2005. **33**(11): p. 1469-1490.
56. Sjaastad, M.D., et al., *Feedback regulation of cell-substratum adhesion by integrin-mediated intracellular Ca2+ signaling.* Proc Natl Acad Sci U S A, 1994. **91**(17): p. 8214-8.
57. Tomaselli, K.J., *Beta 1-integrin-mediated neuronal responses to extracellular matrix proteins.* Ann N Y Acad Sci, 1991. **633**: p. 100-4.
58. Weiss, P., *Experiments on cell and axon orientation in vitro: the role of colloidal exudates in tissue organization.* J Exp Zool, 1945. **100**: p. 353-386.
59. Carter, S., *Haptotaxis and the mechanism of cell motility.* Nature, 1967. **213**(5073).
60. Fromherz, P., H. Schaden, and T. Vetter, *Guided outgrowth of leech neurons in culture.* Neuroscience Letters, 1991. **129**(1): p. 77-80.
61. Hammarback, J., et al., *Growth cone guidance by substrate-bound laminin pathways is correlated with neuron-to-pathway adhesivity.* Developmental biology(Print), 1988. **126**(1): p. 29-39.
62. Curtis, A., C. Wilkinson, and L. Breckenridge, *Living Nerve Nets*, in *Enabling Technologies for Cultured Neural Networks*, M.T.M. Stenger D.A., Editor. 1994, Academic Press: New York. p. 99-120.
63. Clark, P., et al., *Topographical control of cell behaviour. I. Simple step cues.* Development, 1987. **99**(3): p. 439-448.
64. Clark, P., et al., *Topographical control of cell behaviour: II. Multiple grooved substrata.* Development, 1990. **108**(4): p. 635-644.
65. Clark, P., et al., *Cell guidance by ultrafine topography in vitro.* Journal of Cell Science, 1991. **99**(1): p. 73-77.
66. Cohan, C.S. and S.B. Kater, *Suppression of neurite elongation and growth cone motility by electrical activity.* Science, 1986. **232**(4758): p. 1638-1640.

67. Fields, R.D., E.A. Neale, and P.G. Nelson, *Effects of patterned electrical activity on neurite outgrowth from mouse sensory neurons.* Journal of Neuroscience, 1990. **10**(9): p. 2950-2964.
68. Gross, G.W. and K.V. Gopal, *Emerging Histotypic Properties of Cultured Neuronal Networks*, in *Advances in Network Electrophysiology Using Multi-Electrode Arrays*, B.M. Taketani M., Editor. 2006, Springer Science+Business Media Inc.: New York. p. 193-214.
69. Getting, P.A., *Emerging principles governing the operation of neural networks.* Annual Review of Neuroscience, 1989. **12**(1): p. 185-204.
70. Beggs, J.M. and D. Plenz, *Neuronal avalanches in neocortical circuits.* Journal of Neuroscience, 2003. **23**(35): p. 11167-11177.
71. Beggs, J.M. and D. Plenz, *Neuronal avalanches are diverse and precise activity patterns that are stable for many hours in cortical slice cultures.* Journal of neuroscience, 2004. **24**(22): p. 5216-5229.
72. Kamioka, H., et al., *Spontaneous periodic synchronized bursting during formation of mature patterns of connections in cortical cultures.* Neuroscience letters, 1996. **206**(2-3): p. 109-112.
73. Muramoto, K., et al., *Frequency of synchronous oscillations of neuronal activity increases during development and is correlated to the number of synapses in cultured cortical neuron networks.* Neuroscience letters, 1993. **163**(2): p. 163-165.
74. Nakanishi, K., et al., *Recurrent subthreshold electrical activities of rat neocortical neurons progress during long-term culture.* Neuroscience letters, 2001. **304**(1-2): p. 85-88.
75. Turrigiano, G., L. Abbott, and E. Marder, *Activity-dependent changes in the intrinsic properties of cultured neurons.* Science, 1994. **264**(5161): p. 974.
76. Turrigiano, G. and S. Nelson, *Homeostatic plasticity in the developing nervous system.* Nature Reviews Neuroscience, 2004. **5**(2): p. 97-107.
77. Giugliano, M., et al., *Emerging Network Activity in Dissociated Cultures of Neocortex: Novel Electrophysiological Protocols and Mathematical Modeling*, in *Advances in Network Electrophysiology Using Multi-Electrode Arrays*, B.M. Taketani M., Editor. 2006, Springer Science+Business Media, Inc: New York. p. 243-273.
78. Hightower, M., *Electrical and morphological analysis of mouse spinal cord mini-cultures grown on multimicroelectrode plates*. 1988, The University of North Texas: Denton, TX.
79. Jordan, R., *Investigation of inhibitory influences in neuronal monolayer networks cultured from mouse spinal cord*. 1992, University of North Texas.
80. Rhoades, B.K. and G.W. Gross, *The effects of extracellular potassium in epileptiform burst dynamics in cultured monolayer networks*, in *Society of Neuroscience*. 1991.
81. Gross, G. and J. Kowalski, *Experimental and theoretical analysis of random nerve cell network dynamics*, in *Neural Networks. Concepts, Applications, and Implementation*. 1991. p. 47-110.

82. Gross, G., B. Rhoades, and J. Kowalski, *Dynamics of burst patterns generated by monolayer networks in culture*, in *Neurobionics: An Interdisciplinary Approach to Substitute Impaired Functions of the Human Nervous System*. 1993. p. 89–121.
83. Snodgrass, S., et al., *Biochemical correlates of GABA function in rat cortical neurons in culture.* Brain Research, 1980. **190**(1): p. 123.
84. Ramakers, G., et al., *Activity-dependent plasticity of inhibitory and excitatory amino acid transmitter systems in cultured rat cerebral cortex.* International journal of developmental neuroscience: the official journal of the International Society for Developmental Neuroscience, 1994. **12**(7): p. 611.
85. Voigt, T., T. Opitz, and A. de Lima, *Synchronous oscillatory activity in immature cortical network is driven by GABAergic preplate neurons.* Journal of Neuroscience, 2001. **21**(22): p. 8895.
86. De Lima, A., M. Merten, and T. Voigt, *Neuritic differentiation and synaptogenesis in serum-free neuronal cultures of the rat cerebral cortex.* The Journal of Comparative Neurology, 1997. **382**(2).
87. Wagenaar, D., J. Pine, and S. Potter, *An extremely rich repertoire of bursting patterns during the development of cortical cultures.* BMC neuroscience, 2006. **7**(1): p. 11.
88. Cotman, C.W., D.H. Cribbs, and J. Kahle, *Toward Establishing Neural Networks in Culture*. Biological Neural Networks in Invertebrate Neuroethology and Robotics, 1993: p. 3.
89. Hockberger, P.E., D.K. Racker, and J.C. Houk, *Culturing Neural Networks*, in *Enabling Technologies for Cultured Neural Networks*, M.T.M. Stenger D.A., Editor. 1994, Academic Press: San Diego.
90. Coates, P. and R. Nathan, *Feasibility of electrical recordings from unconnected vertebrate CNS neurons cultured in a three-dimensional extracellular matrix.* Journal Of Neuroscience Methods, 1987. **20**(3): p. 203.
91. Ma, W., et al., *CNS stem and progenitor cell differentiation into functional neuronal circuits in three-dimensional collagen gels.* Experimental Neurology, 2004. **190**(2): p. 276-288.
92. Standen, N., P. Gray, and M. Whitake, *Microelectrode Techniques*, *The Plymouth Workshop Handbook*. 1987: Company of Biologists.
93. Tam, D., *A hybrid time-shifted neural network for analyzing biological neuronal spike trains*, in *Progress in Neural Networks*, O. Omidvar, Editor. 1994, Ablex: Norwood. p. 129.
94. Gerstein, G. and A. Aertsen, *Representation of cooperative firing activity among simultaneously recorded neurons.* Journal of neurophysiology, 1985. **54**(6): p. 1513-1528.
95. Lindsey, B., R. Shannon, and G. Gerstein, *Gravitational representation of simultaneously recorded brainstem respiratory neuron spike trains.* Brain Research, 1989. **483**(2): p. 373.
96. Discher, D., P. Janmey, and Y. Wang, *Tissue cells feel and respond to the stiffness of their substrate.* Science, 2005. **310**(5751): p. 1139-1143.
97. Stabenfeldt, S., A. Garcia, and M. LaPlaca, *Thermoreversible laminin-functionalized hydrogel for neural tissue engineering.* Journal of Biomedical Materials Research Part A, 2006(4).

98. Cullen, D., M. Lessing, and M. LaPlaca, *Collagen-dependent neurite outgrowth and response to dynamic deformation in three-dimensional neuronal cultures.* Annals Of Biomedical Engineering, 2007. **35**(5): p. 835-846.

CHAPTER 5

TRAUMA-INDUCED PLASMALEMMA DISRUPTIONS IN THREE-DIMENSIONAL NEURAL CULTURES ARE DEPENDENT ON STRAIN MODALITY AND RATE

Summary

Traumatic brain injury (TBI) results from supra-threshold physical loading, resulting in acute cell death or sub-lethal cellular and network damage. Compromise of the neural plasmalemma has been observed following traumatic neural insults; however, the mechanisms and time-course of such disruptions remain poorly understood. In order to investigate plasma membrane disruption as a function of time post-insult and the effect on long-term cell viability, we induced complex, three-dimensional shear or compressive strain fields on neuronal-astrocytic co-cultures distributed throughout a bioactive matrix (>500μm thick). Co-cultures underwent bulk mechanical loading (0.50 shear or compressive strain at 1, 10, or 30 s^{-1} strain rate) or static control conditions in the presence of impermeant dyes, which enter the cell upon a breach in membrane integrity. Following both bulk shear and compressive loading, permeability markers entered cells in a strain rate dependent manner. Real-time imaging revealed increased membrane permeability in a sub-population of cells immediately upon deformation. Cells were more sensitive to bulk shear deformation than compression in terms of acute permeability changes as well as subsequent cell survival. Moreover, alterations in cell membrane permeability were transient and biphasic over the ensuing hour post-insult, consistent with acute membrane disruptions and resealing followed by a phase of secondary membrane damage. At 48 hrs post-insult, cell death significantly increased in the high

strain rate group but not after quasi-static loading, suggesting that cell survival relates to the initial extent of transient structural compromise. These results provide insight into the temporally varying alterations in membrane stability affecting neural cell survival, which will be critical for elucidating physical cellular tolerances. [1]

Key words. neurotrauma, traumatic brain injury, cell mechanics, biomechanics, compression, shear, neuron, astrocyte, strain rate, 3-D culture, membrane permeability

---

This chapter is an adaptation of a manuscript written along with D.K. Cullen and M.C. LaPlaca to be submitted for review to the Biophysical Journal

Introduction

Traumatic mechanical loading to central nervous system cells can lead to devastating consequences. Neural cells in the brain have a unique fluidic and osseous protection system, and; therefore, are not normally subjected to large deformations. Supra-threshold physical loading can lead to traumatic brain injury (TBI), which is a leading cause of death and disability in the United States [1-2]. TBI is unique from any other neurological affliction in that it is induced by a physical event. The long-term outcomes of TBI are dependent on the severity of the primary physical event and are compounded by multi-faceted secondary events (see [3-5] for reviews). Collectively, these events may result in significant functional deficits and progressive neural degeneration [6-7]. Currently, there are no effective therapeutic interventions that directly attenuate injury-induced neural pathology. Therefore, attention to the tissue and cellular biomechanics of injury is critically important in refining neural tolerance criteria to injury and developing targeted therapies for this affliction.

The mechanics of brain trauma can be quite complex due to the uniqueness of loading parameters from individual to individual. Typically, closed head injury is caused by impact and/or acceleration-deceleration based inertial loading of the head, leading to overt lesions or contusions, and/or, multi-focal or diffuse damage, and possibly, disruption of the vasculature [8-10]. The resulting injuries are a function of complex, three-dimensional (3-D) strain fields consisting of compressive, tensile, and shear strain patterns throughout the brain (Figure 5.1). Based on these biomechanical considerations, as well as heterogeneous brain tissue properties, it is predicted that both shear and compressive deformation are relevant modes of tissue loading in impact (focal/contusion)

injuries, whereas shear deformation is predicted to be the dominant mode of tissue loading in inertial (diffuse/acceleration-deceleration) injuries [11-15]. In turn, these tissue-level strain patterns translate into complex combinations of cellular strains that are dependent on cellular orientation, cytoarchitecture, and cell-cell/cell-matrix interactions [16-17].

The immediate physical consequences of loading on the cellular level may range from complete structural failure, such as major somatic disruption and axotomy, to more subtle damage, such as cytoskeletal breakdown, decoupling of sub-cellular structures/organelles, and micro- or nano-tears in the plasmalemma. However, it is challenging to establish these potentially subtle physical effects as a direct consequence of loading, because secondary pathophysiology can induce similar structural damage. In particular, physical disruption of the plasmalemma, termed "mechanoporation", may be one of the initial responses and is particularly devastating as it may trigger disruption of normal cell function in a positive feedback manner. We postulate that there is an important link between the physical parameters of traumatic loading and physiological consequences of neural injury, and thus trauma-specific mechanisms of physical damage should be identified.

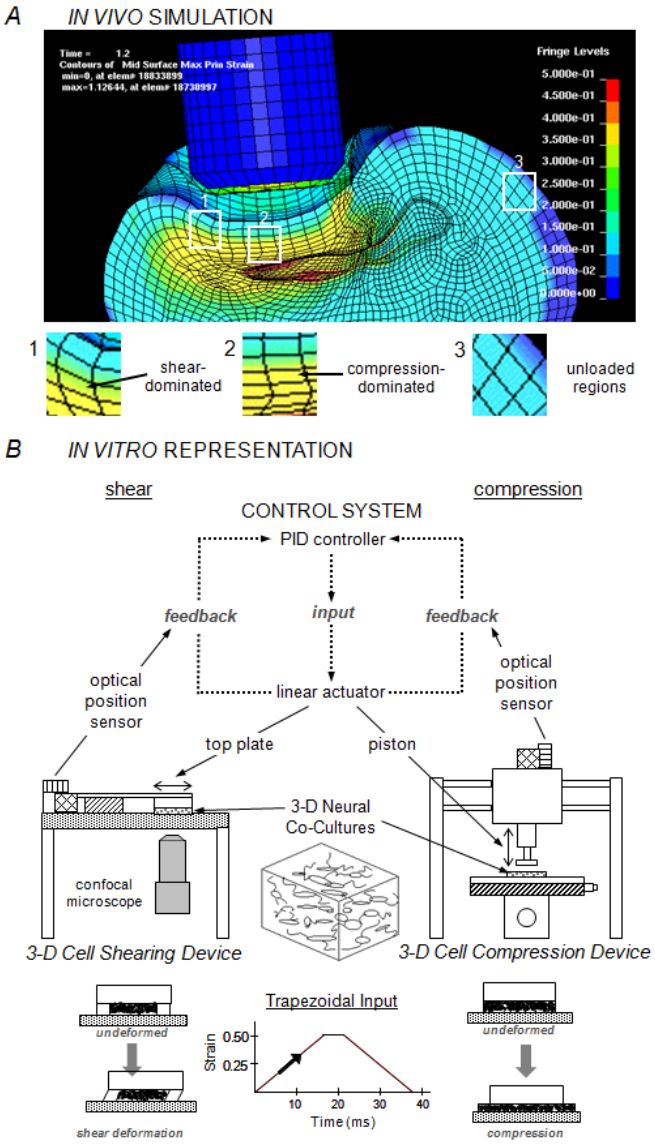

Figure 5.1. Finite element analysis (FEA) simulations following traumatic loading *in vivo* and corresponding isolation of tissue bulk loading components *in vitro*. The strain propagation following a focal insult (controlled cortical impact) in a rodent as predicted by FEA (A). In this example, a focal insult results in heterogeneous strain fields at the tissue level, with regions experiencing shear- or compression-dominated strain fields or regions left relatively unloaded. We developed custom *in vitro* devices for shear or compressive loading of engineered 3-D tissue surrogates (B). These linear-actuator driven systems impart a precise deformation based on proportional-integral-derivative (PID) control with positional feedback from optical sensors. The bulk loading occurs at a prescribed strain magnitude over a specified time, thus controlling strain rate, based on a trapezoidal input. These experimental models provide control over bulk material deformation, while local cellular strains vary based on cellular orientation(s) within the matrix, resulting in various proportions of strain type (e.g., normal versus shear), complexity of the strain field, and strain magnitudes.

In the current work, we evaluated alterations in plasmalemma permeability as a function of bulk deformation mode (shear versus compression), loading parameters (strain and strain rate), and time post-insult (milliseconds to hour) in 3-D tissue surrogates. Neural cells were cultured in a 3-D microenvironment, consisting of a controlled ratio of neurons and astrocytes distributed throughout a bioactive matrix (>500μm thick; ~1 cm in diameter). Precise control of mechanical inputs, using custom built electromechanical devices, enabled delivery of a single stimulus (physical insult) to the 3-D neural constructs reproducibly for a range of strains and strain rates; for these studies we used a high shear or compressive strain (0.50) over slow ("quasi-static") or dynamic (≤50 ms) durations to evaluate the effects of strain rate. Because of the anisotropy and three-dimensionality of the neural network structure in these cultures, the resulting strain fields at the cellular level, upon dynamic deformation, are inherently heterogeneous [16]. The incidence and severity of acute membrane compromise were then correlated with longer-term cell death. This experimental design replicates key features of traumatic loading *in vivo*, such as 3-D dynamic loading conditions, multi-cellular composition, and a 3-D distribution of cell-cell/cell-matrix interactions. With the added benefits of real-time imaging and precise micro-environmental control, this system was utilized to examine the acute temporal profile of membrane disruptions.

Materials and Methods

Isolation of Primary Cortical Neurons and Cortical Astrocytes

All procedures involving animals were approved by the IACUC of the Georgia Institute of Technology. All reagents were from Invitrogen (Carlsbad, CA) unless otherwise noted. Timed-pregnant Sasco Sprague-Dawley rats (embryonic day 17-18; Charles River, Wilmington, MA) were anesthetized using 3% isoflurane and rapidly decapitated. The uterus was removed by Caesarian section and placed in calcium- and magnesium- free Hank's Balanced Salt Solution (CMF-HBSS). Each fetus was removed and rapidly decapitated. After removal of the brain, cerebral cortices were isolated and dissociated using pre-warmed trypsin (0.25%) + EDTA (1 mM) (10 min at 37ºC). The trypsin-EDTA was removed and deoxyribonuclease I (DNase I, 0.15 mg/mL, Sigma, St. Louis, MO) in CMF-HBSS was added. The tissue was triturated with a flame-narrowed Pastuer pipette, centrifuged (1000 rpm, 3 min), and the dissociated cells resuspended in co-culture medium (Neurobasal medium + 2% B-27 + 1% G-5 + 500 μM L-glutamine).

Astrocytes were isolated from postnatal (day 0-1) Sasco Sprague-Dawley rats following anesthesia (3% isoflurane) and decapitation. The cortices were isolated as described above. Further, they were minced and dissociated following the same process as described above to give a cell pellet upon centrifugation that were resuspended in DMEM/F12 + 10% FBS, and transferred to culture flasks. To isolate type I astrocytes, the flasks were mechanically agitated to dislodge less adherent cell types. As the cells approached ~90% confluence they were replated (300 cells/mm^2). Astrocytes were used between passages 4-12 to permit phenotypic maturation [18-19]

Generation of 3-D Neuronal-Astrocytic Co-Cultures

Co-cultures were plated in 3-D using neurons and astrocytes that were separately isolated and dissociated (as described above) within Matrigel™ matrix in custom-made cell culture chambers consisting of a glass coverslip below a circular silicone-based elastomer mold (1:1 ratio of Sylgard 184 and 186, Dow Corning; Midland, MI; cross-sectional area = 2 cm^2). Prior to plating, the chambers were pre-treated with 0.05 mg/mL poly-L-lysine (PLL, Sigma) followed by a Matrigel™ pre-coat (0.5 mL/well at 0.6 mg/mL; Becton Dickinson Biosciences; Bedford, MA) in Neurobasal medium. Matrigel™ exhibits fluid-like behavior at 4°C (permitting even dispersion of dissociated cells throughout matrix) and gels at physiological temperature (entrapping cells in 3-D) [20]. Co-cultures were plated at 2500 cells/mm^3 at a 1:1 neuron:astrocyte ratio (final Matrigel™ concentration 7.5 mg/mL) across a thickness of 500-750 μm, and immediately placed at 37°C for matrix gelation, after which 0.5 mL of co-culture medium was added to each culture well. Co-cultures were maintained at 37°C and 5% CO_2-95% humidified air and medium exchanged at 24 hrs and every 2 days thereafter. This co-culture system has previously been characterized, demonstrating robust neurite outgrowth, network formation, neuronal maturation, and high viability (approx. 95%) at 21 days *in vitro* (DIV) [16, 21-22].

Application of Shear or Compressive Loading

Controlled deformation of the neuronal-astrocytic co-cultures was applied using custom-built electromechanical devices (Figure 5.1). *Compressive deformation* was applied using a 3-D Cell Compression Device (CCD) and *shear deformation* was applied

using a 3-D Cell Shearing Device (CSD) [16-17, 22-23]. For each device, the mechanical action was driven by a linear-actuator (BEI Kimco; San Marcos, CA) coupled to a custom-fabricated digital proportional-integral-derivative controller (25 kHz sampling rate, 16 bit sampling resolution) with closed-loop motion control feedback from an optical position sensor (RGH-34, 400 nm resolution; Renishaw, New Mills, United Kingdom). A trapezoidal input was generated by a code written in LabVIEW® (National Instruments; Austin, TX), permitting application of prescribed strain type magnitudes and strain rates using the same parameters and control system.

All experiments were performed between 21-33 DIV. At the time of injury, cultures were removed from the incubator and mounted in one of the devices. For compression, the linear actuator drove an impactor (piston) compressing the entire construct (piston diameter of 10 mm was greater than construct diameter which ranged from 7-9 mm) to impart uniform compressive loading. For shear deformation, a cell chamber top plate affixed to a linear actuator permitted lateral motion of the top plate with respect to the fixed base of the cell chamber to impart simple shear deformation to the entire 3-D construct. Experimental groups consisted of static (unloaded) control cultures or mechanical loaded cultures. Both compressive or shear deformations were delivered using the same parameters: a trapezoidal input of 0.50 strain at a "quasi-static" strain rate of 1 s^{-1} or at "dynamic" strain rates of 10 s^{-1} or 30 s^{-1} (loading onset times of 500 ms, 50 ms, and 16.7 ms, respectively). During the static unloaded control conditions for compression and shear, the constructs were placed into the respective device, but the device was not activated. After mechanical deformation or static control conditions,

warm medium or buffer with permeability marker (based on the type of assay to be performed) was added and the cultures returned to the incubator. .

Assaying Cell Permeability

Assaying Acute Permeability in Shear and Compression Deformed Cultures

The normally cell-impermeant molecule calcein (629 Da) was utilized to assess acute alterations in plasmalemma permeability following shear and compressive loading at 0.50 strain at strain rates of 1 s^{-1}, 10 s^{-1}, 30 s^{-1} or static control conditions (n = 3-4 constructs per loading condition per deformation mode). Calcein only accesses cells with increased membrane permeability, and will remain sequestered provided membrane integrity is re-established. Prior to injury, medium was removed, calcein solution ($3.2x10^{-4}$ M in HBSS) was added, and the cultures were incubated at 37°C for 10 min to allow the calcein to saturate the 3-D culture construct. Prior to mechanical loading, excess calcein buffer was removed to avoid the potential artifact of fluid movement during the insult stimulus. Calcein buffer remained available within the construct, however, due to the tortuosity of the matrix (as observed from real-time viewing, see Figure 5.4). Immediately following the insult, calcein solution was re-added and the constructs were placed at 37°C for 10 min. Constructs were then rinsed with HBSS and intracellular calcein uptake was immediately imaged using confocal microscopy (LSM 510, Zeiss, Oberkochen, Germany) (ex: 495nm / em: 515nm). Confocal images were acquired across the full thickness of the cultures. These z-stacks were converted to 3-D reconstructions using the LSM Image Browser. At least three regions (defined as having minimum dimensions of 460.7 μm x 460.7 μm x 100 μm) per culture were counted.

Cells with compromised membranes (i.e. calcein^{+}) were counted and the density of permeabilized cells per unit volume was calculated.

The fluorescent intensity of randomly selected calcein^{+} cells from the same cultures was measured to assess the *degree* of altered permeability. Z-stacks from 3-4 regions per culture were converted into 3-D reconstructions using LSM Image Browser. Within each reconstruction, fluorescent intensity line traces, proportional to the amount of calcein uptake, were acquired such that they crossed the cell body of discernable, randomly selected calcein^{+} cells (Figure 5.2). An intensity ratio was calculated based on the formula: (peak intensity – background intensity)/(background intensity). Experimental groups were as follows: shear loading (0.50 strain) at strain rates of 1 s^{-1} (n = 5 cells), 10 s^{-1} (n = 44 cells), 30 s^{-1} (n = 51 cells); and compressive loading (0.50 strain) at strain rates of 1 s^{-1} (n = 19 cells), 10 s^{-1} (n = 22 cells), 30 s^{-1} (n = 75 cells). Of note, the range in the number of cells analyzed per group was due to fewer calcein^{+} cells per frame following lower strain rate loading (see Results).

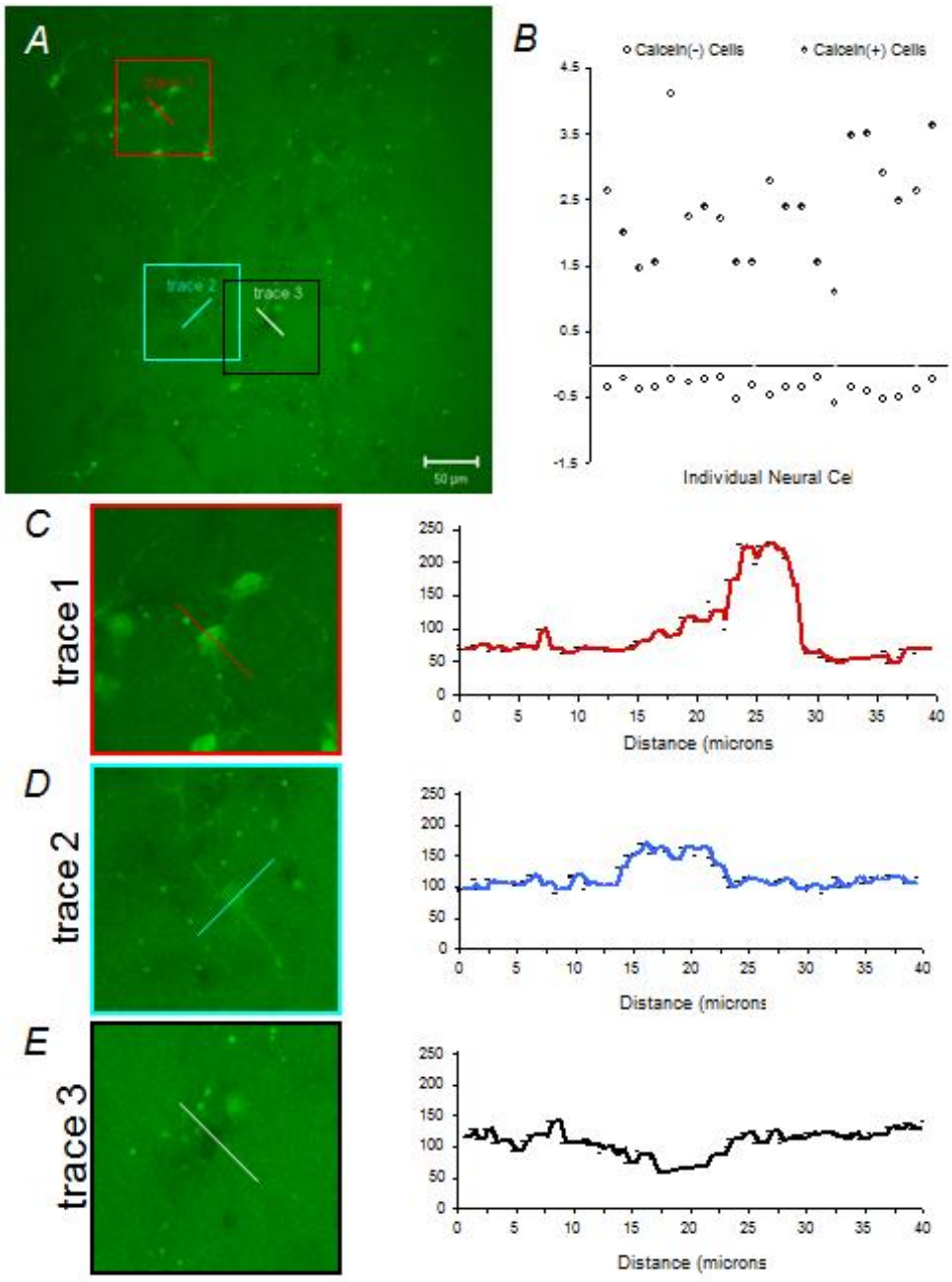

Figure 5.2. Methodology employed to quantify the degree of permeability marker uptake. Fluorescent intensity traces, proportional to amount of calcein uptake, from sample cells in (A) are shown in (C), (D) and (E). Cells were classified into two populations (i.e. calcein^{+} and calcein^{-}) based on fluorescent intensity relative to background (B). Cells with a significant calcein uptake exhibited much higher fluorescence relative to background (C). Cells with low calcein uptake exhibit a smaller increase in fluorescence relative to background (D). Cells that did not uptake calcein exhibited lower fluorescence than background (E). This technique was used to quantify the degree of membrane permeability following trauma. Similar methodology was employed to evaluate membrane permeability changes in real-time following loading.

Assaying Acute Permeability in Real Time

Separate 3-D co-cultures were imaged in real-time on a confocal microscope during and immediately following shear strain (0.50 shear strain, 10 s^{-1} or 30 s^{-1} strain rate) to investigate the temporal pattern of acute membrane disruptions (n=8 constructs total). Imaging was performed using a 10x (921.4 μm x 921.4 μm) or 20x (460.7 μm x 460.7 μm) objective. The optical slice thickness was set to establish a suitable signal-to-noise ratio, and ranged from 5-10 μm based on the magnification. Images were captured at a rate of 1-2 frames/second at a resolution of 256 x 256 or 512 x 512 pixels. On a per-cell basis, changes in intracellular fluorescent intensity were measured as a function of time post-insult using LSM Image Browser (Zeiss). Real-time analyses were only performed using the 3-D CSD because it was designed to mount on an inverted microscope stage with a glass bottom cell chamber. Moreover, the simple shear deformation occurs through in-plane translation of the top plate [17], permitting tracking of individual cells within the focal plane. The compression device was not built to mount on a confocal microscope and out-of-plane z-axis displacement does not lend the system to individual cell tracking.

Assaying Sub-Acute Permeability

To assess the sub-acute time-course of post-insult alterations in permeability, additional constructs were incubated with calcein solution and/or ethidium homodimer-1 (EthD-1; 4 μM, Molecular Probes, Eugene, OR) before and at various time-points up to 60 minutes following shear deformation (0.50 strain, 10 s^{-1} strain rate). Specifically, calcein was added prior to loading (0^{-}) or at 10 min post-insult; EthD-1 was added at 0^{-}, 10 min or 60 min post-insult (n = 2-4 each). Cultures were imaged 10 min following the

EthD-1 incubation. Both calcein and EthD-1 gain intracellular access following compromise to the plasmalemma. However, while calcein requires resealing for intracellular sequestration, EthD-1 labels compromised cells irrespective of membrane resealing by irreversibly binding DNA (causing the nuclei of the cell to fluoresce red (ex: 495nm / em: 635nm)). Together, calcein and EthD-1 permit distinction between re-sealed and non-resealed cell populations.

Assaying Permeability by Cell Type

The subpopulation of neural cells exhibiting permeability changes was evaluated in separate cultures using neurons derived from transgenic mice expressing green fluorescent protein (GFP) cultured with wild-type rat astrocytes (isolated as described above). This permitted neuronal identification (GFP^+). These studies used rhodamine (fluorescing red) as the permeability marker ($3.2x10^{-4}$ M in HBSS), which was added to the construct prior to loading (as described for calcein). These co-cultures were subjected to 0.50 shear strain at a strain rate of 10 s^{-1} and neuronal versus astrocytic rhodamine uptake was qualitatively assessed at 10 min post-insult (n = 3 constructs).

Assaying Cell Viability

Culture viability was assessed, using fluorescent probes for distinguishing live and dead cells, at 48 hrs following either shear or compressive loading (0.50 strain each) at strain rates of 1 s^{-1}, 10 s^{-1}, 30 s^{-1} or static control conditions on 20-21 day old cultures (n = 3-7 constructs per loading condition per deformation mode). Cell cultures were incubated with EthD-1 (4 μM) and calcein AM (2 μM) (Molecular Probes) at 37°C for 30 min and then rinsed with Dulbecco's phosphate-buffered saline. The percentage of

surviving cells was calculated by counting the number of live cells (fluorescing green by AM-cleavage) and the number of cells with compromised membranes - dead or dying cells (nuclei fluorescing red by EthD-1). This assay is distinct from that described above because when AM is conjugated to calcein, it is lipid soluble and readily crosses the plasma membrane. AM cleavage occurs via esterase activity, which is indicative of metabolically active cells. Following this cleavage, the calcein fluoresces green (ex: 495nm / em: 515nm) and cannot pass through the plasma membrane. Of note, percentage of viable cells was based on the total cells present at the time point evaluated, and not on the total cells originally plated. Also, we have previously found that post-insult astrocyte proliferation can mask reductions in survival [22]; therefore, we also calculated the density of dead cells normalized relative to the density of dead cells found in static control cultures.

Statistical Analysis

Analysis of variance (ANOVA) was performed for the permeability and viability studies (with deformation mode and level as independent variables). When differences existed between groups, post hoc Tukey's pair-wise comparisons were performed. Additionally, linear regression analyses were performed to assess potential correlations between permeability measurements and subsequent culture viability. For all statistical tests, $p < 0.05$ was required for significance. Data are presented as mean ± standard deviation

Results

Shear vs. Compression Permeability

3-D neuronal-astrocytic co-cultures were subjected to static (unloaded) conditions or bulk compressive or shear deformation (0.50 strain each) at quasi-static (1 s^{-1}) or dynamic (10 s^{-1} or 30 s^{-1}) strain rates. The normally cell-impermeant molecule calcein was utilized to investigate non-physiological membrane disruptions following the prescribed loading conditions. Since calcein rinses out of cells if membrane integrity is not reestablished, the presence of calcein^{+} cells directly indicates transient alterations in membrane permeability (i.e. membrane resealing). Minimal calcein uptake occurred under either static control or quasi-static conditions (for both shear and compression groups) (Figure 5.3A). However, there was increased calcein uptake following dynamic deformation, indicating that calcein diffused intracellularly and became sequestered during or within minutes following loading. The density of calcein^{+} cells depended on strain rate ($p < 0.001$), but not the mode of deformation, and there were no significant interactions between these factors. Specifically, permeability increased as a function of strain rate and was highest at the maximum rate for both compression and shear ($p < 0.05$ each). However, the density of calcein^{+} cells did not vary between compression versus shear at any matched strain rates (Figure 5.3B). Qualitatively, more calcein^{+} cellular processes were observed following shear compared to compression. In addition, we estimated the percentage of permeabilized cells based on the overall cell density of control cultures. This showed that for both shear and compressive deformation, static and quasi-static controls contained less than 1% and 3% calcein^{+} cells, respectively.

Following 10 s^{-1} loading, approximately 10.0% of the cells took up calcein following shear deformation, compared to 1.5% following compression (not significant). Moreover, for 30 s^{-1} conditions these levels rose to over 27% of cells following shear or compression.

To determine the degree of cell permeability, we evaluated the intracellular fluorescence intensity of calcein on a per-cell basis (from the above cultures). This revealed a significant increase in the mean intensity of the calcein^{+} cells strained at 30 s^{-1} compared to quasi-static loading ($p<0.05$) for both shear and compression (Figure 5.3C). The mean intensity of calcein^{+} cells was significantly increased at 10 s^{-1} versus quasi-static loading only for shear ($p<0.05$). Additionally, at a matched strain rate of 10 s^{-1}, there was enhanced calcein uptake in cells following shear versus compression ($p<0.05$) (Figure 5.3C).

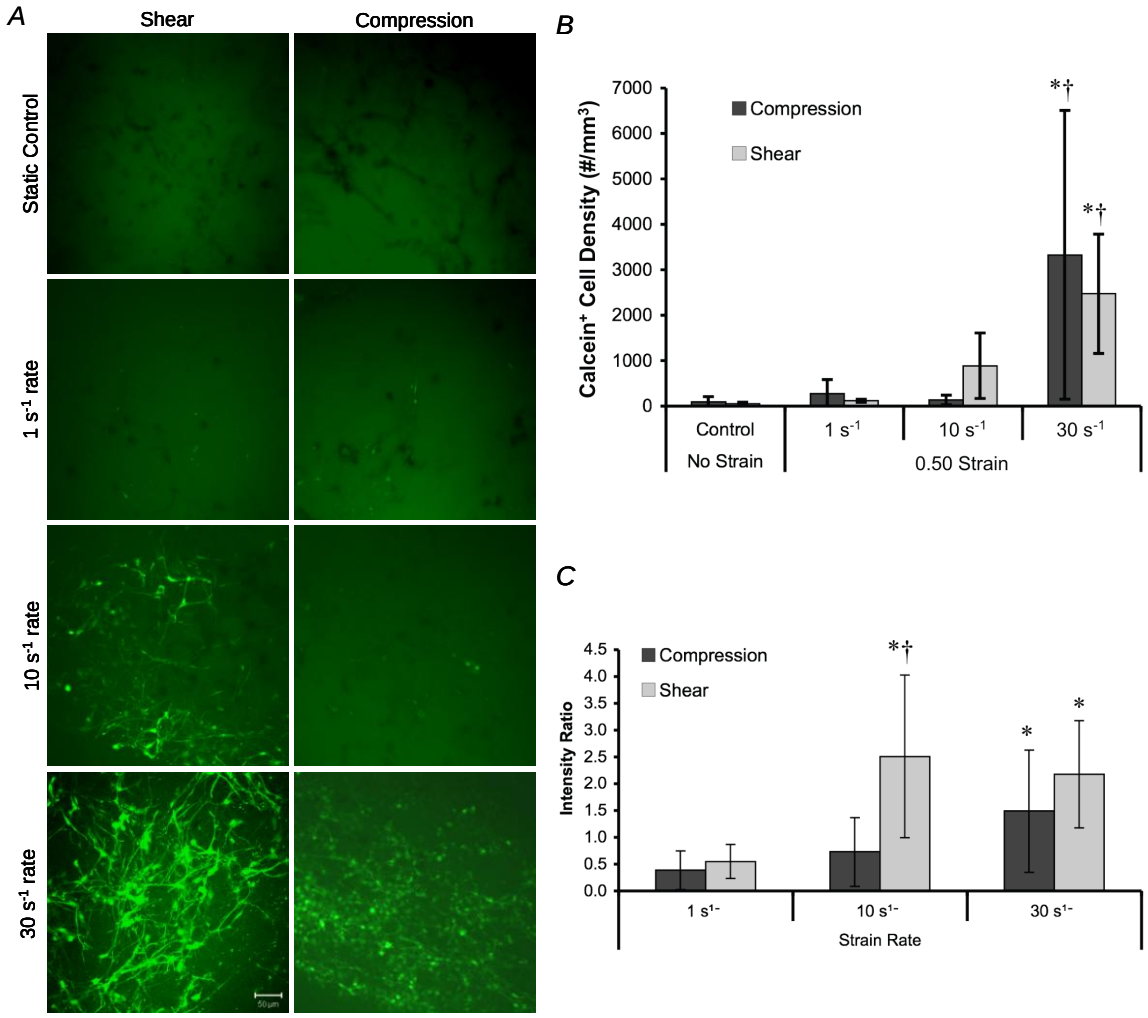

Figure 5.3. Alterations in acute membrane permeability in shear versus compression. Representative confocal reconstructions of calcein stained 3-D cultures following static control conditions or mechanical loading (0.50 strain at 1 s^{-1}, 10 s^{-1}, or 30 s^{-1} strain rate) (A). Calcein, a normally cell-impermeant green fluorescent molecule, was added to the extracellular space prior to loading but becomes intracellularly sequestered in some of the cells in 3-D culture during or immediately following loading (reconstructions from 50 µm thick z-stacks; scale bar = 50 µm). Cell density of permeabilized (calcein^{+}) cells (B). The 3-D cell density and percentage of calcein^{+} cells increased as a function of strain rate and was highest at the maximum strain rate for both compressive and shear loading (*$p < 0.05$ vs. static control; †$p < 0.05$ vs. lower strain rate(s)). However, these parameters did not vary based on mode of deformation. Degree of cell permeability following variable rate shear or compressive (0.50 strain) loading (C). There was a significant increase in the mean intensity of calcein^{+} cells vs. quasi-static loading for both shear and compression at 30 s^{-1} and shear only at 10 s^{-1} (*$p < 0.05$). Also, at 10 s^{-1} loading, there was enhanced calcein uptake following shear vs. compression (†$p < 0.05$). Data: mean ± standard deviation.

Acute Time Course of Permeability Changes

Immediate trauma-induced alterations in cell membrane permeability were investigated on a cell-by-cell basis by imaging shear strain application in real-time. Three-dimensional neuronal-astrocytic co-cultures were subjected to dynamic shear deformation (0.50 strain). Calcein was present in the extracellular space prior to loading (as before), causing it to fluoresce bright green whereas cells with intact plasmalemma excluded the dye and appeared dark. Immediately post-insult, a modest subset of cells immediately became calcein^{+} throughout the cell bodies, whereas in other cells a widespread loss of cell/process definition was apparent (Figure 5.4A). These observations were quantified, revealing that roughly half (47.4%) of the cells showed no change (defined as less than a 10% change in intracellular fluorescence relative to background) immediately following loading. Conversely, 42.1% of cells showed an immediate increase in intracellular intensity between 10-50%. Additionally, 10.5% of the cells had a greater than 50% change in intracellular intensity (these cells either completely blended with the background or appeared brighter than background).

We then used continuous monitoring to qualitatively track calcein entry on a per-cell basis as a function of time post-insult (Figure 5.4B-C). As before, clear intracellular calcein exclusion was observed pre-loading. Immediately following loading, intracellular (in somata as well as in processes) calcein intensity increased in a small portion of cells consistent with earlier observations. However, in most cells a gradual increase in intracellular intensity was observed over seconds to minutes post-insult leading to the somata and processes slowly blending into the background as calcein gradually diffused into the cells post-insult. These observations provide direct evidence of plasmalemma

pores/tears as an immediate and direct result of high strain rate loading. Moreover, the relatively protracted diffusion over the acute period post-injury likely results in the substantial uptake observed following rinsing (refer to Figure 5.3).

The Sub-Acute Time-Course of Altered Membrane Permeability

The time-course of plasmalemma disruptions was investigated following traumatic shear loading at 0.50 strain, 10 s^{-1} strain rate. The density of permeabilized cells was evaluated when permeability marker was added either pre-loading or at specific time points post-loading. Here, there was significant calcein uptake when present during loading (consistent with our earlier results); however, when calcein was added 10 min post-insult, uptake was minimal (Figure 5.5). This indicated that within minutes of the insult, either the cell had reestablished membrane integrity (for appropriate exclusion of calcein) or there was a state of dynamic pore cycling (opening and closing, preventing intracellular calcein sequestration).

To differentiate between these possibilities, we evaluated the density of permeabilized cells at discrete time-points post-insult using calcein and an additional membrane-impermeant marker, EthD-1. These are complimentary markers since calcein requires resealing for intracellular sequestration, whereas EthD-1 irreversibly binds DNA and will thus label compromised cells irrespective of membrane resealing. Here, calcein was only added pre-insult (to track calcein sequestration over time), but EthD-1 was added either pre-insult or at 10 min or 60 min post-insult (to assess potential membrane resealing and secondary poration; imaging occurred 10 min after EthD-1 addition). This revealed that both the density of calcein^{+} and EthD-1^{+} cells varied over time post-insult.

In particular, the density of EthD-1^{+} cells increased immediately after the insult, decreased precipitously when added 10 min post-insult, but then increased again gradually over hours, thus revealing a bi-phasic relationship (Figure 5.6). In addition, the density of calcein^{+} cells increased at 20 min post-insult, possibly due to intracellular diffusion of calcein and/or persistent uptake in processes remote from the somata. Also, by 60 min post-insult, calcein^{+} cellular debris was present, potentially indicating active removal of calcein or the breakdown of some initially calcein^{+} cells. Collectively, these observations demonstrate that there is a primary, transient phase of mechanoporation that concludes within minutes, perhaps ten of seconds, of loading. Also, these results suggest a phase of secondary poration possibly represented by persistent, cycling, or permanent pores and/or the initiation of cell death.

Neuronal vs. Astrocytic Permeability Changes

Acute trauma-induced alterations in membrane permeability were investigated in neurons versus astrocytes following shear loading at 0.50 strain at 10 s^{-1}. For these studies, a group of 3-D co-cultures were generated using GFP^{+} neurons mixed with wild-type astrocytes to permit neuronal identification, and a red permeability marker, rhodamine, was used. Qualitative assessment revealed that alterations in membrane permeability occurred in both neurons (GFP^{+}/rhod^{+}) and astrocytes (GFP^{-}/rhod^{+}), with robust rhodamine uptake in both the somata and cellular processes (Figure 5.7).

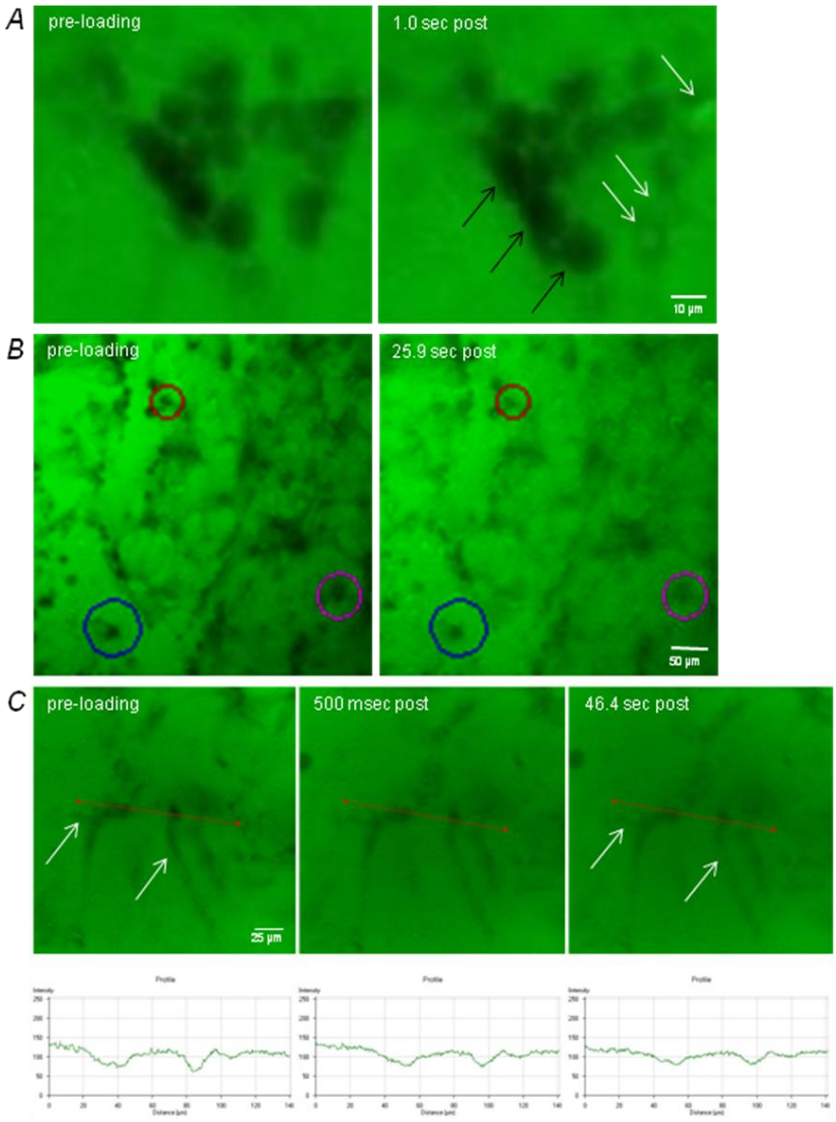

Figure 5.4. Real-time analyses of calcein uptake following shear deformation. Our custom-built shear deformation device was designed to mount on a confocal microscope to permit real-time imaging across the 3-D constructs before, during, and after loading. Calcein diffused throughout the extracellular space prior to loading. The 3-D cultures were then dynamically deformed at 0.50 shear strain (10 s^{-1} or 30 s^{-1} strain rate). Pre-loading, there were clear margins delineating neural somata and processes, indicating intact plasmalemma appropriately excluding calcein. However, immediately post-insult, there was a subset of cells that became calcein^{+} (A, white arrows). Although, most cells continued to exclude calcein (A, black arrows). In other cases, a widespread loss of definition was apparent in neurites as well as somata (B). Calcein uptake was tracked on a per-cell basis throughout loading (C). Here, clear intracellular calcein exclusion was observed pre-loading. Within 500 ms post-insult, intracellular calcein intensity increased. This process continued throughout the first minute, resulting in processes gradually blending with the background (white arrows).

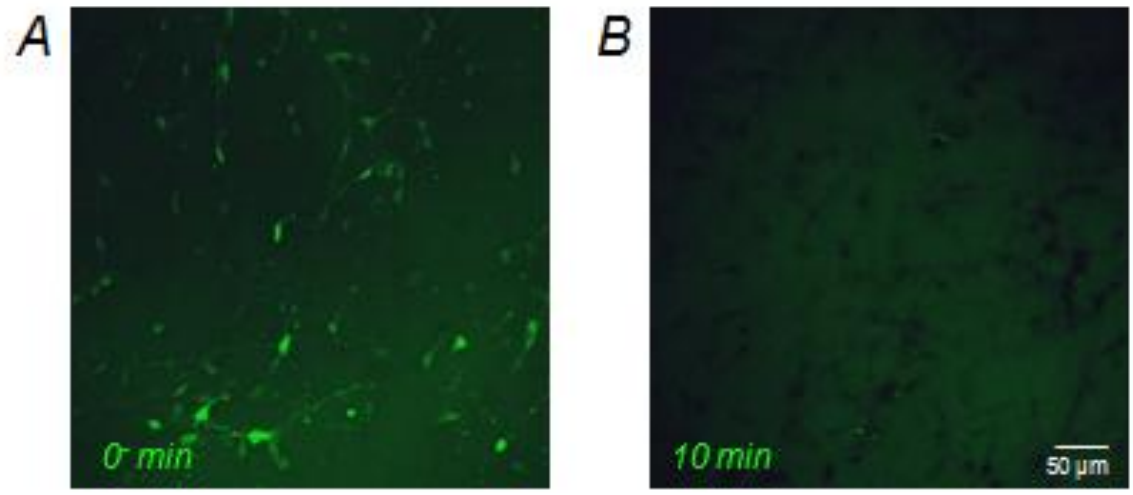

Figure 5.5. Sub-acute permeability alterations. Representative confocal reconstructions of 3-D neuronal-astrocytic co-cultures following mechanical loading at 0.50 shear strain, 10 s^{-1} strain rate. Calcein was added to the cultures either prior to loading (0^-) (A) or 10 min post-loading (B). There was modest uptake when the calcein was present during loading but minimal uptake when calcein was added minutes post-insult (reconstructions from 50 µm thick z-stacks).

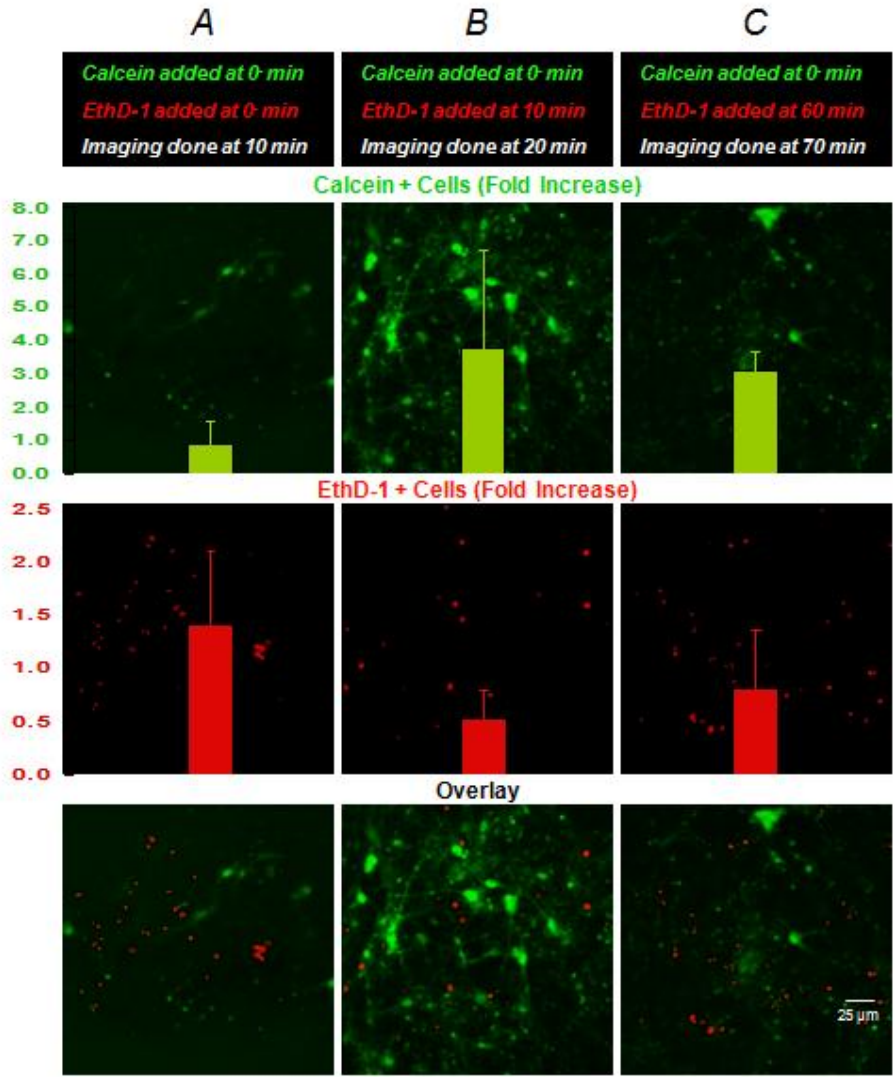

Figure 5.6. Sub-acute time-course of permeability alterations. Representative confocal reconstructions of 3-D neuronal-astrocytic co-cultures following mechanical loading at 0.50 shear strain, 10 s^{-1} strain rate. In addition to calcein, an alternate permeability marker was used, EthD-1, which permanently binds an intracellular substrate. Calcein was added to the cultures *only* prior to loading (0^{-}), whereas EthD-1 was added either prior to loading (A, imaging done at 10 min), or 10 min (B, imaging done at 20 min) or 60 min (C, imaging done at 70 min) post-loading (reconstructions from 60µm thick z-stacks). Over time, intracellular calcein increased given an additional 10 min for intracellular diffusion (B); however, by 60 min intracellular calcein had decreased markedly, suggesting a second phase of altered permeability, with indications of cellular debris (C). In contrast, when EthD-1 was added 10 min post-insult, there was a decrease in EthD-1^{+} cells (C) compared to both earlier and later time points. These results were quantified and normalized to the density of EthD-1^{+} cells in static control cultures, revealing a bi-phasic relationship, where EthD-1^{+} cells decreased precipitously by 10 min post-insult, but increased gradually over one hour post-insult. Data: mean ± standard deviation.

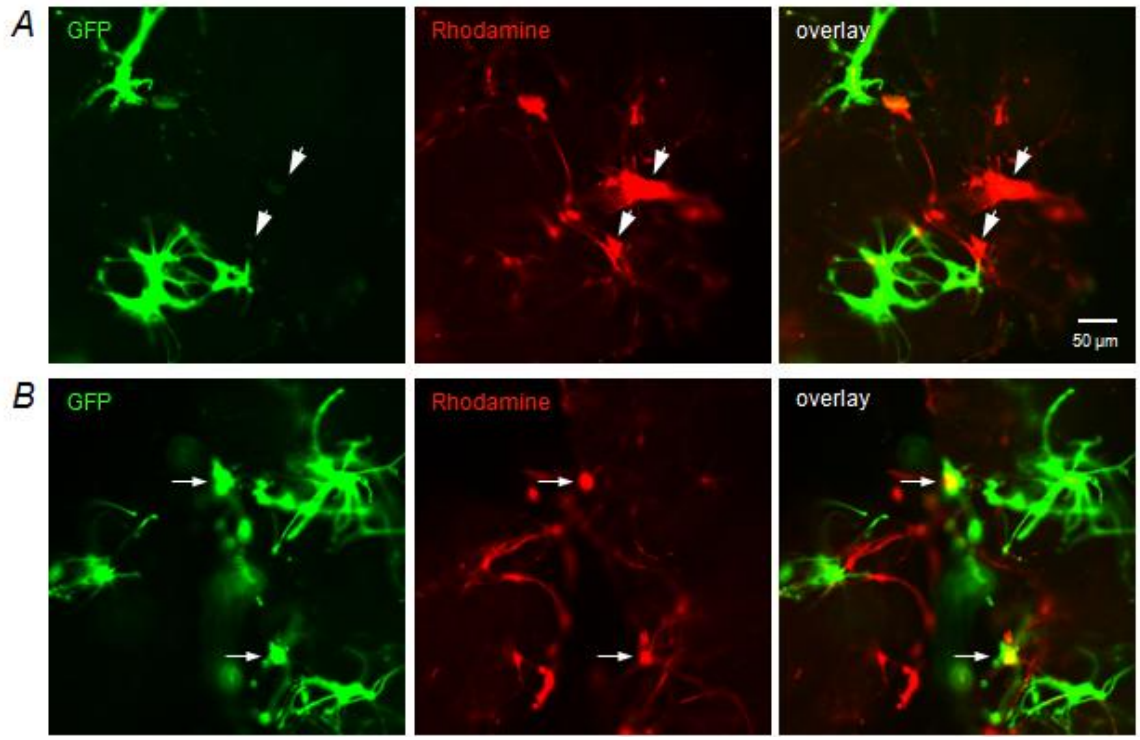

Figure 5.7. Trauma-induced alterations in membrane permeability in neurons versus astrocytes. A subset of co-cultures was generated using GFP^+ neurons mixed with wild-type astrocytes to permit neuronal identification, and a red permeability marker was utilized (rhodamine). Here, there was a mix of both $Rhod^+/GFP^-$ astrocytes (A, denoted by arrowheads) and $Rhod^+/GFP^+$ neurons (B, denoted by arrows) exhibiting altered membrane permeability following injury. This demonstrated the susceptibility of both cell types to acute plasmalemma disruptions following dynamic loading.

Shear vs. Compression Viability

At 48 hours post-insult, a live/dead assay was performed to evaluate the consequences of traumatic loading on cell survival (Figure 5.8A). Following static control conditions or mechanical loading (0.50 shear or compressive strain at 1 s^{-1}, 10 s^{-1}, or 30 s^{-1} strain rate), the percentage of viable cells depended significantly on strain rate ($p < 0.01$) but not the mode of deformation, with no significant interaction between these factors. In particular, following shear loading, the percentage of viable cells was

significantly reduced at 30 s^{-1} versus quasi-static (1 s^{-1}) loading or static control cultures ($p < 0.05$) (Figure 5.8B). We have previously shown that a mechanical insult may directly initiate astrocyte proliferation [22], making the density of dead cells a more accurate marker of post-injury survival. The fold-increase in the density of dead cells (compared to static controls) varied significantly based on strain rate ($p < 0.05$) as well as deformation mode ($p < 0.001$), with no significant interaction between these factors. Specifically, following shear loading at 10 s^{-1} or 30 s^{-1}, the density of dead cells increased by over 5-fold ($p < 0.05$) (Figure 5.8C). Additionally, at matched strain rates of 10 s^{-1} and 30 s^{-1}, there were significant increases in cell death in shear versus compression ($p < 0.05$ each) (Figure 5.8C).

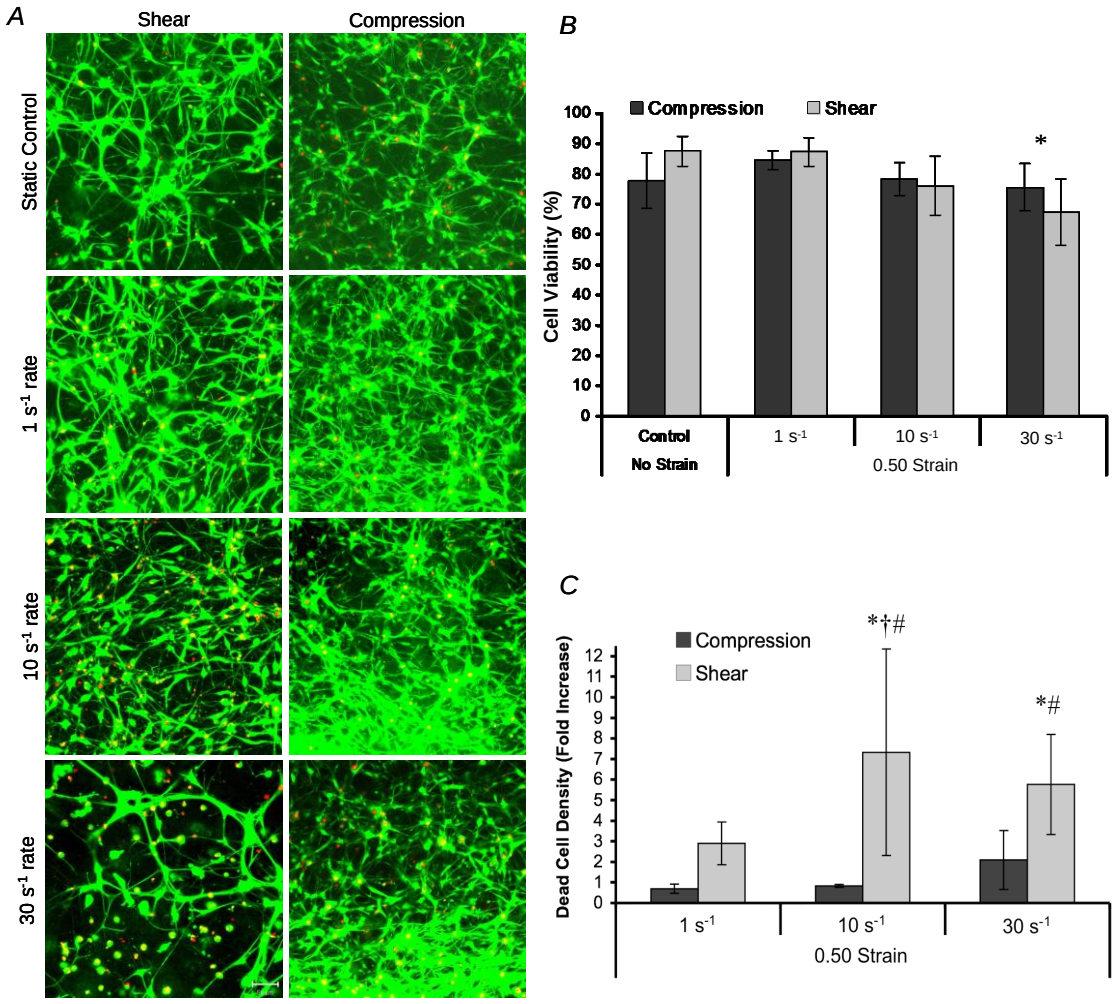

Figure 5.8. Post-insult viability in shear versus compression. Representative confocal reconstructions of culture viability following static control conditions or mechanical loading (0.50 strain at 1 s^{-1}, 10 s^{-1}, or 30 s^{-1} strain rate) (A). Live cells were stained green and the nuclei of dead/dying cells red (reconstructions from 100 µm thick z-stacks; scale bar = 50 µm). Percentage of viable cells (B). The percentage of viable cells 48 hrs following shear deformation depended significantly on injury level (*$p < 0.05$ vs. static and quasi-static controls). Dead-cell density (C). Post-insult proliferation can mask reductions in survival, thus the density of dead cells was calculated (normalized relative to static controls). The density of dead cells varied significantly based on injury level ($p < 0.05$) as well as deformation mode ($p < 0.001$). Pair-wise comparisons: *$p < 0.05$ vs. static control; †$p < 0.05$ vs. quasi-static; #$p < 0.05$ vs. matched strain rate. Data: mean ± standard deviation.

Correlation between Permeability and Viability

Linear regression analyses were performed to assess the potential relationship between acute cell damage and subsequent cell death. Specifically, the acute density of compromised cells ($calcein^{+}$) and the degree of per-cell calcein uptake measured at 10 min post-insult were correlated with the density of dead cells across all loading conditions at 48 hours post-insult. The density of permeabilized cells correlated poorly with later cell death following shear loading ($R^2 = 0.22$). In contrast, this parameter correlated strongly with cell death following compressive loading ($R^2 = 0.98$) (Figure 5.9A); however, there was a lack of distinction between quasi-static and 10 s^{-1} loading in this case. Alternatively, the degree of per-cell calcein uptake, potentially proportional to the degree of cell damage, correlated strongly with cell death for both shear and compression ($R^2 = 0.96$ and $R^2 = 0.95$, respectively, Figure 5.9B). Additionally, the increase in cell death was markedly greater with respect to strain rate for shear versus compression, suggesting that shear deformation is the prevalent mechanism of cellular damage that ultimately induces cell death. Together, these results indicate that the degree of initial transient structural compromise was a stronger predictor of cell death than the number of compromised cells.

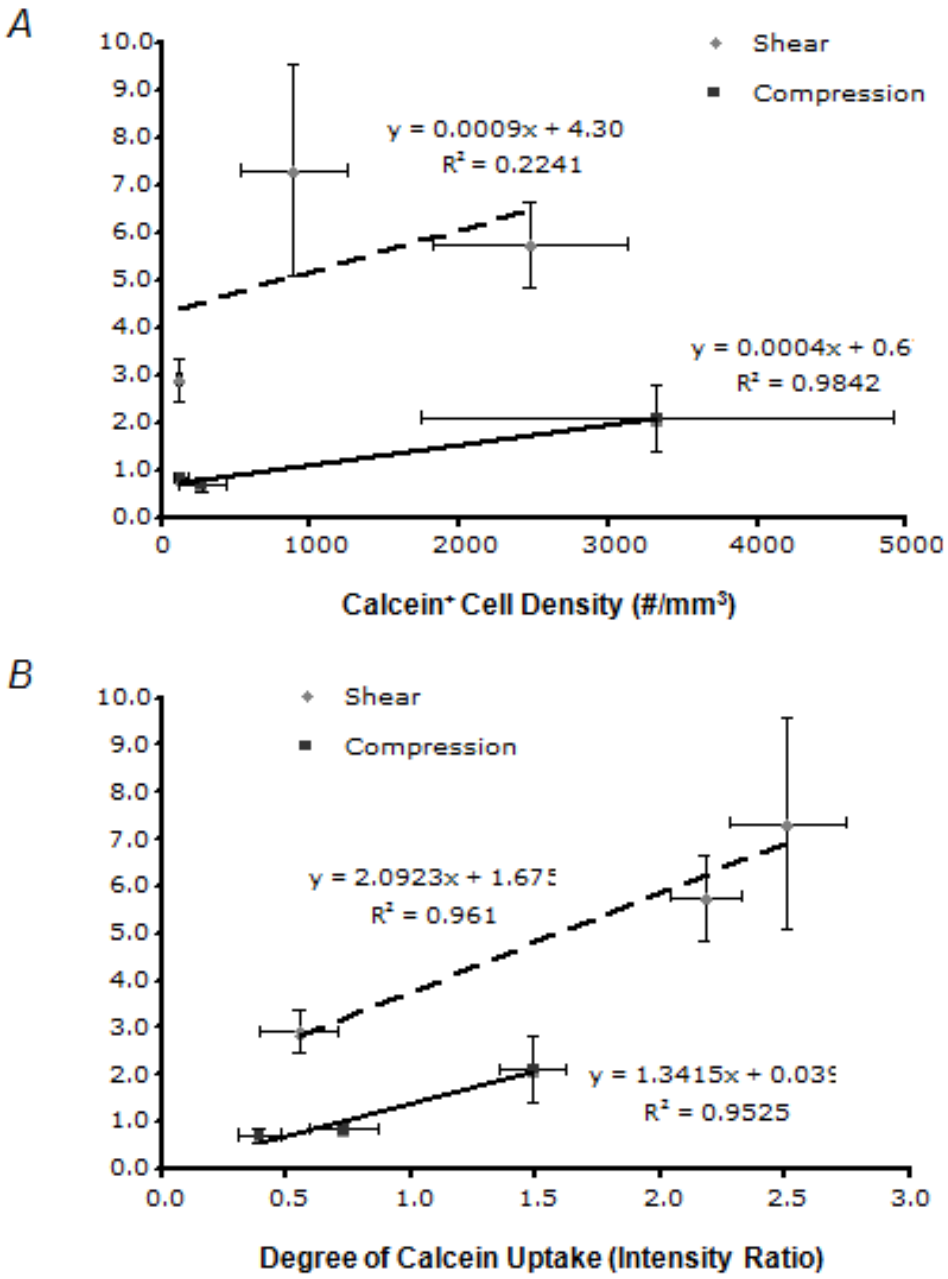

Figure 5.9. Regression analyses to assess potential correlations between acute markers of cell damage and subsequent longer-term cell death. Cell death versus the density of permeabilized cells (A) or versus the degree of per-cell permeability (B). The degree of calcein uptake on a per cell basis was overall a stronger indicator of cell death than the density (or percentage) of calcein$^+$ cells. This implicates the degree of damage rather than the presence of damage in subsequent cell death. Additionally, this increase in cell death was markedly greater for shear versus compression across all strain rates, substantiating that shear deformation is the prevalent mechanism of cellular damage that ultimately induces cell death. Data: mean ± SEM.

Discussion

Traumatic loading to the brain results in complex strain fields; therefore, using custom-built electromechanical devices, we reproducibly imparted controlled shear and compressive deformation on a 3-D neural culture model. This 3-D model is more appropriate to evaluate acute responses to traumatic loading than planar counterparts due to similarities to *in vivo* conditions, such as the three dimensionality of neural network structure, cytoarchitecture, and the distribution of cell-cell/cell-matrix interactions. Using defined inputs to a heterogeneous, anisotropic culture is intended to represent different tissue-level deformation patterns (i.e. shear- or compression-dominated) that may occur at different locations or in varying loading directions within the brain during a traumatic insult. We subjected 3-D neural co-cultures to mechanical loading (0.50 shear or compressive strain at 1, 10, or 30 s^{-1} strain rate) or static control conditions in order to investigate acute and sub-acute plasma membrane disruptions and cell viability. Our major findings were as follows: (1) disruptions of the plasmalemma occurred immediately upon shear or compressive loading and persisted over seconds post-insult; (2) the loading thresholds for these acute plasmalemma disruptions were lower following shear versus compression (≥ 10 s^{-1} in shear; ≥ 30 s^{-1} in compression), with shear resulting in increased degree of per-cell failure and increased compromise of cellular processes; (3) acute alterations in membrane permeability occurred in both neurons and astrocytes; (4) membrane compromise was bi-phasic over one hour post-insult, with acute disruptions immediately upon loading which resealed within minutes, followed by secondary loss of membrane integrity; and (5) both shear and compressive loading induced cell death by 48

hrs post-insult, with shear resulting in significantly higher cell death than compression, when loaded at a relatively high strain rate.

Our results demonstrate that acute plasma membrane compromise following mechanical loading was strain rate-dependent, consistent with previous studies [22, 24-26]. This behavior is due to the viscoelastic nature of cells, which predicts that in the case of high strain rate loading, characteristic of traumatic neural injury, the elastic component will be dominant causing cells to behave in a more rigid manner (i.e. failure given sufficiently large deformation). On the other hand, low strain rate loading entails an increasing effect of the viscous component, whereby structural components are able to comply with even large deformations [27]. In particular, we found that the degree of calcein uptake per permeabilized cell – potentially a gauge of local stress/strain concentrations – increased in a strain rate-dependent manner. A noteworthy caveat in this analysis is that calcein will not necessarily stain all permeabilized cells, since it will not be retained in cells that were permeabilized but not resealed. Likewise, pores smaller than a critical diameter will prevent calcein entry, which may also be affected by molecular charge, shape, and binding affinity. Thus, additional studies of the nature of mechanically-induced membrane damage may require alternative permeability markers with defined characteristics.

The acute cellular responses in 3-D cultures exposed to bulk shear or compression has relevance to loading profiles in TBI (see Figure 5.1). We did not find significant differences in the density of permeabilized cells between these two bulk modes of deformation at matched strain rates. However, the degree of damage (i.e. calcein uptake) on a per-cell basis was greater following shear deformation than compression

deformation. Shear conditions led to increased calcein uptake at lower strain rates, demonstrating a lower threshold for membrane permeability following shear versus compression. Moreover, we observed preferential calcein presence in cellular processes following shear versus compression. This indicates that cellular processes are either more vulnerable to shear loading, or increased somatic permeability leads to enhanced diffusion of calcein. Sensitivity of cellular processes to deformation was also observed in a recent *in vivo* study of spinal cord contusion, which noted persistent permeability in axons [28]. The ramifications of immediate plasmalemma compromise may be devastating, triggering the loss of membrane potential, permeation of molecules, electrokinetic transport, and osmotic imbalance, and even cell rupture [29]. The resulting loss of ionic homeostasis, particularly Ca^{2+} homeostasis in neurons, has been shown to disrupt action potential firing and synapse function, impair axonal conduction, and play a role in excitotoxicity, cytoskeletal breakdown, mitochondrial dysfunction, necrosis, and apoptosis [5, 26-27, 30-38].

We investigated the mechanisms of strain-induced membrane disruption by imaging shear strain application to 3-D neural cultures in real-time, revealing at least three subpopulations of cells with regard to calcein uptake, despite a uniform bulk insult. One subpopulation showed calcein uptake from the extracellular space immediately upon deformation, another subpopulation showed gradual calcein uptake that built up over tens of seconds to minutes, and a third subpopulation showed no calcein uptake even over minutes post-insult. Local cellular strains are functions of cell morphology and orientation [16] and therefore it is not surprising to observe this heterogeneous response within individual cultures. These responses vary due to differences in the following: cell

type morphologies (affecting cellular mechanical properties), orientation with respect to the bulk strain field (affecting principal axes of local cellular strains), and the number of cellular processes (affecting the complexity of the strain field). Also, this varied response may indicate local differences in mechanical properties and thus cell tolerances [39-40] and is consistent with other studies that suggest that multiple types of primary neuronal and axonal injury co-exist following trauma [41-45].

We also investigated the sub-acute time-course of alterations in membrane permeability discriminating between cells that were transiently porated (labeled using a marker requiring resealing for intracellular sequestration - calcein) and cells with transient or prolonged poration (labeled using a marker that bound an intracellular substrate – EthD-1). Although we found significant numbers of permeable cells at the time of injury, membrane integrity appeared re-established by 10 minutes post injury, as previously reported [24-25]. Additionally, cells that became calcein^{+} at the time of injury became "leaky" within one hour, indicating some initially compromised cells developed a second phase of membrane compromise, potentially a progression towards cell death. Likewise, based on the number of EthD-1^{+} cells, intracellular access of EthD-1 spiked immediately post-insult when EthD-1 was present during injury, but decreased when EthD-1 was added 10 minutes post-injury. This trend then reversed as EthD-1^{+} cells increased by 60 minutes. This increased cellular uptake of EthD-1 at 60 minutes post-injury also suggests a secondary, developing phase of membrane compromise which may include dying or dead cells. This cell population may consist of initially compromised cells that experienced secondary membrane damage, or cells that were affected by the mechanical insult independent from acute mechanoporation. Of note, EthD-1 is

commonly used to identify dead cells, because live cells have intact membranes and thus are able to exclude it. Implicit in this distinction is that a compromised plasmalemma indicates a dead or dying cell. Our results suggest that EthD-1 may be used as a marker of membrane permeability at acute time points, because despite no cell loss in the first hour post-insult, EthD-1 labeled cells immediately and at 60 minutes after loading, while cells exclude EthD-1 (and calcein) when added 10 minutes after the insult. Similar to our use of EthD-1 as a membrane permeability marker, other studies have used propidium iodide [46] and ethidium bromide [47], both irreversible DNA binding dyes commonly used for identifying dead cells, as markers of membrane permeability following traumatic brain injury in animals.

In light of the many potentially damaging consequences of high strain rate deformation, we evaluated cell survival within the 3-D co-cultures at 48 hours after shear or compressive loading. There were significant reductions in cell viability after high (30 s^{-1}) strain rate loading compared to quasi-static (1 s^{-1}) loading or static control cultures, indicating a strain rate-dependence for post-insult survival. We found an over 5-fold increase in cell death following 10 s^{-1} and 30 s^{-1} shear strain loading, but only a 2-fold increase in the cell death following 30^{-1} compressive loading. We correlated two acute responses, the density of permeabilized cells and the degree of per-cell permeability changes, with this subsequent cell death. For both shear and compressive loading, the degree of acute permeability changes on a per–cell basis was a stronger predictor of cell death than the density of permeabilized cells. These results implicate the degree of damage rather than the presence of damage in trauma-induced cell death. Possibly, increased severity of the initial structural compromise may directly predispose a cell for

subsequent death, whereas less severe compromise is survivable. Alternatively, different populations of cells may subsequently die, which is unknown, given we did not track individual cells. Indeed, calpain-mediated spectrin proteolysis, an indicator of necrotic cell death, has been shown to occur independent of membrane disruption *in vivo* [41]. On the other hand, neural cell survival following early post-traumatic permeability increases has also been observed [41, 44]. Thus, these studies suggest that many initially permeabilized cells survive the insult; however, there may be prolonged alteration in physiology or later death in this population. Not surprising, there is also evidence of delayed cell death in cells that initially survive membrane compromise *in vivo* [46]. Thus, the long-term survivability of initially permeabilized cells, as well as the functional state of these cells, is not completely understood and warrants further investigation.

While further study is needed, our data suggest that many of the initial disruptions in the plasma membrane are repaired within minutes (perhaps seconds) of injury, indicating that reparative mechanisms are rapidly deployed. These may include lowering the thermodynamic state of the lipid bilayer to reseal ruptures in the plasma membrane and/or vesicle release and fusion to the plasma membrane via calcium-dependent mechanisms [48-54]. Some of these emergency cellular repair mechanisms may be energetically taxing [55], and may occur when metabolic demands in the injured cell are increasing. These reparative mechanisms may be limited or not available as secondary degradative events are initiated, such as calcium-dependent activation of proteases and phospholipases that may enzymatically digest the cytoskeleton and plasma membrane [56-60] - thus causing a secondary poration. Although these secondary mechanisms of cell damage are not unique to trauma (see [61-62] for reviews), primary (physical)

damage as well as the damaged/reparative context in which the secondary events ensue are unique to trauma.

Collectively, our observations lead us to postulate a time-course of events involving post-trauma alterations in membrane permeability that may ultimately lead to cell death (Figure 5.10). As a direct physical consequence of traumatic loading, a primary phase of mechanoporation is initiated in a subset of cells. In some cases, this may be irreparable damage. In other cases, this phase is marked by transient disruptions, ending within tens of seconds or minutes of the physical insult. In our study, these populations were indicated by high levels of intracellular calcein and EthD-1 at the time of injury. In cells that are able to reseal, the initial physical insult may provide sufficient perturbation to lead to a secondary phase of membrane poration/damage due to non-mechanical causes (e.g., phospholipase and/or protease-mediated processes). In the sub-acute period, this phase is marked by dynamic pore turnover, captured in our studies by the differential levels of EthD-1 staining with respect to time, that may ultimately lead to cell death [56-60]. Thus, over the first hour post-insult, two related yet distinct mechanisms of membrane damage appear as biphasic alterations in membrane permeability.

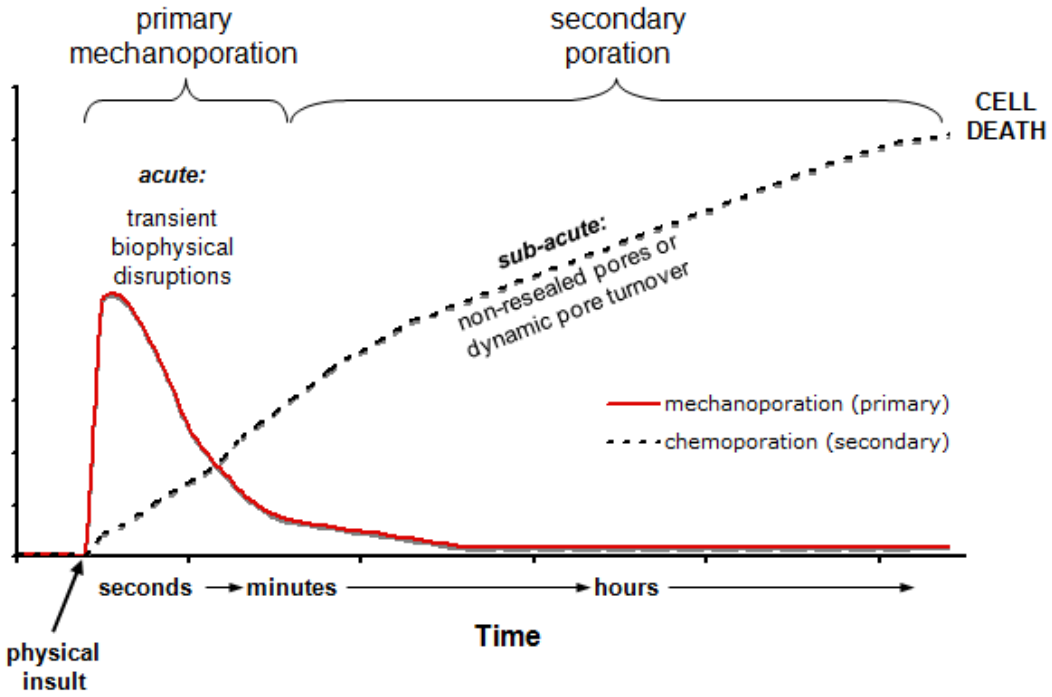

Figure 5.10. Postulated permeability time-course. Mounting evidence suggests that the primary phase of mechanoporation ends within seconds of the physical insult, and thus is marked by transient, acute biophysical disruptions. A protracted phase of secondary poration ensues as time progresses in some cases. This phase is likely enzymatically-mediated and potentially marked by dynamic pore turnover that may ultimately lead to cell death. Collectively, these two related yet distinct mechanisms yield the appearance of bi-phasic alterations in membrane permeability over the first several hours post-insult.

Conclusion

In summary, our demonstrate a particular vulnerability to shear deformation, which resulted in increased cell structural damage/failure and death compared to compression. We observed a biphasic response in cell membrane permeabilization upon injury, with a primary mechanoporation phase lasting seconds to minutes post injury, and a secondary phase of membrane damage ensuing in the hours post injury. These results are the basis for a proposed sequence of membrane damage and repair dynamics that should be considered in light of other consequences of mechanical injury for both neural and other systems, as mechanoporation may be a key trigger for cellular dysfunction. In addition, elucidation of acute mechanisms of structural damage using biomechanically-characterized reduced (i.e. *in vitro*) models can then be extrapolated to cellular or tissue loading responses in human TBI. Further investigation of these events and their time course will contribute to our increased understanding of cellular tolerances and be useful in computer modeling to more accurately predict structural and functional damage in response to large magnitude, high rate deformation.

Acknowledgements

The authors thank Albert King and Liying Zhang at Wayne State University for finite element modeling of strain propagation following controlled cortical impact, Crystal M. Simon for valuable input regarding experimental design and data analysis, Christopher E. Gonzales for technical contributions, and Rebekah M. Hamrick for editorial assistance.

This work was partially supported by NSF (CAREER Award BES-0093830), NIH/NIBIB (EB001014), NSF (EEC-9731643) and the Southern Consortium for Injury Biomechanics at the University of Alabama Birmingham-Injury Control Research Center, through a grant from the National Center for Injury Prevention and Control, Centers for Disease Control and Prevention, Award R49/CE000191 and Cooperative Agreement TNH22-01-H-07551 with the National Highway Traffic Safety Administration. This work made use of shared facilities from the Georgia Tech/Emory Center (GTEC) for the Engineering of Living Tissues, an ERC (EEC-9731643).

References

1. Langlois, J., W. Rutland-Brown, and K. Thomas, *Traumatic brain injury in the United States: emergency department visits, hospitalizations, and deaths*. 2004, Centers for Disease Control and Prevention, National Center for Injury Prevention and Control: Atlanta, GA. p. 1–68.
2. Langlois, J.A., W. Rutland-Brown, and M.M. Wald, *The epidemiology and impact of traumatic brain injury: a brief overview*. J Head Trauma Rehabil, 2006. **21**(5): p. 375-8.
3. McIntosh, T.K., et al., *Secondary brain injury: neurochemical and cellular mediators.* Traumatic brain injury, 1999.
4. Saatman, K., et al., *Classification of traumatic brain injury for targeted therapies.* Journal of neurotrauma, 2008. **25**(7): p. 719-738.
5. Raghupathi, R., *Cell death mechanisms following traumatic brain injury.* Brain Pathol, 2004. **14**(2): p. 215-22.
6. Smith, D., et al., *Progressive atrophy and neuron death for one year following brain trauma in the rat.* Journal of neurotrauma, 1997. **14**(10): p. 715-727.
7. Stein, S., et al., *Delayed and progressive brain injury in closed-head trauma: radiological demonstration.* Neurosurgery, 1993. **32**(1): p. 25.
8. Gennarelli, T.A., *Mechanisms of brain injury.* J Emerg Med, 1993. **11 Suppl 1**: p. 5-11.
9. Margulies, S.S. and L.E. Thibault, *A proposed tolerance criterion for diffuse axonal injury in man.* J Biomech, 1992. **25**(8): p. 917-23.
10. Meaney, D.F., et al., *Biomechanical analysis of experimental diffuse axonal injury.* J Neurotrauma, 1995. **12**(4): p. 689-94.
11. Sahay, K., et al., *Elastomechanical characterization of brain tissues.* Journal of biomechanics, 1992. **25**(3): p. 319-326.
12. McLean, A.J. and R.W.G. Anderson, *Biomechanics of Closed Head Injury.* Head Injury, 1997.
13. LaPlaca, M., et al., *CNS injury biomechanics and experimental models.* Progress in brain research, 2007. **161**: p. 13.
14. Thibault, L.E. and T.A. Gennarelli, *Biomechanics of diffuse brain injuries.* Proc. 10th Int. Tech. Conf. on Experimental Safety Vehicles. DOT, NHTSA., 1989.
15. Holbourne, A., *Mechanics of head injury.* Lancet, 1943. **2**: p. 438-41.
16. Cullen, D. and M. LaPlaca, *Neuronal response to high rate shear deformation depends on heterogeneity of the local strain field.* Journal of neurotrauma, 2006. **23**(9): p. 1304-1319.
17. LaPlaca, M., et al., *High rate shear strain of three-dimensional neural cell cultures: a new in vitro traumatic brain injury model.* Journal of biomechanics, 2005. **38**(5): p. 1093-1105.
18. Hatten, M.E., et al., *Astroglia in CNS injury.* Glia, 1991. **4**(2): p. 233-43.
19. Liao, S.L. and C.J. Chen, *Tyrosine kinase signaling involved in glutamate-induced astrocyte proliferation.* Neuroreport, 2001. **12**(16): p. 3519-22.
20. Kleinman, H., et al., *Basement membrane complexes with biological activity.* Biochemistry, 1986. **25**(2): p. 312-318.

21. Irons, H., et al., *Three-dimensional neural constructs: a novel platform for neurophysiological investigation.* Journal of Neural Engineering, 2008. **5**(3): p. 333-341.
22. Cullen, D., C. Simon, and M. LaPlaca, *Strain rate-dependent induction of reactive astrogliosis and cell death in three-dimensional neuronal–astrocytic co-cultures.* Brain Research, 2007. **1158**: p. 103-115.
23. Cullen, D., M. Lessing, and M. LaPlaca, *Collagen-dependent neurite outgrowth and response to dynamic deformation in three-dimensional neuronal cultures.* Annals Of Biomedical Engineering, 2007. **35**(5): p. 835-846.
24. Prado, G., et al., *Mechanical trauma induces immediate changes in neuronal network activity.* Journal of Neural Engineering, 2005. **2**(4): p. 148-158.
25. Geddes, D., R. Cargill, and M. LaPlaca, *Mechanical stretch to neurons results in a strain rate and magnitude-dependent increase in plasma membrane permeability.* Journal of neurotrauma, 2003. **20**(10): p. 1039-1049.
26. LaPlaca, M., V. Lee, and L. Thibault, *An in vitro model of traumatic neuronal injury: loading rate-dependent changes in acute cytosolic calcium and lactate dehydrogenase release.* Journal of neurotrauma, 1997. **14**(6): p. 355-368.
27. Galbraith, J., L. Thibault, and D. Matteson, *Mechanically induced depolarization in the squid giant axon to simple elongation.* J. Biomech. Eng, 1993. **115**: p. 13-22.
28. Simon, C., et al., *Spinal cord contusion causes acute plasma membrane damage.* Journal of neurotrauma, 2009. **26**(4): p. 563-574.
29. Bartoletti, D.C., G.I. Harrison, and J.C. Weaver, *The number of molecules taken up by electroporated cells: quantitative determination.* FEBS Letters, 1989. **256**(1-2): p. 4-10.
30. Dumont, R.J., et al., *Acute spinal cord injury, part I: pathophysiologic mechanisms.* Clin Neuropharmacol, 2001. **24**(5): p. 254-64.
31. McIntosh, T., et al., *Review. The Dorothy Russell Memorial Lecture. The molecular and cellular sequelae of experimental traumatic brain injury: pathogenetic mechanisms.* Neuropathology and Applied Neurobiology, 1998. **24**(4): p. 251-267.
32. Rami, A., D. Ferger, and J. Krieglstein, *Blockade of calpain proteolytic activity rescues neurons from glutamate excitotoxicity.* Neuroscience research, 1997. **27**(1): p. 93-97.
33. Villa, P., et al., *Calpain inhibitors, but not caspase inhibitors, prevent actin proteolysis and DNA fragmentation during apoptosis.* Journal of Cell Science, 1998. **111**(6): p. 713-722.
34. Weber, J., *Calcium homeostasis following traumatic neuronal injury.* Current neurovascular research, 2004. **1**(2): p. 151.
35. Weber, J.T., et al., *Alterations in calcium-mediated signal transduction after traumatic injury of cortical neurons.* Cell Calcium, 1999. **26**(6): p. 289-99.
36. Goforth, P., E. Ellis, and L. Satin, *Enhancement of AMPA-mediated current after traumatic injury in cortical neurons.* Journal of Neuroscience, 1999. **19**(17): p. 7367-7374.

37. Shi, R. and J. Whitebone, *Conduction deficits and membrane disruption of spinal cord axons as a function of magnitude and rate of strain.* Journal of Neurophysiology, 2006. **95**(6): p. 3384-3390.
38. Zhang, L., et al., *Reduction of voltage-dependent Mg2+ blockade of NMDA current in mechanically injured neurons.* Science, 1996. **274**(5294): p. 1921.
39. Elkin, B.S. and B. Morrison, 3rd, *Region-specific tolerance criteria for the living brain.* Stapp Car Crash J, 2007. **51**: p. 127-38.
40. Elkin, B.S., et al., *Mechanical heterogeneity of the rat hippocampus measured by atomic force microscope indentation.* J Neurotrauma, 2007. **24**(5): p. 812-22.
41. Farkas, O., J. Lifshitz, and J. Povlishock, *Mechanoporation induced by diffuse traumatic brain injury: an irreversible or reversible response to injury?* Journal of Neuroscience, 2006. **26**(12): p. 3130-3140.
42. Farkas, O. and J.T. Povlishock, *Cellular and subcellular change evoked by diffuse traumatic brain injury: a complex web of change extending far beyond focal damage.* Prog Brain Res, 2007. **161**: p. 43-59.
43. Kelley, B.J., et al., *Traumatic axonal injury in the perisomatic domain triggers ultrarapid secondary axotomy and Wallerian degeneration.* Exp Neurol, 2006. **198**(2): p. 350-60.
44. Singleton, R.H. and J.T. Povlishock, *Identification and Characterization of Heterogeneous Neuronal Injury and Death in Regions of Diffuse Brain Injury: Evidence for Multiple Independent Injury Phenotypes.* J. Neurosci., 2004. **24**(14): p. 3543-3553.
45. Stone, J., et al., *Impaired axonal transport and altered axolemmal permeability occur in distinct populations of damaged axons following traumatic brain injury.* Experimental Neurology, 2004. **190**(1): p. 59-69.
46. Whalen, M.J., et al., *Acute plasmalemma permeability and protracted clearance of injured cells after controlled cortical impact in mice.* J Cereb Blood Flow Metab, 2008. **28**(3): p. 490-505.
47. Koob, A.O., et al., *Intravenous polyethylene glycol inhibits the loss of cerebral cells after brain injury.* J Neurotrauma, 2005. **22**(10): p. 1092-111.
48. Chang, D. and T. Reese, *Changes in membrane structure induced by electroporation as revealed by rapid-freezing electron microscopy.* Biophysical Journal, 1990. **58**(1): p. 1-12.
49. McNeil, P.L., K. Miyake, and S.S. Vogel, *The endomembrane requirement for cell surface repair.* Proc Natl Acad Sci U S A, 2003. **100**(8): p. 4592-7.
50. McNeil, P., et al., *Patching plasma membrane disruptions with cytoplasmic membrane.* Journal of Cell Science, 2000. **113**(11): p. 1891-1902.
51. Miyake, K. and P. McNeil, *Vesicle accumulation and exocytosis at sites of plasma membrane disruption.* Journal of Cell Biology, 1995. **131**(6): p. 1737-1745.
52. Nehrt, A., et al., *The critical role of voltage-dependent calcium channel in axonal repair following mechanical trauma.* Neuroscience, 2007. **146**(4): p. 1504-12.
53. Schlicher, R., et al., *Mechanism of intracellular delivery by acoustic cavitation.* Ultrasound in medicine & biology, 2006. **32**(6): p. 915-924.
54. Shi, R., et al., *Dimethylsulfoxide enhances CNS neuronal plasma membrane resealing after injury in low temperature or low calcium.* J Neurocytol, 2001. **30**(9-10): p. 829-39.

55. Togo, T., J.M. Alderton, and R.A. Steinhardt, *The mechanism of cell membrane repair.* Zygote, 2000. **8 Suppl 1**: p. S31-2.
56. Lyeth, B., et al., *Effects of muscarinic receptor antagonism on the phosphatidylinositol bisphosphate signal transduction pathway after experimental brain injury.* Brain research, 1996. **742**(1-2): p. 63-70.
57. Saatman, K., et al., *Traumatic axonal injury results in biphasic calpain activation and retrograde transport impairment in mice.* Journal of Cerebral Blood Flow & Metabolism, 2003. **23**(1): p. 34-42.
58. Serbest, G., et al., *Temporal profiles of cytoskeletal protein loss following traumatic axonal injury in mice.* Neurochemical research, 2007. **32**(12): p. 2006-2014.
59. Büki, A., et al., *The role of calpain-mediated spectrin proteolysis in traumatically induced axonal injury.* Journal of neuropathology and experimental neurology, 1999. **58**(4): p. 365-375.
60. Homayoun, P., et al., *Cortical impact injury in rats promotes a rapid and sustained increase in polyunsaturated free fatty acids and diacylglycerols.* Neurochemical research, 2000. **25**(2): p. 269-276.
61. Adibhatla, R. and J. Hatcher, *Phospholipase A 2, reactive oxygen species, and lipid peroxidation in CNS pathologies.* BMB Rep, 2008. **41**(8): p. 560–567.
62. Vosler, P., C. Brennan, and J. Chen, *Calpain-mediated signaling mechanisms in neuronal injury and neurodegeneration.* Molecular Neurobiology, 2008. **38**(1): p. 78-100.

CHAPTER 6

DISCUSSION AND CONCLUSION

Summary and Significance

This section integrates the major findings of the research and discusses their collective implications.

Evaluating the cytotoxicity of SU-8 2000 (a microfabrication material that enables the fabrication of high aspect-ratio structures) and devising treatments to improve its cytocompatibility was the first aim of this research work. The results suggested a link between SU-8 2000 cytotoxicity in neuronal cultures to poor adhesive properties and toxic components, such as solvents and photo acid generator associated elements. Several post-processing strategies were developed to improve SU-8 2000 cytocompatibility, including combinations of heat and isopropanol sonication followed by surface treatments of either oxygen plasma or parylene coating. Overall, these treatments diminished the cytotoxicity and poor cell adhesion of SU-8 2000, expanding its potential as a microfabrication material for bioMEMS and other biomedical applications.

After enhancing the cytocompatibility of SU-8 2000, in the second aim of this research work a 3-D co-culture system of neurons and astrocytes within a bioactive scaffold of extracellular matrix-derived proteins and proteoglycans was generated and optimized. This 3-D neural network was used to study the *in vitro* network development of both electrophysiological (functional) properties via 3-D MEA recording and structural properties through viability and immunocytochemical techniques. This is the first

investigation of the network-level electrophysiological activity of dissociated 3-D cultures. Our culture system maintained considerable neurite outgrowth and complex 3-D network architecture that developed over time *in vitro*. The cultures exhibited high long-term viability up to three weeks *in vitro* with functional network synaptic connections and spontaneous and evoked electrophysiological activity. The 3-D culture environment appears to better promote the electrophysiological activity of these cultures as compared to a 2-D environment, as measured in terms of average spike and burst rates per electrode. This electrophysiological activity may be strongly influenced by the changing inhibitory synaptic character of these cultures. This work shows that physiologically relevant 3-D micro-environments can be created with control over cell density, cell types, and media conditions. However, weaknesses remain with our 3-D co-culture, as cells were isolated from critical factors usually provided in an *in vivo* nervous system, such as normal synaptic inputs, blood supply, immunological factors, systemic inputs, and the *in vivo* tissue developmental program. Additionally, these neural cultures exhibited reduced synaptic density, randomized architecture, and reduced glia number as compared to an *in vivo* system. Nevertheless, 3-D co-cultures still represent an important step towards engineering more physiologically-conformant neural tissue models for *in vitro* testing and tissue engineering. Such tissue-engineered constructs may serve as investigative platforms to study neurobiological phenomena by more accurately representing *in vivo* interactions with the control and precision realized by *in vitro* systems. In addition, the random architecture of the neural networks in the 3-D co-culture allows for general statistical analyses of the gross behavioral features, patterns, and responses of neural networks to various physiologically relevant stimuli. Such

analysis can be useful in testing drugs, understanding the structure-function relationship in developing neural networks, designing better tissue engineered neural constructs, and interfacing neural tissue with neural prostheses. The engineering of such novel culture models is critical for *in vitro* advances in neuroscience and neural engineering, providing custom and modular design capabilities for the mechanistic study of cell growth, cell-cell / cell-matrix interactions, as well as the responses to chemical or mechanical perturbations.

As a demonstration of the utility of 3-D cultures to study neural network response under a pathological condition and to potentially serve as a high-throughput drug-testing platform, we developed a method of 3-D culture injury and analysis in the third aim of this work. Physiologically relevant 3-D culture systems have the potential to be high-throughput systems because *several* 3-D cultures can be *reproducibly* generated, in controlled and defined environments (with respect to cell type, cell ratios, and orientation) for use in *varied* assays both in sequence and in parallel in *real-time* with *precise* micro-environmental manipulation and control, from very little source animal tissue at a time. Furthermore, the amount of cell markers available for study is magnified given that the three-dimensionality allows the presence of more cells within a given space. We developed a compression injury device capable of delivering controlled high magnitude strains at high, uniform rates throughout the 3-D co-cultures. This injury device was then validated for its ability to induce cellular trauma in the 3-D cultures, by measuring the number of permeabilized cells post insult from the device and the quantification of subsequent neuronal death. In parallel, injury was induced using on a previously built shear injury device. For the purpose of investigating neural network

properties throughout compressive injury, we created a hybrid device to use with commercially available Multi Electrode Array (MEA) system (Multi Channel Systems, Germany). In the future, this device can potentially allow for injury directly within the MEA, concomitant recording of the electrophysiological activity during the injury and drug treatment to investigate the injury response. By enabling simultaneous and subsequent electrophysiological recording from injured 3-D cultures, this technology would provide information on network property changes (such as changes in synapse strength, signal spread and velocity, etc.) following a traumatic neuronal injury.

Our injury experiments demonstrated that disruptions of the cellular plasmalemma occurred immediately upon shear or compressive loading and persisted over seconds post-insult. For both shear and compression loading, these acute plasmalemma disruptions resulted in significant increases in membrane permeability in a strain rate dependent manner. However, the loading thresholds for these acute plasmalemma disruptions were lower following shear versus compression, with shear resulting in increased degree of per-cell failure and increased compromise of cellular processes. Acute alterations in membrane permeability occurred in both neurons and astrocytes. Membrane compromise was bi-phasic over one hour post-insult, with acute disruptions immediately upon loading which resealed within minutes, followed by secondary loss of membrane integrity. Both shear and compressive loading induced cell death by 48 hrs post-insult, with shear resulting in significantly higher cell death than compression, when loaded at a relatively high strain rate. For both shear and compressive loading, the degree of acute permeability changes on a per–cell basis was a stronger predictor of cell death than the density of permeabilized cells. These results

implicate the degree of damage rather than the presence of damage in trauma-induced cell death. Our 3-D co-culture model *in vitro* not only generated a rapid and reproducible injury, but, since local cellular strains in *in vivo* traumatic neural injury may be heterogenous and a function of cell orientation with respect to the bulk strain field, a 3-D model such as ours may better represent neural trauma-related biomechanics and pathophysiology than 2-D models. Overall, our 3-D co-culture model could be important in elucidating cellular tolerances and in developing mechanistically-motivated intervention strategies for neural injury.

Future Directions and Applications

The results of our first study (Aim 1) have provided a methodology for increasing the cytocompatibility of SU-8 2000, enabling its use as a primary microfabrication material for biological microelectromechanical systems (bioMEMS) and other biomedical applications. This can allow greater microfabrication advances towards the development of small, cheap, precise, and biocompatible devices for bioMEMS applications. Since our work suggested a link between SU-8 2000 cytotoxicity in neuronal cultures to poor adhesive properties and toxic components, such as solvents and photo acid generator associated elements, future research can focus on developing SU-8 with alternative components that are more biocompatible. Furthermore, the methodologies developed in this work can be extended to testing and improving the cytocompatibility of any other material of interest.

Studying 3-D neural networks with microelectrodes and an *in vitro* 3-D culture model (Aim 2) allowed us to study the interfacing and development of 3-D neural networks *in vitro*. Further study along these lines can delve into studying the nervous systems's information processing capabilities. Likewise, our *in vitro* 3-D culture model, can help gain insight in neural prosthesis actuation and control by providing a high-throughput economical testing option for data acquisition and analysis.

Additionally, the 3-D culture model offers an excellent pre-clinical test-bed for the simulation and study of neural pathologies in a controlled environment. New insights from these studies can lead to new therapeutic strategies in neural regeneration for the treatment of both traumatic damage and neurodegenerative disorders. For example, drug and cell therapeutic strategies for the remyelination of neurons in multiple sclerosis can

be developed using the 3-D culture MEA system by testing for the increase in the conduction velocities of demyelinated neurons upon addition of the therapeutic test agent.

Likewise, the 3-D culture model could electrophysiologically characterize stroke response, by testing under ischemic conditions. Using this information, an implanted microchip could be programmed to detect stroke-related brain signals and notify you and a health care provider, quickening diagnosis and treatment. The chip's design could even enable the immediate release of device-stored medication, such as tissue plasminogen activator, which needs to be administered within the "golden time window" of 90 minutes post-stroke for effective counter-action. Likewise, many other possibilities exist: such implants could seamlessly function within the body, owing their biocompatibility. Likewise, they could resorb upon biological or external stimulus. Physico-chemical phenomena could assist in the implant's functions; for instance, a chemical reaction could cause allosteric changes inducing drug-release or immune-response.

The 3-D culture model could also aid in the research of stem-cell therapy. Currently, a robust testing arena is needed to verify that artificially induced stem cells have developed into electrophysiologically active neurons that network with each other. The 3-D MEA culture model would allow thorough network-level testing of neuronal induction of stem cells by both the recording and stimulation of the test cultures and comparison with standard neuronal cultures.

This work has implication on tissue engineering research as well. The presence of laminin in the 3-D matrix studied aids in the development of 3-D tissue microstructure in our cultures. Future studies can throw light on how neurons develop networks in 3-D, and how do these networks change their structure and function with time under neural

developmental conditions. This information can be used for tissue engineering surrogate neural tissue *in vitro*, that can be used to replace their damaged or degenerated counterparts *in vivo*.

As demonstrated in the last study of this work (Aim 3), the 3-D culture model can be applied for studying traumatic afflictions and their subsequent pathology. Our results are the basis for a proposed sequence of membrane damage and repair dynamics that should be considered in light of other consequences of mechanical injury for both neural and other systems, as mechanoporation of cells following injury may be a key trigger for cellular dysfunction. In addition, elucidation of acute mechanisms of structural damage using biomechanically-characterized reduced (i.e. *in vitro*) models, such as ours, can then be extrapolated to cellular or tissue loading responses in human TBI. Further investigation of these events and their time course will contribute to our increased understanding of cellular tolerances and be useful in computer modeling to more accurately predict structural and functional damage in response to large magnitude, high rate deformation.

As a closing note, the general methodology of 3-D co-culture analysis developed in this investigation provides an experimental framework on which to build, including varying the cell type, adding additional cell types, modifying or changing the scaffold, or interfacing with other systems, such as electrodes, fluidic support, or other cell systems. This model can be used to test various therapies such as single dose, time-release, mono- and combination drug therapies; drug-releasing devices; cell-based therapies such as stem cell delivery; study pathological conditions; characterize and validate tissue engineering strategies; characterize and validate neural implants for continuous monitoring,

diagnostic, and therapeutic applications to the nervous system; or simply to understand the development of neural networks.